University of Glasgow

Doctoral Thesis

Effects of the Dzyaloshinskii-Moriya interaction on spin waves in domain walls

Pablo
Borys

A thesis submitted in fulfilment of the requirements for the degree of Doctor of Philosophy

in the

Materials and Condensed Matter Physics
School of Physics and Astronomy

December 2015

Declaration of Authorship

I, Pablo Borys, declare that this thesis titled, 'Effects of the Dzyaloshinskii-Moriya interaction on spin waves in domain walls' and the work presented in it are my own. I confirm that:

- This work was done wholly or mainly while in candidature for a research degree at this University.
- Where any part of this thesis has previously been submitted for a degree or any other qualification at this University or any other institution, this has been clearly stated.
- Where I have consulted the published work of others, this is always clearly attributed.
- Where I have quoted from the work of others, the source is always given. With the exception of such quotations, this thesis is entirely my own work.
- I have acknowledged all main sources of help.
- Where the thesis is based on work done by myself jointly with others, I have made clear exactly what was done by others and what I have contributed myself.

Signed: _____

Date: _____

"Por mi raza hablará el espíritu."

José Vasconcelos

Abstract

We propose novel ways of manipulating spin wave propagation useful for data processing and storage within the field of magnonics. We analyse the effects of the Dzyaloshinskii-Moriya interaction (DMI) on magnetic structures using an analytical formalism. The DMI is the antisymmetric form of the exchange interaction and becomes relevant in magnetic structures where surface phenomena are important as in thin ferromagnetic films. The antisymmetric nature of the DMI modifies the magnetic ground state stabilising chiral structures. In particular, the DMI favours one kind of domain wall, Néel wall, over the common Bloch-type wall. In this thesis, we focus on taking advantage of the new features found in the small fluctuations, or spin waves, around a DMI driven-Néel type wall in order to propose new magnonic devices.

Studies about the influence of the DMI on spin waves in uniformly magnetised films show that the dispersion can be non-reciprocal, i.e. the frequency is not symmetric with respect to the wave vector, $\Omega(k) \neq \Omega(-k)$. In domain walls, we observe that the non-reciprocity phenomenon arises for propagation parallel to the plane of the wall. In this direction, the domain wall acts as a confining potential and provides a way of channelling the spin waves even in curved geometries. The non-reciprocity increases the spin wave group velocity to a range useful for information technologies.

For propagation perpendicular to the wall plane we find that spin waves are reflected due to the DMI. We consider a periodic array of Néel walls and calculate the band structure in which frequency gaps appear. The reflection phenomenon in the periodic array is the basis of a tunable frequency filter device

Examining the symmetries of the magnetic Lagrangian, we find that energy and linear momentum are conserved. We analyse how energy conservation explains the non-reciprocal dispersion and how linear momentum conservation is achieved by spin waves transferring linear momentum to the domain wall and moving it.

Following similar symmetry considerations, we calculate the continuity equation for the total angular momentum of the system. We find that the total angular momentum of the system consists of an orbital and a spin contribution. We demonstrate that an angular momentum transfer from the orbital part, associated with the DMI, to the spin part, given by the magnetic moments, needs to occur for the total angular momentum to be conserved. We propose that this mechanism leads to spin wave-driven domain wall motion.

Acknowledgements

Completion of a PhD is a difficult task that cannot be achieved alone. I want to thank the people and institutions that have made this possible.

Thank you, Prof. Robert Stamps, for not only being a mentor in science related matters, but also for showing me by example the abilities needed to become a productive member of the academic community. I sincerely hope to continue learning from you.

The collaboration with the research group at the University of Paris-Sud has been very productive and my research stay there allowed me to form a network useful for future projects. Thank you, Dr. Felipe García for a friendly collaboration. Thank you, Dr. Joo-Von Kim for being my honorary supervisor.

Thank you, friends and staff at the Materials and Condensed Matter Physics group for a very pleasant stay in Glasgow.

My thankfulness to Prof. Volodymyr Kruglyac and Dr. Christian Korff for revising this thesis.

I am forever in debt with my parents, Antonio Borys and Beatriz Sosa. Your infinite and constant support is key for this achievement. Thank you, dad and mum. I feel so proud of having a person like my brother, Rodrigo Borys, in my life. Without you this would not be possible. Thanks brother.

My *madrina*, Spanish for Godmother, has really lived up to the name. I strongly believe that everything I have become is mostly because of you and what you have taught me. Thank you so much *madrina*, Estela Borys.

I am specially grateful for having an extraordinary wife who has supported me throughout every step we have decided to take. In addition to your love and patience which has allowed me to endure through bad moments, your optimism and joy have always filled our home with hope and happiness. Thank you, Veronica.

Thank you, my baby girl Odarka, for reorienting my whole life in the best possible way. I hope all the efforts made on our side someday become fruitful for you.

This PhD was funded by the National Council of Science and Technology of Mexico (CONACyT).

Contents

List of Figures

List of Original Publications

This thesis is based on the following articles. In all of them I contributed with the theoretical calculations.

(1) Felipe Garcia Sanchez, Pablo Borys, Arne Vansteenkiste, Joo-Von Kim, Robert Stamps. Nonreciprocal spin-wave channeling along textures driven by the Dzyaloshinskii-Moriya interaction. *Phys. Rev. B* **89**, 224408, (2014)

(2) Felipe Garcia Sanchez, Pablo Borys, Rémy Soucaille, Jean-Paul Adam, Robert Stamps, Joo-Von Kim. Narrow Magnonic Waveguides Based on Domain Walls. *Phys. Rev. Lett.*, **114** 247206, (2015)

(3) Pablo Borys, Felipe Garcia Sanchez, Joo-Von Kim, Robert Stamps. Spin Wave Eigenmodes of Dzyaloshinskii Domain walls. *Advanced Electronic Materials.* Accepted. In production. (2015)

Physical parameters used in this thesis

Parameters correspond to typical
values found in the perpendicular material
Pt(3 nm)/Co(0.6 nm)/AlO_x(2 nm) [1, 2].

Saturation magnetisation	M_s	=	1100×10^3 A/m
Isotropic exchange	A	=	18 pJ/m
Vacuum permeability	μ_0	=	1.26×10^{-6} N/A^{-2}
Volume dipolar anisotropy	$K_\perp$	=	17×10^3 J/m^3
Effective uniaxial anisotropy	K_0	=	1.3×10^6 J/m^3
Gyromagnetic ratio	γ	=	1.76×10^{11} rad A m/N s

For Odarka and Veronica

Chapter 1

Introduction

The research field of spintronics focuses on taking advantage of the extra degree of freedom given by the spin in electron currents carrying information. The discovery of Giant magneto resistance by Albert Fert and Peter Grünberg was recognised with the Nobel prize in 2007 and is based on this premise [3, 4]. Spintronics has the disadvantage of relying on the movement of electrons for the transport and processing of data and hence with an inherent generation of Joule heating. An alternative mechanism for transporting information in the spin variable has been studied for over 80 years.

Spin waves and their particle-like counterpart, magnons, are the low-lying energy states of spin systems coupled by exchange interactions and were first predicted by Bloch in 1929 [5–8]. Not only do they present a wide variety of linear and non-linear properties which makes them interesting for fundamental research but also they are in the GHz region of the frequency spectrum which is appropriate for telecommunications. New technologies that allow the fabrication of devices in the nano-scale together with new physical phenomena discovered as spin pumping [9], spin transfer torque [10], and spin Hall effect [11, 12] have made the study of spin waves reach a peak recently. The name *magnonics* was coined to refer to the transport and processing of data by spin waves [13–16]. The main advantage of magnonics resides in the fact that the transport and processing of information occurs without any real particle moving, as depicted in figure (1.1).

There are several important challenges to overcome before magnonics or the combination magnonics-spintronics can represent an option for conventional electronics in the figure of semiconductor technologies. Issues related with further developments in materials science include decreasing large spin wave damping, miniaturisation of the devices [17],

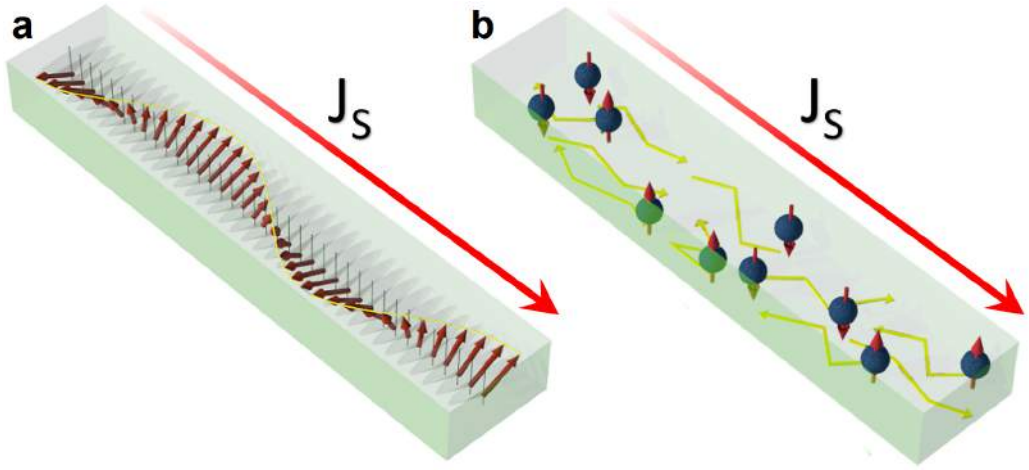

FIGURE 1.1: Sketch of the difference between spintronics and magnonics. The red arrows indicate the spin current. In (a), spin waves induce the spin current, while in (b) moving electrons are responsible for the spin current.

and fabrication of artificial magnonic crystals [18], the magnetic analogue of photonic crystals [19–21]. Magnon manipulation is another desirable feature in the field of magnonics. In all of these challenges the Dzyaloshinskii-Moriya interaction (DMI) can play an important role.

The DMI arises in low-symmetry materials with a strong spin orbit coupling and is the antisymmetric form of the exchange interaction. Dzyaloshinskii in 1958, based entirely on symmetry considerations, first used this chiral interaction to explain weak ferromagnetism in antiferromagnets [22]. A few years later Moriya included spin orbit coupling and exchange interactions in the electronic Hamiltonian and treated them as a perturbation. He calculated the second order energy terms for the perturbation to get the same result [23, 24] as Dzyaloshinskii. In some non-centrosymmetric magnetic crystals the DMI is responsible for the formation of heliciodal and skyrmionic structures which have been a centre of attention lately [25, 26]. Skyrmions in particular have unique properties such as propagation under spin-polarized currents [27] with a high tolerance to material defects as they are topologically protected [28, 29] which makes them suitable structures for information storage and processing. An induced, interface form of the DMI can appear because of inversion symmetry breaking at the surface between magnetic films and non-magnetic substrates made out of heavy atoms that provide the spin orbit coupling regardless of the crystal symmetry of the component materials [30]. In bulk materials the effect is negligible but can be significant for thin films. Experiments have shown that this induced form of the DMI leads to chiral spin structures in manganese monolayers on top tungsten [31] and skyrmion lattices in iron monolayers on iridium[32].

For a Pt/Co system which has a perpendicular magnetic anisotropy and is relevant for storage applications, a three-site indirect exchange mechanism is predicted to lead to a chiral interaction. In Co this has the form of the interface DMI [33] in agreement with a phenomenological approach used for the same symmetry [25].

As spin waves are primarily exchange dominated in the nano-scale it is important to determine what is the effect of the antisymmetric form of this interaction. A common feature is non-reciprocity in the spin wave dispersion, $\omega(k) \neq \omega(-k)$, where ω is the frequency of the wave and k its wave number. Udvardi and Szunyogh in 2009 first raised the possibility that the spin wave chiral degeneracy that results from the isotropic part of the exchange could be lifted in the presence of DMI [34]. With a first principles calculation they found an asymmetric magnon dispersion for a Fe monolayer on tungsten for a certain direction of propagation that was explained by the presence of the DMI. Shortly after, a first experimental result came from Zakeri et. al., in which, by using spin-polarised electron energy loss (SPEEL) analysis on a Fe double-layer grown on tungsten, it was possible to determine a DMI driven asymmetry in the spin wave dispersion [35]. While surface spectroscopy techniques such as SPEEL allowed to quantify the DMI in these systems through asymmetry in the dispersion, they are less useful for nanostructures where measuring the DMI strength is still a challenge. Several experimental methods were proposed to this end, but in each case the determination of the DMI through its parameter D was indirect and relied on strong assumptions involving domain wall dynamics [36–38]. At the same time theoretical studies were being made to determine the effect of the DMI in the spin wave dispersion in thin films. They all concluded that non-reciprocity should be found [39–42].

It was not until this year that many experimental groups, by using Brillouin light spectroscopy (BLS), published results [43–46] where non-reciprocal dispersion phenomenon has made possible a measurement of the strength D and, in some cases, determination of its sign [47]. Also using BLS, recent studies have determined that the interface form of the DMI is inversely proportional with the thickness of the magnetic layer, a clear indication of its surface nature [48, 49]. The influence of the DMI on the field of magmonics has been intensively studied over the last few years. Nucleation and stabilisation of magnetic skyrmions in thin films [29], and a fast current-controlled domain wall motion [50] are important examples in this sense. Now it is time to find possible applications.

Domain walls. Homogeneously magnetised areas, or domains, spontaneously appear in a ferromagnet to minimise the internal energy of the material. Neighbouring domains are separated by transition regions, or domain walls, in which the magnetisation direction varies gradually. Control over the domain wall motion is a very desirable feature because of possible applications such as magnetic storage and logic devices. Unlike conventional hard drive disks and magnetic tapes that rely on mechanical motion, novel solid state magnetic storage devices based on domain walls such as the racetrack memory are fast and non-volatile [51]. Basic logic gates using movable domain walls have been demonstrated [52] and magnetic sensors are already being commercialised [53].

Two main approaches have been used to move a domain wall. Magnetic field-driven motion is a well studied phenomenon [54] and allows high velocities without any electrical connections. However, applying external magnetic fields parallel to the spin orientation results in the problem that the magnetic fields enlarge or shrink domains and eventually lead to their collapse [55]. The ability to move neighbouring domain walls in the same direction is also difficult [56]. Current-driven domain wall motion has been proposed based on the idea of spin transfer torque [57–59]. This mechanism arises from a torque acting on the local spins as a result of an applied electric current as a consequence of angular momentum transfer from the conducting electron spins to the localised spins in the domain wall [60–62].

Recently, experimental results have shown that in ultra thin films the appearance of two spin-orbit induced effects makes a domain wall move at high speeds under the influence of an electrical current [63, 64]. The DMI stabilises a Néel-type domain wall with a given handedness [1, 65, 66]. Then, the spin Hall [11, 12] effect induces a flow of spins or spin current that transfers a torque to the wall and moves it. The origin of the spin Hall effect is the spin orbit interaction, which leads to the coupling of spin and charge currents. The spin Hall effect finds an analogy in the classical Hall effect [67] in which the Lorentz force deflects electrons so that a longitudinal electron current results in a transverse electron flow, which leads to a voltage difference at the transverse edge. Even though current driven-domain wall motion overcomes most of the problems related to field-driven motion, the use of electric current through the sample releases heat, Joule heating, decreasing the efficiency of the device.

The role of spin waves in current-driven domain wall motion has been shown to be important. Spin waves act as a thermal bath with which energy can be exchanged with the domain wall. It has been shown that power is diverted from the domain wall motion through the amplification of some thermal spin waves [54]. Several studies

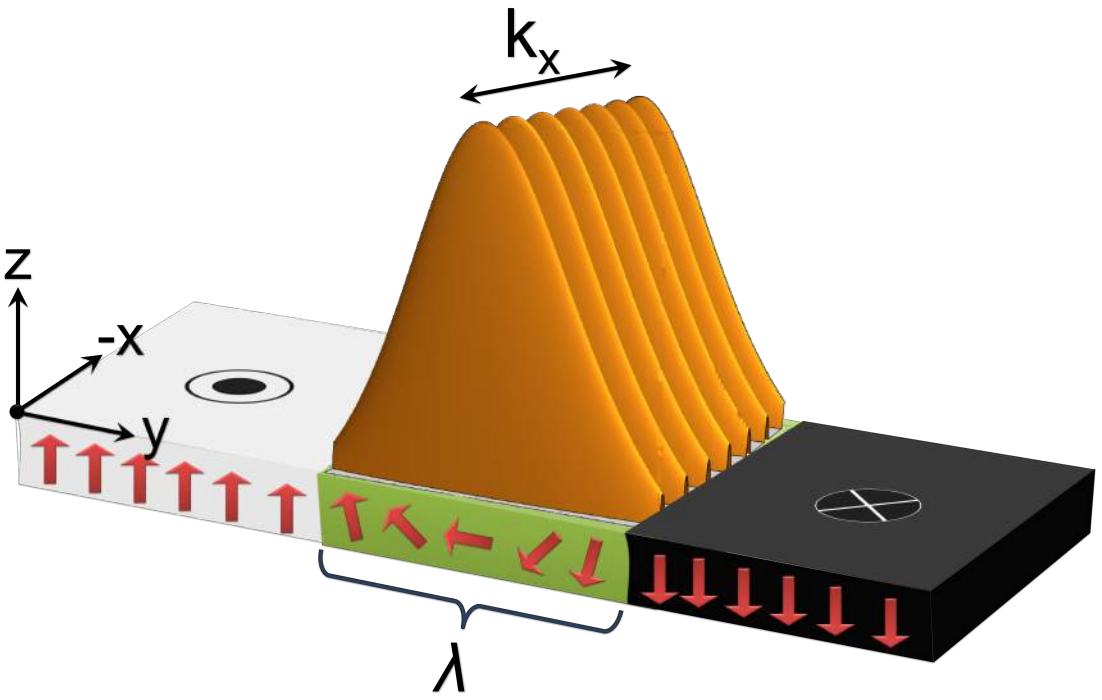

FIGURE 1.2: Mode localised to the centre of a Néel type domain wall (green layer) with a width λ. The localised wall excitation is represented by the gold waves that moves as a plane wave in the x direction.

have focused their attention to theoretically understand the physical ideas behind the interplay between the thermally originated spin waves in a wall and the current-induced domain wall motion [68–74]. A starting point to understand spin waves in domain walls are the so called Winter modes, which are the spin waves allowed in a domain wall.

Winter first calculated the spin waves modes in a Bloch domain wall to study the properties of nuclear magnetic resonances in 1961 [75]. He solved the equations of motion for exchange coupled spins using a Bloch-type domain wall profile as the static state and found that the spin wave spectrum is divided in two branches. One is a localised wall excitation that does not exist outside the wall. In the direction perpendicular to the plane of the wall, there is a bound state with zero energy. This results from the fact that there is no energy change associated with a smooth, global,rigid rotation of spins from the up to the down magnetisation state. This also indicates that the domain wall is a metastable configuration [69, 76]. In figure (1.2), we depict the wall excitation (gold waves) localised to the centre of the wall (green layer) with width λ. This mode propagates, confined within the domain wall width, in the x direction (see figure(1.2)).

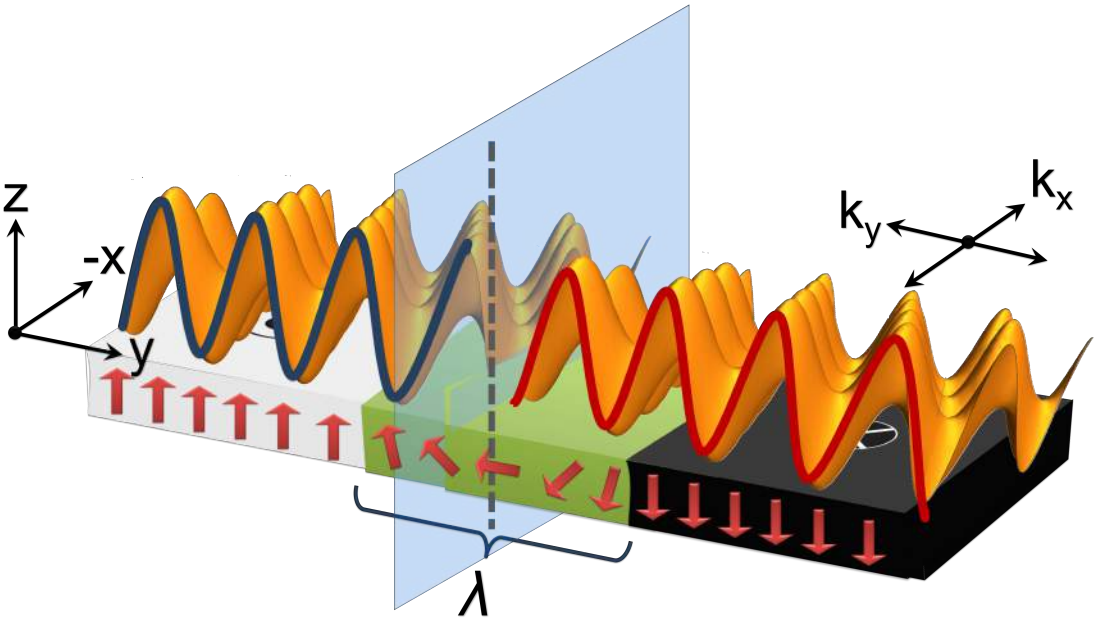

FIGURE 1.3: Travelling modes (gold waves) propagating in the film plane. The semi-transparent blue plane indicates the domain wall plane. Propagation parallel to the wall plane is the same as for plane waves, while propagation perpendicular to the plane is distorted because of the domain wall as compared to plane waves. Spin waves propagating perpendicular to the wall plane are not reflected by the domain wall and only acquire a phase shift indicated by the red and blue lines on top of the spin waves.

Translational invariance of the static magnetisation is assumed in the x direction. This mode has a quadratic, gap-less dispersion.

The other branch corresponds to travelling modes with a plane-wave character far from the wall but distorted in the vicinity of the wall. This branch has a quadratic dispersion in both directions of propagation with a finite energy due to the magneto-crystalline interaction at wave vector $\mathbf{k} = 0$ similar to the spin wave spectrum in a uniform ferromagnet [77].

An interesting feature of the travelling modes is that they are not reflected by the domain wall and only acquire a phase shift when propagating through it. In figure (1.3) we depict the travelling spin waves (gold waves) propagating in the film with wave vectors k_x and k_y. We indicate the phase shift with the blue and red lines on top of the spin waves. This reflectionless phenomenon has been studied in the field of optics [78], acoustics and quantum mechanics and is basically related to a specific symmetry of the potential[79–82].

It has been shown within the Wentzel–Kramers–Brillouin (WKB) approximation that, in addition to being completely transmitted, the travelling spin waves acquire a phase shift after crossing a domain wall [83]. By considering two different paths in which spin waves propagate and a domain wall in only one of the paths it has been shown by micromagnetic simulations that complete transmission, and phase shift can be used to create a device where logic operations can be realised because of spin wave interference [84].

Lately, studies have proposed an all magnonic-driven domain wall motion [85–87]. Magnons, in a similar way as phonons, can be assigned a momentum, $\hbar k$, usually called the crystal momentum or quasi-momentum. While this is not a physical momentum, it interacts with particles such as other magnons, photons, and phonons. In particular, it is known that domain walls behave as a particle-like object with inertial mass. The appearance of mass is phenomenologically explained by dynamical generation of the demagnetising field which causes the magnetisation to be tilted out of the plane of the static wall [88, 89]. In this sense, magnons can transfer momentum when they are reflected by the domain wall and move it. While spin wave reflection is not achievable by only considering the effective potential associated with a domain wall, some mechanisms such as the dipole interaction can in fact lead to spin wave reflection [90]. Damping plays an important part in linear momentum transfer-domain wall motion through a damping torque. Without damping linear momentum transfer results only in a rotation of the plane of the wall. Magnons also carry an angular momentum $\pm\hbar$, where the sign depends on the direction of the magnetisation. When magnons cross from one domain to another their angular momentum changes by $2\hbar$. In order for the total angular momentum of the system to be conserved the domain wall absorbs angular momentum from the magnons and moves. The domain wall moves in different directions depending on the underlying physical mechanism. Recently, it has been shown for materials uniformly magnetised in the plane of the film that the DMI enhances the linear momentum transfer increasing the wall velocity [91].

The domain wall width is determined by a competition between the isotropic exchange energy that prefers a gradual variation of the magnetisation and the magnetostatic interaction that prefers an abrupt variation from one to domain to another. For materials where the magnetisation lies in the plane of the film, normally called soft materials such as permalloy, the domain wall width is in the hundreds of nano-meters while in perpendicularly magnetised or hard materials it can be of only a few nano-meters. The perpendicular magnetic anisotropy in hard materials is an essential property for ultra

high density magneto-optical recording medium [92, 93] and hence these materials are the main interest of this work.

It is the intention of this work to propose novel ways for spin wave manipulation under the influence of the DMI in a specific spin texture, namely, a domain wall. In particular, we propose a domain wall magnonic wave guide based on the theoretical results found in Chapter 3 in which the spin wave dispersion is calculated under the influence of the DMI. We propose in Chapter 4 a periodic array of domain walls stabilised by the DMI that has similar features to the ones found in a magnonic crystal and that may find applications as a tunable device. Finally, based on symmetry considerations, we analyse the conservation of total angular momentum in thin films with the DMI in Chapter 5. We find that angular momentum transfer from spin waves to the domain wall leads to wall motion. The general outline of the thesis is:

In Chapter 2 the DMI is formally defined, the interface form is deduced, and the effect it has on the static configuration of domain walls is shown. We find that the stable configuration is a Néel type wall due to the competition between the dipole interaction in the centre of the wall and the DMI. These walls have been recently called Dzyaloshinskii domain walls.

In Chapter 3 we calculate the dispersion of spin waves in a Dzyaloshinskii domain wall. Calculations were made by treating the DMI as a perturbation in the magnetic energy of the system. We consider the two possible branches of the domain wall spin waves. For the localised modes we find that propagation parallel to the plane of the wall leads to a non-reciprocal dispersion. We investigate how the domain wall acting as a confining potential can be used as a channel for spin wave propagation. Furthermore, based on our theoretical work, micromagnetic simulations made by our colleagues at the University of Paris-Sud show that domain walls can work as magnonic wave guides in curved geometries.

We, then, address the effect of the DMI on the travelling modes. While for propagation parallel to the plane of the wall the spin wave dispersion is non-reciprocal as for the localised modes, for propagation perpendicular to the plane of the wall the energy degeneracy is lifted due to the DMI. This gives a hint that spin waves are reflected by the wall.

In Chapter 4 we investigate in detail the spin wave reflection and propose a model that can work as a field-tunable frequency filter. Spin waves propagating perpendicular to the plane of the wall are reflected because of an extra chiral term in the effective

potential that describes the wall that arises because of the DMI. We propose a periodic array of domain walls stabilised by the DMI and calculate the band structure. We find that, because of the reflection, our proposed model resembles a magnonic crystal in which frequency gaps emerge in the band structure. We briefly discuss the implications of spin wave reflection to domain wall motion.

In Chapter 5, we apply symmetry arguments to the magnetic Lagrangian and find the conserved physical quantities in a ferromagnetic film perpendicularly magnetised and under the influence of the DMI. We find the continuity equations for the energy, linear momentum and angular momentum. The conservation law of the total angular momentum requires angular momentum transfer from an orbital part to the spin part described by the magnetic moments within the continuum approximation. We analyse the consequences of the angular momentum transfer to domain wall motion.

Chapter 2

Dzyaloshinskii domain walls

In this chapter the DMI is formally introduced and its effect on a domain wall is discussed. Domain walls are regions in a magnetic material where the magnetic moment varies rapidly as a function of position. The walls form boundaries between regions of zero variation called domains. Bloch first studied theoretically these structures [94] followed by Landau and Lifshitz [95], and Néel [96]. Within a continuum approximation the material is assumed as a magnetic continuum characterised by a spontaneous magnetisation M_s, exchange stiffness A, and effective uniaxial anisotropy K_o and given a magnetisation distribution $\mathbf{M}(\mathbf{r})$. Energies arise from each of these parameters: demagnetising energy, isotropic exchange and anisotropy, respectively. It is the competition between these energies that determine the static equilibrium structure of a domain wall.

An additional energy term in low symmetry materials, the DMI, described by a parameter D modifies the static configuration of a domain wall favouring a Néel type wall recently named a Dzyaloshonskii domain wall.

2.1 Dzyaloshinskii-Moriya Interaction

The antisymmetric form of the exchange interaction can be written microscopically as,

$$\epsilon_D = \sum_{i,j} \mathbf{D}_{i,j} \cdot (\mathbf{S}_i \times \mathbf{S}_j) \,, \tag{2.1}$$

where D_{ij} is the Dzyaloshinskii vector and $\mathbf{S}_{i,j}$ are the spins on the atomic sites i, j. Equation (2.1) is called the DMI and manifests in different forms. It has been

used to explain weak ferromagnetism where there is a net magnetic moment in an antiferromagnet because of a misalignment of the sublattices with respect to the totally antiparallel configuration. Another manifestation of this interaction occurs in non-centrosymmetric magnetic crystals where it competes with the isotropic exchange and anisotropies to create different spin textures as helical and skyrmionic structure.

Even in centrosymmetric magnetic crystals it is possible to have a finite DMI if there is an external mechanism to break the symmetry at the interfaces. For bulk materials the strength of the DMI is supposed to be very weak but for artificial structures such as ferromagnetic thin films, multilayers, and nanowires the situation is different. The lack of inversion symmetry at the interface between a thin ferromagnetic film and a non-magnetic substrate with strong spin-orbit coupling results in an important DMI contribution to the energy of the system.

In the continuum approximation the DMI is expressed as a combination of invariants that are linear with respect to the first spatial derivatives of the magnetisation,

$$D\, L_{ij}^{k} = D\left(m_i \frac{\partial m_j}{\partial x_k} - m_j \frac{\partial m_i}{\partial x_k}\right), \tag{2.2}$$

where D is the Dzyaloshinskii constant related to the strength of the interaction and i, j, k are the Cartesian coordinates x, y, z. The L_{ij}^{k} are known in mathematical physics as the Lifshitz invariants and were first studied in the theory of phase transitions [97]. The exact form of these invariants is determined by symmetry considerations and given by the direction of the Dzyaloshinskii vector $\mathbf{D}_{i,j}$. For a thin film geometry where the sample is isotropic in the plane XY and the symmetry breaking is in the z direction there are two distinct forms for the Lifshitz invariants. The bulk form of DMI occurs when $\mathbf{D}_{i,j}$ points along the displacement vector between spins $\mathbf{S}_i$ and $\mathbf{S}_j$, in this case

$$\epsilon_B = D(L_{zx}^{y} + L_{zy}^{x}). \tag{2.3}$$

However, it has been argued that the bulk form tends to cancel out due to the impurities in the film arising from the fabrication processes [41]. An interface form occurs when $\mathbf{D}_{i,j}$ points perpendicular to the displacement vector between the two neighbouring spins, $\mathbf{S}_1$ and $\mathbf{S}_2$ as shown in figure 2.1. The spin orbit interaction arises from the coupling of the heavy atoms, (blue spheres), and the localised spins, (purple arrows), of the ferromagnetic material atoms, (red spheres). In this case the form of the interaction

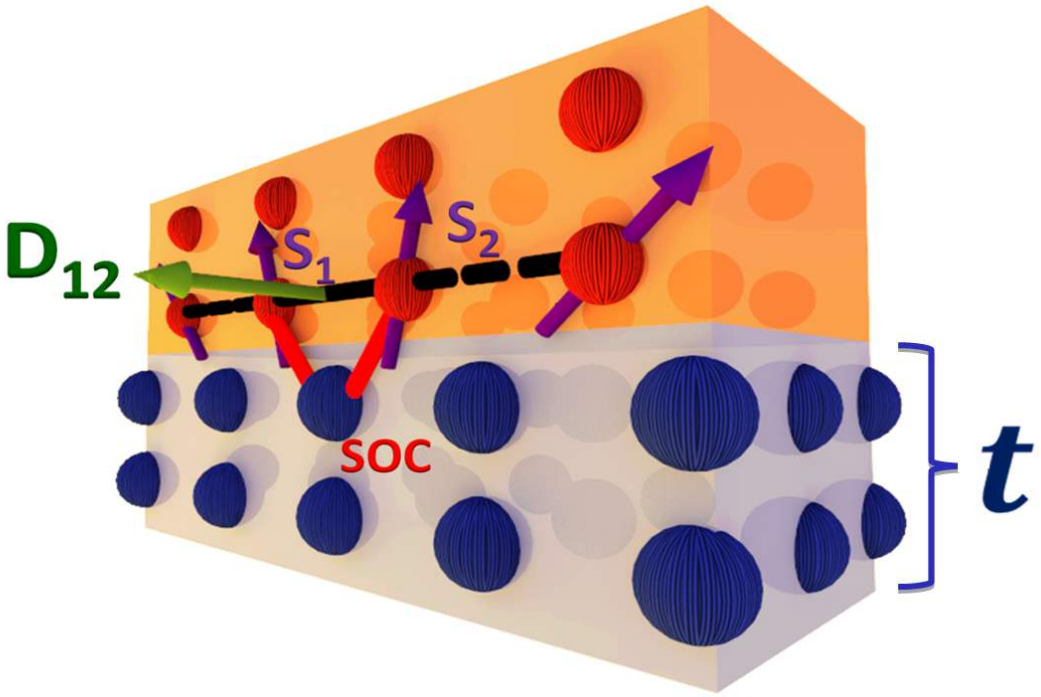

FIGURE 2.1: Visual description of the interface form DMI. The Dzyaloshinskii vector points perpendicular to the displacement vector between spins $\mathbf{S}_i$ and $\mathbf{S}_j$. t is the thickness of the substrate and the red lines represent the spin orbit coupling (SOC) between the heavy atoms of the substrate and the localised spins in the ferromagnet.

in the continuum approximation is

$$\epsilon_I = D(L^x_{zx} + L^y_{zy}), \tag{2.4}$$

This is the form considered throughout this work as it is expected to be the one most relevant for magnonic applications.

2.2 Dzyloshinskii domain walls

In this section we show how the DMI affects the stable configuration of a domain wall. In perpendicular materials two kinds of wall may arise as the stable configuration and are presented in figure (2.2). In figure (2.2(a)) a Bloch-type profile is presented. The magnetic moments rotate through the wall in a screw-like rotation in a plane perpendicular to the y axis. These are the most common type of walls because they minimise the demagnetising energy by avoiding surface charges as is depicted in (2.2(b)). Symmetry permits two possible senses of screw-rotation, right or left handed corresponding to $\phi = 0$ and π, respectively, both with the same energy. We show

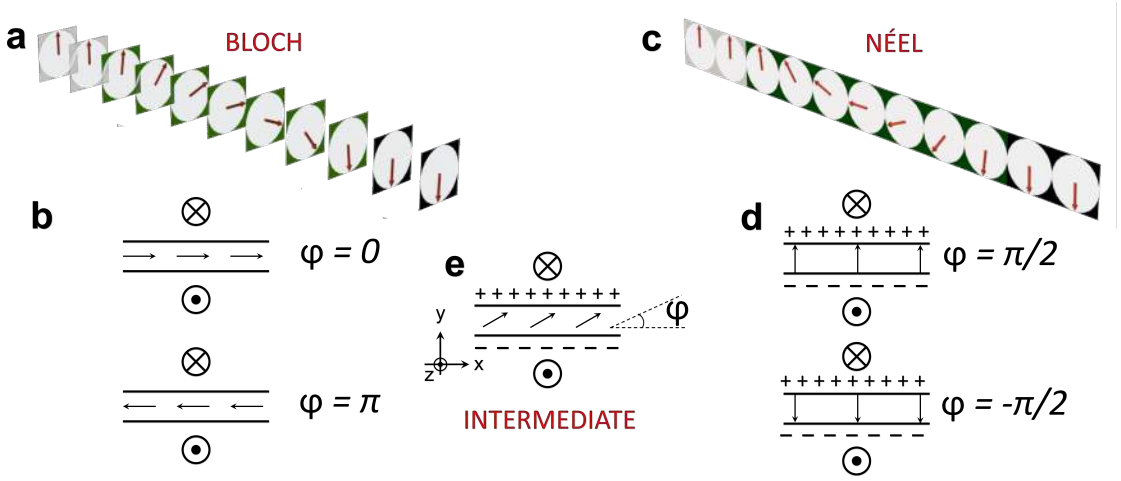

FIGURE 2.2: Bloch and Néel type walls. The Bloch profile is presented in (a) where magnetic moments rotate from one domain to the other in the plane perpendicular to the y axis. In (c) the Néel configuration is shown where the magnetic moments rotate perpendicular to the wall plane. (b), (d) and (e) show the structures as seen from the $+z$ direction, accumulation of magnetic charge is minimum in a Bloch configuration and maximum in for Néel walls.

below that in the absence of the DMI this indeed is the wall profile. By contrast, the magnetostatic energy is maximum for $\phi = \pm\pi/2$, (see figure (2.2(d))). In this case the magnetic moments rotate in a plane perpendicular to the wall plane as shown in (2.2(c)). These are called Néel walls and may become favoured if we include an external in-plane magnetic field or additional anisotropy terms. In this section, we show that the inclusion of the DMI favours a smooth transition from a Bloch configuration to a Néel type wall as shown in figure (2.2(e)) by compensating the demagnetising energy in the centre of the wall. After a critical D value the stable configuration is a Néel type wall with a preferred handedness as a result of the chiral nature of the DMI.

2.2.1 Magnetic energies

A ferromagnet is characterised by a spontaneous magnetisation associated with long range magnetic ordering. Interestingly, the largest energy that gives rise to the magnetic ordering is not the result of the dipolar interaction between the elementary magnetic moments. To see this we compare the thermal energy $k_B T_c$, where k_B is Boltzmann constant and T_c, Curie Temperature, is the critical temperature at which magnetic ordering is lost with the energy of magnetic interaction between two magnetic dipoles. The magnetic interaction is of the order $(\mu_0/M_s)\mu_B^2/a^3 \sim 10^{-18}$ J, where μ_B is Bohr's magneton, a is the lattice parameter, μ_0 is the vacuum permeability, and M_s the

magnetisation. The thermal energy for typical Curie temperatures in ferromagnets is in the range $(10^{-15}, 10^{-13})$ J. Therefore a different interaction is responsible for magnetic ordering.

The electrostatic, Coulomb interaction, $(1/4\pi\epsilon_0)e_0^2/a$, where e_0 is the electron charge, and ϵ_0 the vacuum permittivity, is of the order of 10^{-11} J and then, even a fraction of it would be enough to maintain the magnetic ordering near T_c. From quantum mechanics, we know that the form of a wave function and, consequently, the expectation value of the Coulomb interaction depends on the mutual orientation of their spins. The part of the Coulomb energy that depends on this orientation is called the exchange energy and is the cause of magnetic ordering. In ferromagnets, this energy is minimised at parallel orientation of all electronic moments of the outer shells. Frenkel and Heisenberg proposed this mechanism to explain ferromagnetism in 1928 [98].

Dirac showed [99] that the Hamiltonian of the isotropic part of the exchange interaction is given by $-J\,\mathbf{S}_1 \cdot \mathbf{S}_2$, where $\mathbf{S}_{1,2}$ are the interacting, spins of two neighbour electrons. J is the exchange integral, it decreases rapidly as a function of the relative distance between to particles and hence the short range nature of the interaction.

It is useful to find an expression for the isotropic exchange interaction in a continuum approximation in which the discrete nature of the lattice is ignored. The total contribution of the exchange interaction in its atomistic form is

$$E_A = -J \sum_{i,j} \mathbf{S}_i \cdot \mathbf{S}_j \tag{2.5}$$

where summation runs only over nearest neighbours. When spins are assumed as classical vectors the inner product inside the sum in equation (2.5) depends on the angle ϕ_{ij} between them. Assuming a $\phi_{ij} << 1$, $\cos\phi_{ij} \simeq 1 - \phi_{ij}^2/2$ and we obtain

$$E_A = -JS^2 \sum_{i,j} \cos\phi_{ij} = \text{constant} + \frac{JS^2}{2} \sum_{i,j} \phi_{ij}^2. \tag{2.6}$$

It is possible to neglect the constant term as it just refers to the energy of the fully aligned system. We define the unit vector $\mathbf{m} = \mathbf{M}/M_s$, where $\mathbf{M}$ is the magnetisation and M_s is the saturation magnetisation. The unit vector $\mathbf{m}$ correspond to the direction of the spin at lattice point r_{ij}. As seen in figure (2.3), the small angle ϕ_{ij} can be

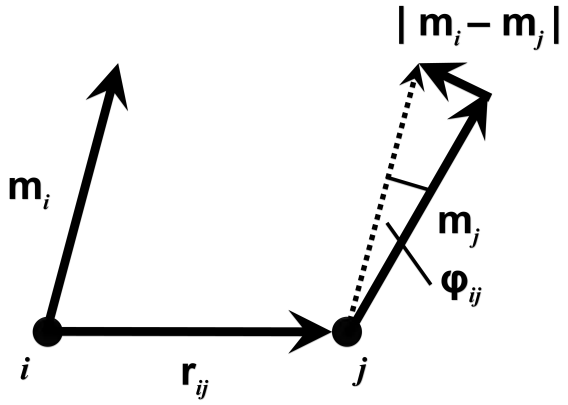

FIGURE 2.3: The magnetic moments are represented by the reduced moments $\mathbf{m}_i$ and $\mathbf{m}_j$ at sites i and j separated by a vector $\mathbf{r}_{ij}$. The angle between the moments is ϕ_{ij}.

approximated as $|\theta_{ij}| \simeq |\mathbf{m}_i - \mathbf{m}_i| \simeq |(\mathbf{r}_{ij} \cdot \nabla)\mathbf{m}|$, so that the energy can be written as

$$E_A = JS^2 \sum_{i,j} [(\mathbf{r}_{ij} \cdot \nabla)\mathbf{m}]^2. \tag{2.7}$$

In the continuum limit we ignore the discrete nature of the lattice and the sum is transformed into an integral

$$E_A = \int dV\, A(\nabla \mathbf{m})^2, \tag{2.8}$$

where $A = 2JS^2 n/a$ is called the exchange stiffness. n is the number of sites in the unit cell and a is the lattice parameter. For a simple cubic-type lattice $n = 1$ and $A = 2JS^2/a$.

The isotropic exchange energy, equation (2.8) is degenerate with respect to spatial coordinates. Real magnetic materials, however, are not isotropic. There is a preferred space direction for which, in the absence of an external field, the material is magnetised. There are several types of anisotropy terms that describe this phenomenon, the most common is the magnetocrystalline anisotropy, described by the parameter K_u. This anisotropy is caused by spin-orbit effects in which the electron orbits are linked to the crystallographic structure. The interaction between the electron orbits and their spin result in a preferred alignment along a well-defined crystallographic axis. The direction of the magnetisation is determined only by anisotropic energies. It is convenient to define the quantisation axis z as the direction for which the anisotropy energy is minimum. In

the continuum approximation a uniaxial anisotropy is given by

$$\epsilon_K = -K_u\, m_z^2. \tag{2.9}$$

Another energy term arises from the magnetic field, $\mathbf{H_d}$, generated by the magnetic body itself. Each magnetic moment in a ferromagnetic sample represents a magnetic dipole and therefore the sum of all of the moments contribute to the total magnetic field in the sample. In the magnetostatic limit, Maxwell's equations state that $\nabla \cdot \mathbf{H_d} = -\nabla \cdot \mathbf{M}$. The total energy due to this so called stray or demagnetising field is

$$E_d = -\frac{\mu_0}{2} \int dV\ \mathbf{M} \cdot \mathbf{H_d}, \tag{2.10}$$

where both $\mathbf{M}$ and $\mathbf{H_d}$ depend on space and time and has a long range interaction nature. This energy is responsible for the formation of domains. In general the integral, equation (2.10), can be notoriously complicated to calculate and cause much difficulty in micromagnetic theory. However, for our purposes the demagnetising energy can be treated with a local approximation that results in a shape anisotropy. To exemplify the procedure consider an infinite film in the XY plane such that the magnetisation only depends on the coordinate z. In this situation, the magnetostatic problem has a simple analytical solution for the stray field, H_d [100],

$$H_d^z = -M_z = -M_s m_z, \qquad E_d = \int dV\ \frac{\mu_0 M_s^2}{2} m_z^2, \tag{2.11}$$

so that now the demagnetising energy is effectively local.

Assuming uniform magnetisation everywhere, the demagnetising energy is described by an effective uniaxial anisotropy with the parameter $K_0 = K_u - \mu_0 M_s^2/2$. When $K_o > 0$ it defines an easy axis of magnetisation and corresponds to perpendicularly magnetised films and when $K_0 < 0$ it defines an easy plane which corresponds to in-plane magnetised films. Throughout this work we consider $K_0 > 0$.

For domain walls in perpendicular materials we sometimes make a local approximation to the demagnetising energy within a wall and include the term

$$E_{K_\perp} = \int dV\ K_\perp m_y^2 \tag{2.12}$$

where $K_\perp = N_y \mu_0 M_s^2/2$ is determined by the demagnetising coefficient $N_y \simeq d/(d+\pi\lambda)$ related with the shape of the sample through the thickness of the film d and the domain wall width λ when the domain wall profile depends on the y coordinate [101].

Extra energy terms such as surface anisotropies are not considered in this thesis.

2.2.2 Bloch domain wall

The stable configuration of a domain wall corresponds to the structure that minimises the energy. To calculate the profile of such a configuration we consider the magnetization orientation, represented by the unit vector $\mathbf{m}$, and parametrized by spherical coordinates as $\mathbf{m} = (\sin\theta\cos\phi, \sin\theta\sin\phi, \cos\theta)$, where $\theta = \theta(\mathbf{r}, t)$ and $\phi = \phi(\mathbf{r}, t)$ and minimise the energy.

The total magnetic energy of this system is given by the functional $E[\theta(\mathbf{r}), \phi(\mathbf{r})]$,

$$E = \int dV \ \left[A\left((\nabla\theta)^2 + \sin^2\theta\,(\nabla\phi)^2\right) + K_\perp \sin^2\theta \sin^2\phi - K_o\cos^2\theta\right]. \tag{2.13}$$

In general, the stable profile is determined by the solution to the Euler-Lagrange equations associated with the functional in equation (2.13), which are obtained by setting the first-order functional derivatives to zero. In this case, we consider two domains uniformly magnetised along the $\pm z$ direction connected by a domain wall that varies in the y direction as shown in figure (3.1). Variations in the x direction are neglected and we assume that $\phi_0(y)$ is a constant ϕ_0. In this case the Euler-Lagrange equations are,

$$\begin{gathered}(K_o + K_\perp \sin^2\phi_0)\sin\theta_0(y)\cos\theta_0(y) = A\frac{d^2\theta_0}{dy^2} \\ 2K_\perp \sin\phi_0\ \cos\phi_0\ \sin^2\theta_0(y) = 0.\end{gathered} \tag{2.14}$$

The second equation has solutions for $\phi_0 = (0, \pi/2)$. The case for $\phi_0 = 0$ corresponds to a Bloch-type wall while $\phi_0 = \pi/2$ is a Néel wall. Once each case is substituted in the first equation of (2.14) they yield

$$\sin 2\,\theta_0 - 2\lambda_{B,N}^2 \frac{d^2\theta_0}{dy^2} = 0, \tag{2.15}$$

with $\lambda_B = \sqrt{\frac{A}{K_o}}$ and $\lambda_N = \sqrt{\frac{A}{K_o + K_\perp}}$ the domain wall widths for Bloch and Néel types respectively. The term $K_\perp$ reduces the domain wall width of a Néel type wall as compared

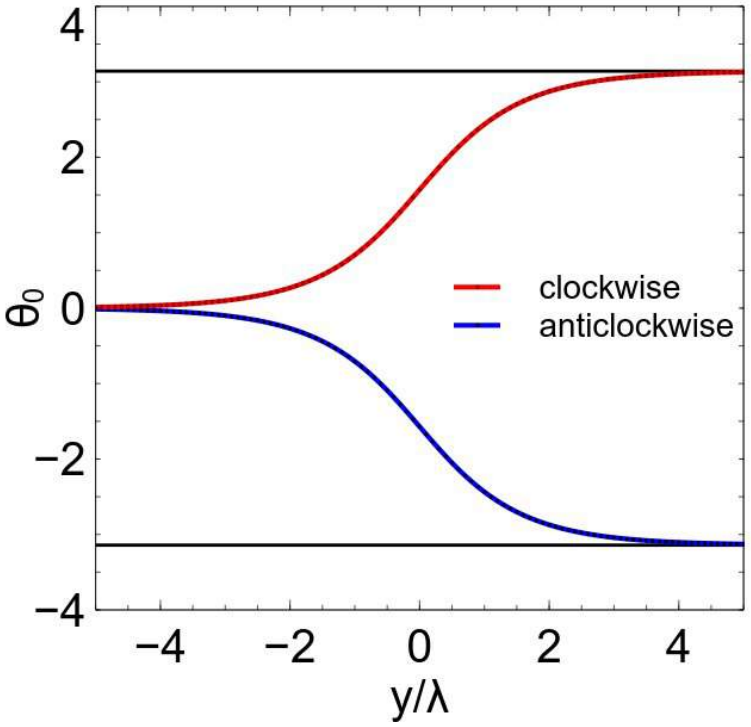

FIGURE 2.4: Two possible senses of rotation given by equation (2.16). The red curve indicates a clockwise rotation from $\theta_0 = 0$ to $\theta_0 = \pi$. The blue curve shows the anti-clockwise rotation.

to a Bloch wall. For the parameters used throughout this work $\lambda_N = (0.984)\lambda_B$, less than a 2% difference. The solution of equation (2.15) gives the domain wall profile, (see Appendix A for details),

$$\theta_0(y) = \pm 2 \arctan\left[\exp\left(\frac{y - Y_0}{\lambda_{B,N}}\right)\right], \tag{2.16}$$

where Y_0 is the (arbitrary) centre of the wall. The two signs represent the two possible senses of rotation of the wall and are presented in figure 2.4, the positive sign indicates a clockwise rotation and the minus sign an anti-clockwise one. The domain wall energy is obtained by inserting $\theta_0(y)$ and ϕ_0 into the magnetic energy functional (2.13), upon integration,

$$\begin{aligned} \sigma_B &= 4\, K_o\, \lambda_B = 4\, \sqrt{K_o\, A} \\ \sigma_N &= 4\, (K_o + K_\perp)\, \lambda_N = 4\, \sqrt{(K_o + K_\perp)\, A}, \end{aligned} \tag{2.17}$$

from where it is clear that a Bloch type wall is preferred energetically, $\sigma_B < \sigma_N$. The wall energy is degenerate with respect to the sense of rotation of the wall as considering the positive or negative sign for $\theta_0(y)$ gives the same result.

2.2.3 Dzyaloshinskii domain walls

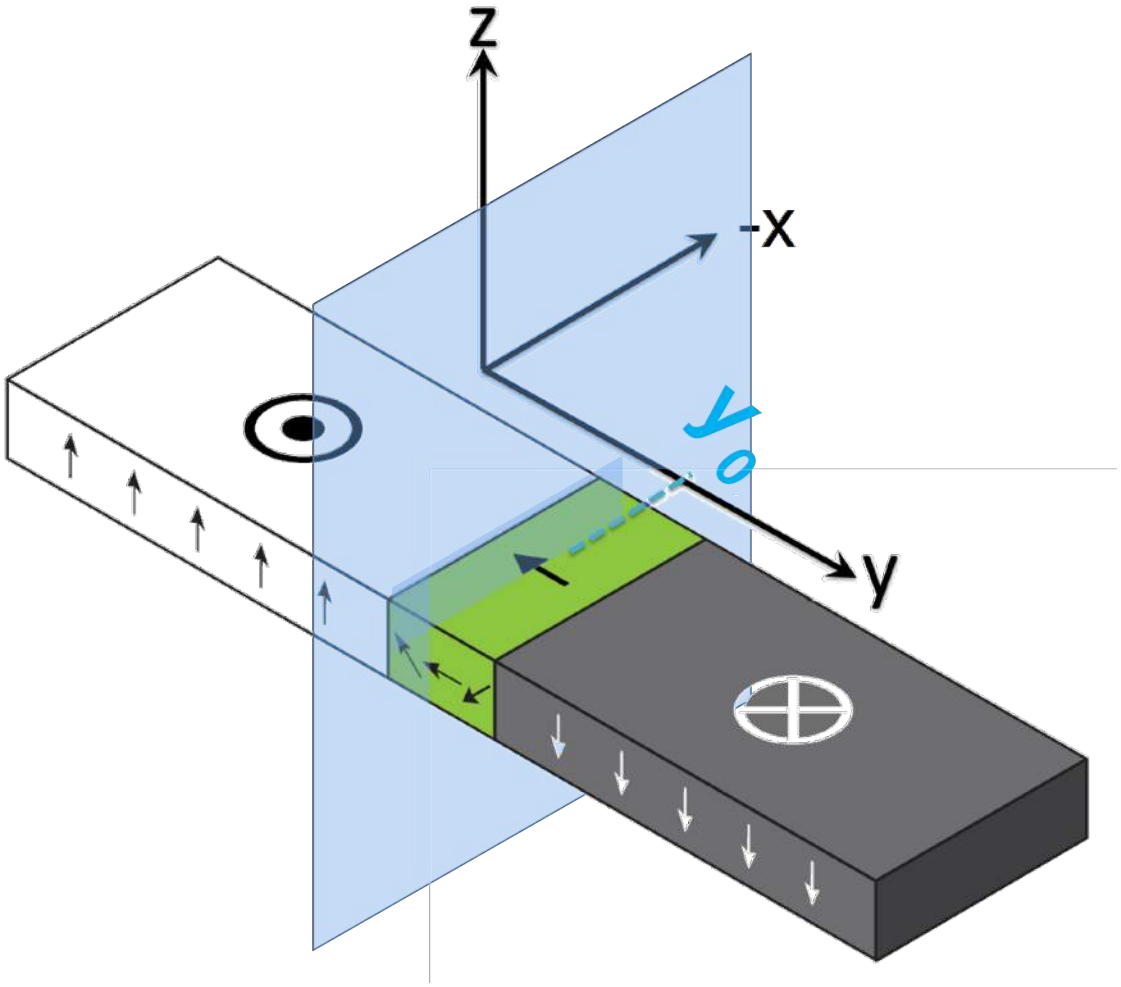

FIGURE 2.5: Geometry under consideration. Two magnetic domains whose magnetisation point in the $\pm z$ axis are connected by a left handed Néel domain wall stabilised by the DMI. Translational invariance is considered in the x direction and the domain wall centre is denoted by Y_0. The semi-transparent blue plane indicates the plane of the wall

We now consider the effect of the DMI on the static configuration. We assume that the domain wall profile is given by $\theta_0(y)$, (equation (2.16)), and let ϕ, the angle that describes the plane of the wall rotate freely. We substitute $\theta_0(y)$ and ϕ in the magnetic energy functional, (equation 2.13), adding the DMI term given in spherical coordinates by

$$E_{DMI} = \int dV\, D\left(\frac{\partial\theta}{\partial x}\cos\phi + \frac{\partial\theta}{\partial y}\sin\phi + \frac{1}{2}\sin 2\theta\left(\frac{\partial\phi}{\partial y}\cos\phi - \frac{\partial\phi}{\partial x}\sin\phi\right)\right). \quad (2.18)$$

We integrate over the volume using the relations $\cos\theta_0(y) = -\tanh(y/\lambda)$ and $\sin\theta_0(y) = -\operatorname{sech}(y/\lambda)$ to obtain the domain wall energy as a function of the ϕ angle,

$$\sigma_{DMI} = 2K_\perp\lambda\sin^2\phi \pm \pi D\sin\phi + 2(K_\perp + K_o)\lambda. \tag{2.19}$$

The stable configuration is that which minimises the energy, so we calculate

$$\frac{d\sigma_{DMI}}{d\phi} = \cos\phi(4\,K_\perp\lambda\sin\phi \pm \pi D) = 0, \tag{2.20}$$

which gives the stability conditions as a function of the D parameter,

$$\begin{aligned} \sin\phi &= +\frac{\pi D}{4K_\perp\lambda} \qquad \texttt{for} \quad \pi D < 4K_\perp\lambda \\ \phi &= \quad \frac{\pi}{2} \qquad\quad \texttt{for} \quad \pi D > 4K_\perp\lambda. \end{aligned} \tag{2.21}$$

It is necessary to take the positive sign in the first equation of (2.21), which corresponds to a counter clockwise rotation of the $\theta_0(y)$ angle, because we are only considering $0 < \phi < \pi/2$ and then $0 < \sin\phi < 1$ in this interval. A critical value $\pi D_c = 4K_\perp\lambda$ appears. When $D > D_c$ there is a Néel type wall called a Dzyaloshinskii wall, below this limit the domain wall reorients smoothly to a Bloch wall. The total energy of the wall when $D > D_c$ is

$$\sigma = 4(K_u + K_\perp)\lambda_N - \pi D = 4\sqrt{(K_o + K_\perp)A} - \pi D. \tag{2.22}$$

Note that the domain wall width λ used in the derivation of the stability conditions (2.19-2.21) does not correspond to the Bloch or Néel definitions, it corresponds to a transition domain wall width $\lambda_N < \lambda < \lambda_B$. It does not depend explicitly on D but the way it varies does depend on the angle ϕ which is related to the DMI in the interval $D < D_c$. From here on it will be assumed that D is above the critical value and that the domain width is $\lambda = \lambda_N = \sqrt{\frac{A}{(K_o+K_\perp)}}$.

The DMI lifts the degeneracy with respect to the sense of rotation as can be seen by considering the opposite sense of rotation, chirality, for $\theta_0(y)$, which results in an energy $\sigma = 4\sqrt{(K_o + K_\perp)A} + \pi D$. For a positive D parameter a left handed wall is energetically preferred.

The static configuration has been established, a left handed Néel domain wall is favoured for $D > D_c$. Thiaville et. al. [2] performed micromagnetic simulations on a similar system and obtained the same result. They explained it analytically and the procedure

followed here is based on their derivation. Also, *ab-initio* calculations [65] report a preferred wall handedness when DMI is considered. For Pt/Co(0.6 nm)/AlO, whose parameters correspond to the ones used in this thesis, this result has been proved experimentally by Tetienne et. al. [1] with magnetic microscopy based on a single nitrogen-vacancy defect in diamond. Field driven-domain wall motion is significantly affected in this configuration. Velocity and the critical field value, Walker field, above which the domain wall starts to precess depend nearly linearly in the D parameter up to very large values before the domains become unstable [2]. A given handedness for a positive or negative value of D can also enhance some features of current-induced domain wall motion. It has been shown that the Spin Hall effect due to the current flowing in the substrate can efficiently move this type of wall at zero field in opposite directions [50, 64, 102].

Chapter 3

Non-reciprocity and spin wave channelling

In this chapter the spin wave dispersion is theoretically calculated using perturbation theory in a Dzyaloshinskii domain wall. We find that the domain wall-spin waves localised to the centre of the wall exhibit a non-reciprocal dispersion [103] just as the one found in uniformly magnetised materials. However, in this case, the domain wall acts as a confining potential to these localised modes in a way that it is possible to channel the spin waves through the centre of the wall [104]. For Dzyaloshinskii walls the channelling is strongly non-reciprocal with high group velocities for this direction of propagation. We show by micromagnetic simulations that spin waves can propagate following the domain wall wave guide even in curved geometries.

The DMI requires the satisfaction of twisted boundary conditions in the magnetic film that leads to a magnetisation tilting at the edges of the film. We observe that similar to the spin wave channelling in the centre of the wall, spin waves are channelled in a non-reciprocal manner at the edges of the film. We propose that by measuring the non-reciprocity it is possible to determine the strength of the DMI.

For the travelling modes in the domain wall, we find that for propagation parallel to the plane of the wall the non-reciprocity is preserved. For propagation perpendicular to the plane of the wall we find that, unlike systems without DMI, the energy degeneracy related with the reflectionless feature of the wall is lifted. We explore this phenomenon in Chapter 4.

3.1 Spin wave equations of motion

In this section we find the spin wave equations of motion by linearising the torque equation. We separate the equation of motion in to a Schrödinger-like part, H_0, that depends on the isotropic exchange and the uniaxial anisotropy and a part, H_1, that depends on the DMI and the dipole interaction in the centre of the wall. While H_1 is treated with perturbation theory in the next section, here we present the solutions to H_0. Following the usual perturbation method, the H_0 solutions define the basis eigenfunctions to treat the perturbation.

3.1.1 Energies and torque equation

The energy densities under consideration as described in Chapter 2 are the isotropic exchange interaction, $\epsilon_A = A(\nabla \mathbf{m})^2$, the uniaxial effective anisotropy along the z axis normal to the plane of the film, $\epsilon_{K_o} = -K_o\, m_z^2$, and a term approximating the dipole interaction in the centre of the wall, $\epsilon_{K_\perp} = K_\perp\, m_y^2$. It has been shown in section (2.2.2) that these energies determine the domain wall profile and the domain wall width $\lambda = \sqrt{A/(K_o + K_\perp)}$. The interface form of the DMI, $\epsilon_{DMI} = D\,(L_{zx}^x + L_{zy}^y)$, stabilises a left handed Néel domain wall, (see section (2.2.3)) as presented in figure (3.1).

In Chapter 2 we determined the static configuration of the system. We are interested now in its dynamic behaviour. Magnetisation dynamics are based on the fundamental mechanical law that relates the time-rate of change of angular momentum to a torque $\mathbf{T}$. For a unit volume in a magnetic material the angular momentum is that of an electron spin. It differs from $M_s\,\mathbf{m}$ only by a constant $\mu_0\gamma$, where μ_0 is the vacuum permeability and γ is the gyromagnetic ratio. The basic equation of motion is then

$$-\frac{1}{\mu_0\gamma}\frac{\partial \mathbf{m}}{\partial t} = \mathbf{T} \tag{3.1}$$

The torque on the magnetic moment is written in terms of an effective field $\mathbf{H_{eff}}$ as $\mathbf{T} = \mathbf{m} \times \mathbf{H_{eff}}$. The effective field is given by the functional derivative of the total energy density, $\epsilon = \epsilon_A + \epsilon_{K_o} + \epsilon_{K_\perp} + \epsilon_{DMI}$,

$$\mathbf{H_{eff}} = \left(-\frac{1}{\mu_0 M_s}\frac{\delta \epsilon}{\delta \mathbf{m}}\right). \tag{3.2}$$

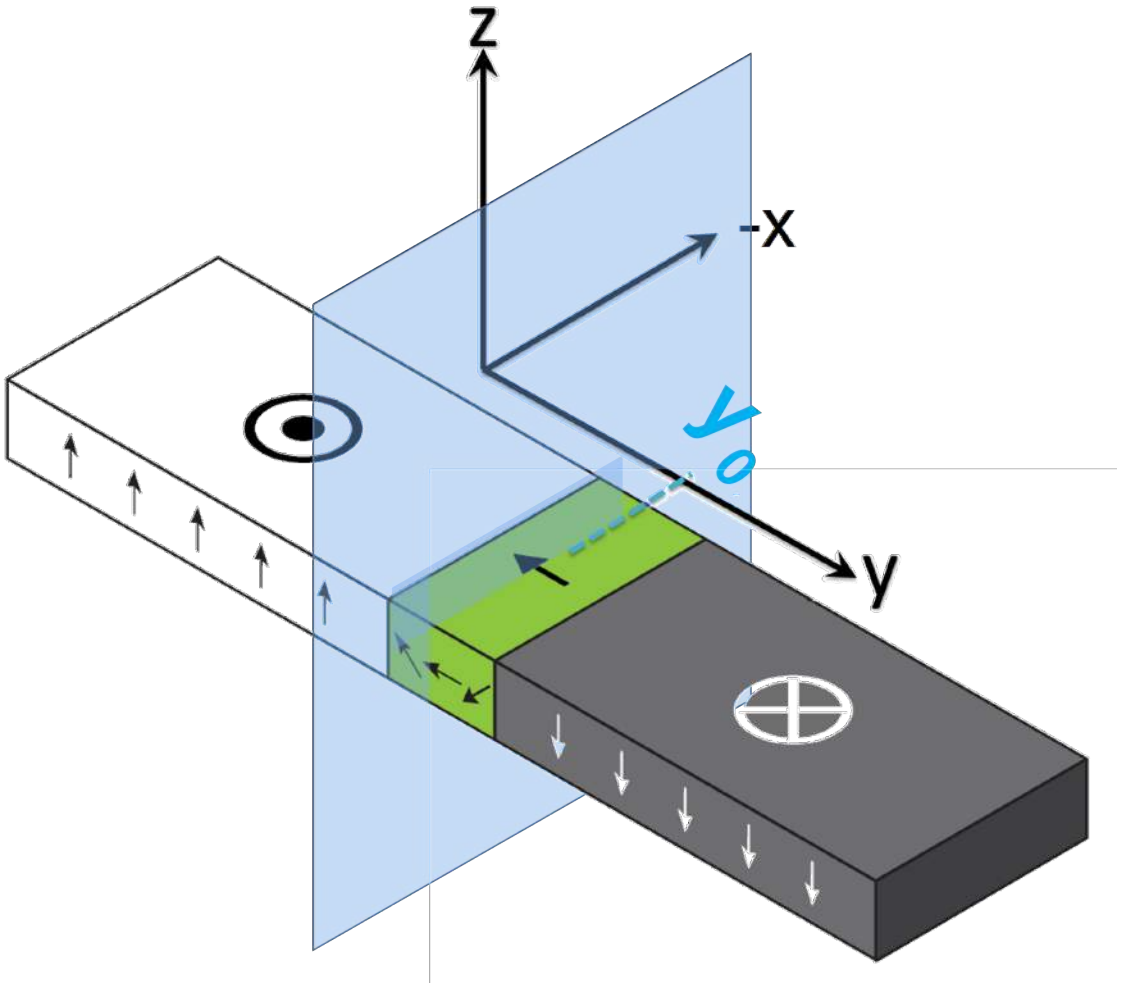

FIGURE 3.1: Geometry under consideration. Two magnetic domains whose magnetisation point in the $\pm z$ axis are connected by a left handed Néel domain wall stabilised by the DMI. Translational invariance is considered in the x direction and the domain wall centre is denoted by Y_0. The semi-transparent blue plane indicates the plane of the wall

The equation of motion of the magnetisation,

$$\frac{\partial \mathbf{m}}{\partial t} = -\gamma \mu_0 \mathbf{m} \times \left(-\frac{1}{\mu_0 M_s} \frac{\delta \epsilon}{\delta \mathbf{m}} \right), \tag{3.3}$$

is known as the Landau-Lifshitz equation without dissipation. A variational procedure provides a more formal way to derive equation (3.3). Consider the system Lagrangian defined in the laboratory frame as

$$L = \int_\Omega dV\, \mathcal{L}, \qquad \mathcal{L} = \frac{M_s}{\gamma} m_z \frac{\partial \phi}{\partial t} - \epsilon \tag{3.4}$$

where $\mathcal{L}$ is the Lagrangian density in the volume Ω and $\phi = \arctan(m_y/m_x)$ is the azimuthal angle.

We can calculate the Poisson brackets to verify that m_z and ϕ are canonical conjugates of the momentum and coordinate. First we define the commutation relations of the components of the magnetisation field using

$$\mathbf{m}(\mathbf{r}) = \hbar\gamma\mathbf{s}(\mathbf{r}), \tag{3.5}$$

where $\mathbf{s}(\mathbf{r})$ is the vector spin density. Then

$$\begin{aligned} \{m_x(\mathbf{r}), m_y(\mathbf{r})\} &= i\hbar\gamma m_z(\mathbf{r})\delta(\mathbf{r}-\mathbf{r}') \\ \{m_+(\mathbf{r}), m_-(\mathbf{r})\} &= 2\hbar\gamma m_z(\mathbf{r})\delta(\mathbf{r}-\mathbf{r}') \end{aligned} \tag{3.6}$$

where $m_\pm = m_x \pm i m_y$. From where

$$\{m_z(\mathbf{r}), \phi(\mathbf{r}')\} = -\delta(\mathbf{r}-\mathbf{r}') \tag{3.7}$$

that results from calculating the Poisson brackets for spin components in the classical limit. The Lagrangian density is written in the form $\mathcal{L} = P\dot{Q} - \mathcal{H}$ where P and Q are the generalised coordinates of the system, and $\mathcal{H}$ is the Hamiltonian. In this respect, we can describe a ferromagnet using a semi-classical approximation in terms of a classical field theory with the fields given by $\phi(\mathbf{r}, t)$ and $m_z(\mathbf{r}, t)$ [90, 105, 106].

The action is defined as,

$$S = \int_{t_1}^{t_2} dt\, L\left(q, \frac{\partial q}{\partial x_i}, x_i\right), \tag{3.8}$$

where $L = \int dV\, \mathcal{L}$, q are the generalised coordinates (ϕ, m_z), and x_i the spatial coordinates (x, y, z). Under the transformation $q \to q + \delta q$ along with the condition that the first variation vanishes results in:

$$\begin{aligned} 0 = \delta S = \int dt\, dV \left[-\frac{\partial}{\partial t}\frac{\partial \mathcal{L}}{\partial(\partial q/\partial t)} - \frac{\partial}{\partial x_i}\frac{\partial \mathcal{L}}{\partial(\partial q/\partial x_i)} + \frac{\partial \mathcal{L}}{\partial q}\right]\delta q + \\ \int dt\, dV \frac{\partial}{\partial x_i}\left(\frac{\partial \mathcal{L}}{\partial(\partial q/\partial x_i)}\delta q\right). \end{aligned} \tag{3.9}$$

The integrand of the first integral on the right hand side correspond to the Euler-Lagrange equations of the system. Equation (3.3) can be calculated from them. The integrand on the second integral is given in the form of a total divergence so it can be transformed to an integral over the surface enclosing the volume. It corresponds to the

boundary conditions,

$$\mathbf{n} \cdot \frac{\partial \mathcal{L}}{\partial(\partial q/\partial x_i)} = 0, \tag{3.10}$$

where $\mathbf{n}$ is a unit vector normal to the surface of the material and x_i are the spatial coordinates (x, y, z). These boundary conditions are used in section 3.2.1 below.

Our main interest is the dynamics of small fluctuations around the static configuration, spin waves, which are described by equations of motion in the low-energy, long-wavelength limit by linearising equation (3.3) with $\mathbf{m}(\mathbf{r}, t) = \mathbf{m}_0(\mathbf{r}) + \delta\mathbf{m}(\mathbf{r}, t)$, and $\mathbf{H_{eff}}(\mathbf{r}, t) = \mathbf{H_{eff}}_0(\mathbf{r}) + \delta\mathbf{h_{eff}}(\mathbf{r}, t)$. The static configuration is given by the domain wall profile, $\mathbf{m}_0(\mathbf{r})$, while $\delta\mathbf{m}(\mathbf{r}, t)$ represents the spin waves. The linearised torque equation is obtained by neglecting terms quadratic in the fluctuations, $\delta\mathbf{h_{eff}}(\mathbf{r}, t) \times \delta\mathbf{m}(\mathbf{r}, t) << 1$, and using the fact that the term, $\mathbf{m}_0(\mathbf{r}) \times \mathbf{H_{eff}}_0(\mathbf{r})$ gives the static configuration. Then,

$$\frac{\partial \delta\mathbf{m}}{\partial t} = -\gamma\mu_0(\mathbf{m_0} \times \delta\mathbf{h_{eff}} + \delta\mathbf{m} \times \mathbf{H_{eff}}_0). \tag{3.11}$$

We define the static magnetisation field by parametrising $\mathbf{m}_0(y)$ in spherical coordinates, $\mathbf{m}_0(y) = (\sin\theta_0 \cos\phi_0, \sin\theta_0 \sin\phi_0, \cos\theta_0)$. We have shown, (Chapter 2), that the domain wall profile in the presence of the DMI is a Néel type wall,

$$\begin{aligned} \theta_0(y) &= -2\arctan\left[\exp\left(\frac{y - Y_0}{\lambda}\right)\right], \\ \phi_0 &= \frac{\pi}{2}. \end{aligned} \tag{3.12}$$

It is convenient to perform a local gauge transformation such that the equilibrium configuration points along the local z' axis everywhere. This can be achieved by rotating about the x axis as depicted in figure 3.2, and given by the rotation matrix,

$$R = \begin{pmatrix} 1 & 0 & 0 \\ 0 & \cos\theta_0 & -\sin\theta_0 \\ 0 & \sin\theta_0 & \cos\theta_0 \end{pmatrix}. \tag{3.13}$$

We verify that $R\,\mathbf{m} = (0, 0, 1)$ indeed rotates the magnetisation components such that they point in the z' direction in the local frame. Fluctuations in this local frame are written as $\delta\mathbf{m}' = (\delta m'_x, \delta m'_y, 0)$. In the laboratory reference frame the fluctuation are calculated in terms of the local frame by $R^{-1}(\delta\mathbf{m}')$,

$$\delta\mathbf{m} = R^{-1}\delta\mathbf{m}' = (\delta m'_x, \delta m'_y \cos\theta_0, -\delta m'_y \sin\theta_0), \tag{3.14}$$

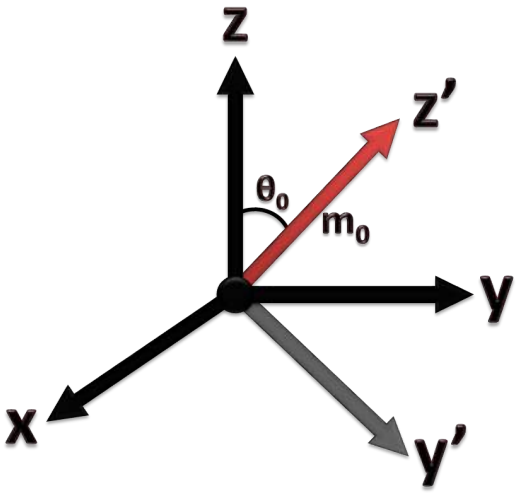

FIGURE 3.2: Rotation around the x axis to transform the magnetisation components such that in the local frame given by the primed coordinates the magnetisation always points along the z' axis.

from where it is possible to calculate the fluctuation contribution to the effective field.

$$\delta\mathbf{h_{eff}} = -\frac{1}{\mu_0 M_s}\frac{\delta\epsilon}{\delta(\delta\mathbf{m})}. \tag{3.15}$$

After calculating the linearised equation of motion ,(3.11), it is necessary to rotate back to the local frame where the fluctuations $(\delta m'_x, \delta m'_y)$ were defined and the static magnetisation points along the local z' axis. We, then, calculate $R\left[-(\mathbf{m}\times\delta\mathbf{h_{eff}} + \delta\mathbf{m}\times\mathbf{H_{eff}})\right]$ to obtain the dynamical matrix,

$$\frac{\partial}{\partial t}\begin{pmatrix}\delta m'_x\\ \delta m'_y\end{pmatrix} = H_0\begin{pmatrix}\delta m'_x\\ \delta m'_y\end{pmatrix} + H_1\begin{pmatrix}\delta m'_x\\ \delta m'_y\end{pmatrix}, \tag{3.16}$$

where H_0 comprises only the isotropic part of the exchange and the uniaxial anisotropy such that the spin wave is circularly polarised.

3.1.2 Domain wall spin wave eigenmodes

We are interested in solving the dynamics of equation (3.16), to do so we first present the eigenvalue solution to H_0. In the next section we apply perturbation theory to the full Hamiltonian and treat the H_1 term as the perturbation.

As we chose H_0 such that the spin waves are circularly polarised, we can perform the usual circular transformation, $\xi = \delta m'_x + i\delta m'_y$, to find,

$$H_0\ \xi = \frac{2\gamma(K_o + K_p)}{M_s}(-\lambda^2\nabla^2 + V_p)\,\xi = \Omega\,\xi. \tag{3.17}$$

where Ω is the eigenvalue. This is a Schrödinger like equation for the spin waves ξ. Note that the same form is found for the complex conjugate, ξ^*. The Laplacian operator in equation (3.17) arises from the isotropic exchange part and determines the spatial variation of the spin waves. The $V_p = 1 - 2\,\mathrm{sech}^2(y/\lambda)$ term is the effective potential that describes the wall and results from terms involving $\cos\theta_0(y) = -\tanh(y/\lambda)$ and $\sin\theta_0(y) = -\,\mathrm{sech}(y/\lambda)$ from equation (3.12). This eigenvalue equation is known as the modified Pöschl Teller potential [77, 79, 80]. There are two families of solutions for this operator. There is a localised wave which we denote by ξ_{loc}, and travelling waves denoted by ξ_{tr}. Together they form a complete orthonormal set. We treat each family of solution separately.

First,

$$\xi_{loc} = \exp\left[i(k_x x - \Omega_{loc}t)\right]\mathrm{sech}(y/\lambda), \qquad \Omega_{loc} = \frac{2\gamma(K_o + K_\perp)}{M_s}\omega_{kx}, \tag{3.18}$$

with $\omega_{kx} = (k_x\lambda)^2$, are spin waves eigenmodes localized in the direction perpendicular to the domain wall (y) on a length scale λ but propagate as plane waves parallel to the domain wall (x). The frequencies are degenerate with respect to the direction of propagation $\Omega_{loc}(k_x) = \Omega_{loc}(-k_x)$, a result of the isotropic nature of the exchange interaction that produces a quadratic spin wave dispersion.

Second,

$$\xi_{tr} = \exp\left[i(\mathbf{k}\cdot\mathbf{r} - \Omega_{tr}t)\right](\tanh(y/\lambda) - ik_y\lambda), \qquad \Omega_{tr} = \frac{2\gamma(K_o + K_\perp)}{M_s}(1 + \mathbf{k}^2\lambda^2) \tag{3.19}$$

which are travelling spin waves eigenmodes propagating in the plane of the film with wave vector $\mathbf{k} = (k_x, k_y, 0)$. Far from the wall these modes behave as plane waves, while in the vicinity of the wall the form of the wave propagating in the y direction is distorted by the term $(\tanh(y/\lambda) - ik_y\lambda)$. The spin wave frequency Ω_{tr} is similar to the one of a uniformly magnetised film where a gap appears due to the effective anisotropy described by K_o, only that in this case the term $K_\perp$ augments the gap. For $\mathbf{k} = 0$ the ferromagnetic resonance is $2\gamma(K_o + K_\perp)/M_s \simeq 21.2$ GHz for the parameters

used in this work and listed in the beginning of this thesis. In reference [1] they use these values to fit experimental results obtained using magnetic microscopy based on a single nitrogen-vacancy defect in diamond to determine the type of domain wall in Pt(3 nm)/Co(0.6 nm)/AlO_x(2 nm).

We note that the degeneracy now arises for both directions of propagation, k_x and k_y such that $\Omega_{tr}(k_x, k_y) = \Omega_{tr}(\pm k_x, \pm k_y)$. This results from an interesting feature of the V_p potential, namely that spin waves propagating perpendicular to the domain wall are not reflected and only acquire a phase shift, so there is no indication in the dispersion of a preferred direction because of the domain wall. The reflectionless phenomenon is a result of a special symmetry of the potential V_p [79, 80]. The acquired phase shift can be understood in terms of the geometrical or Berry phase which occurs when the wave phase varies adiabatically from one initial state to a different, intermediate state and back to the initial state. It is expected for the wave phase, after going through the intermediate and back to the initial state, to be the same as the one in the initial state. However, under certain circumstances the wave phase is changed [107]. In the case of spin waves propagating through a domain wall the initial state corresponds to a uniformly magnetised state, then it goes through the domain wall and returns to an initial state, although the magnetisation vector is now pointing in the opposite direction. That the states can be considered the same is a result of the symmetric energy terms of the system, isotropic exchange and effective uniaxial anisotropy and can only be true if there is no applied field.

The rest of the chapter is focused on using these known solutions, equations (3.18, 3.19) and treat H_1 with degenerate perturbation theory.

3.2 Perturbation theory

For most problems in physics an exact analytical solution is difficult to obtain and approximation methods need to be used. While a numerical approach is always an option, analytical solutions provide further physical insight within the limits of the approximation. Perturbation theory is one of these approximation methods and is based on separating the total Hamiltonian of the system H in two parts $H = H_0 + H_1$ where the $H_1 = 0$ problem is assumed to have been solved in the sense that both the exact eigenfunctions and eigenenergies are known. We formally identify the wave function of our Schrödinger problem with the semi-classical magnetic field describing

the ferromagnet. We take advantage of the clarity given by Dirac notation to present the perturbation theory. We assume the solution to the eigenvalue equation

$$H_0|n^0\rangle = E_n^0|n^0\rangle, \tag{3.20}$$

is known. The goal of perturbation theory is to find approximate eigenenergies and eigenfunctions of the full Hamiltonian,

$$(H_0 + \alpha H_1)|n\rangle = E_n|n\rangle \tag{3.21}$$

where H_1 is known as the perturbation and α is a continuous real parameter that is introduced to keep track of the number of times the perturbation enters the calculation. At the end of the calculation we set $\alpha \to 1$ and recover the original Hamiltonian. The parameter α can be visualised as varying continuously from 0 to 1 such that in the case $\alpha = 0$ we have the unperturbed case, $H = H_0$ and when $\alpha = 1$ we have the complete Hamiltonian. In physical situations we expect a smooth transition from $|n^0\rangle$ to $|n\rangle$ and E_n^0 to E_n as α varies from 0 to 1. In the case under consideration, the DMI parameter D corresponds to the parameter α. It possible to consider the DMI as the perturbation as it is at least one order of magnitude smaller than the isotropic exchange. The method rests on a Taylor expansion of the eigenvalue problem for the full Hamiltonian in powers of α,

$$\begin{aligned} |n\rangle &= |n^0\rangle + \alpha|n^1\rangle + \alpha^2|n^2\rangle \ldots; \\ E &= E^0 + \alpha E^1 + \alpha^2 E^2 \ldots, \end{aligned} \tag{3.22}$$

to obtain an approximate solution to equation (3.21). First order perturbation theory corresponds to take the expansion to first order in α, where $|n^1\rangle$ and E^1 are the first order corrections to the eigenfunctions and eigenenergies respectively.

In our case, however, the unperturbed Hamiltonian, H_0, is degenerate as was discussed in section 3.1.2. Degeneracy means that any linear combination of unperturbed eigenfunctions have the same energy so it is not possible to know the exact combination to which the corrected eigenfunction, $|n\rangle$, is reduced when $\alpha \to 0$. Degenerate perturbation theory addresses this complication. Consider two eigenfunctions $|n_a^0\rangle$ and $|n_b^0\rangle$ such that they both have the same energy E^0, any linear combination of these states, $|n^0\rangle = a|n_a^0\rangle + b|n_b^0\rangle$, also has the same energy. We are interested in the solution of $(H_0 + \alpha H_1)|n\rangle = E|n\rangle$, with $E = E^0 + \alpha E^1$ and $|n\rangle = |n^0\rangle + \alpha|n^1\rangle$ to first order in α.

Then, using equations (3.21, 3.22) and orthogonality relations

$$H_0|n^1\rangle + H_1|n^0\rangle = E^0|n^1\rangle + E^1|n^0\rangle, \tag{3.23}$$

Taking the inner product with $|n^0_{a,b}\rangle$ we obtain

$$\begin{aligned} a\,W_{aa} + b\,W_{ab} &= a\,E^1; \\ a\,W_{ba} + b\,W_{bb} &= b\,E^1, \end{aligned} \tag{3.24}$$

where

$$W_{ij} = \langle n^0_i|H_1|n^0_j\rangle, \qquad (i,j = a,b). \tag{3.25}$$

Note that W_{ij} are known as they are the matrix elements of H_1 with respect to the unperturbed eigenfunctions $|n^0_a\rangle$ and $|n^0_b\rangle$. Solving for E^1 we obtain a fundamental result of the degenerate perturbation theory,

$$E^1_{\pm} = \frac{1}{2}\left(W_{aa} + W_{bb} \pm \sqrt{(W_{aa} - W_{bb})^2 + 4|W_{ab}|^2}\right), \tag{3.26}$$

the perturbation lifts the degeneracy as can be seen from the two signs in the squared root in equation (3.26). We now apply this result to our problem.

The perturbation H_1 is given by the second term on the right hand side of equation (3.16) and it depends on the DMI and on the dipolar interaction in the centre of the wall. The DMI and the dipole interaction are treated as perturbation as they are at least one order of magnitude smaller than the isotropic exchange interaction, ($A \sim 10^{-21}$ J, $D \sim 10^{-22}$ J). Explicitly,

$$H_1 = \frac{2\gamma D}{\lambda M_s}\begin{pmatrix} \lambda\,\mathrm{sech}(y/\lambda)\frac{\partial}{\partial x} & 0 \\ \kappa_D - \mathrm{sech}(y/\lambda) & \lambda\,\mathrm{sech}(y/\lambda)\frac{\partial}{\partial x} \end{pmatrix}, \tag{3.27}$$

defining $\kappa_D = K_\perp \lambda / D$. We have to treat each element of equation 3.27 as a perturbation term.

The unperturbed part of the Hamiltonian, H_0, is degenerate with respect k and $-k$, which means that spin waves propagating in opposite directions have the same energy.

We calculate the correction to the energy due to the perturbation H_1 by computing the eigenvalues of

$$W = \begin{pmatrix} W_{k,k} & W_{k,-k} \\ W_{-k,k} & W_{-k,-k} \end{pmatrix}, \tag{3.28}$$

as in equation (3.26). The matrix elements are,

$$W_{\alpha,\beta} = \langle \xi^\alpha | H_1 | \xi^\beta \rangle; \qquad \langle \mathbf{r} | \xi^\alpha \rangle = \xi^\alpha(\mathbf{r}), \tag{3.29}$$

where $\alpha, \beta = k, -k$ indicate the twofold degeneracy with respect to the direction of propagation. We consider two linearly independent solutions, ξ^α and ξ^β, in the same eigenspace to address the degeneracy in the unperturbed Hamiltonian.

Using $\xi_{loc}(\mathbf{r})$, equation (3.18), results in the energy correction to the localised modes, while using $\xi_k(\mathbf{r})$, equation (3.19), leads to the energy correction of the travelling modes. We address each case in the following sections.

3.2.1 Correction to the localised modes

When the localised solutions $\xi_{loc}(x, y)$ are used as the scattering basis to calculate the energy first order corrections, integrals of the form,

$$\begin{aligned} &\int dV\, \xi^*_{loc}(x,y)(-D\,\mathrm{sech}(y/\lambda))\xi_{loc}(x,y) \\ &\int dV\, \xi^*_{loc}(x,y)(D\lambda\,\mathrm{sech}(y/\lambda))\frac{\partial}{\partial x}\xi_{loc}(x,y) \end{aligned} \tag{3.30}$$

need to be calculated. The degeneracy subspace is defined by considering $\pm k_x$ in $\xi_{loc}(x, y)$ and all the possible combinations as described by equation (3.28). The result,

$$H_1 = \frac{2\gamma D}{\lambda M_s} \begin{pmatrix} \pm i\frac{\pi\lambda^2}{2}k_x & 0 \\ \kappa_D - \frac{\pi\lambda}{2} & \pm i\frac{\pi\lambda^2}{2}k_x \end{pmatrix}, \tag{3.31}$$

is a matrix that contains the correction terms for each matrix element in H_1. We are now in the position to calculate the total correction to the energy as the eigenenergies of H_0 are known and the corrections to H_1 are given by 3.31. Finding the solution to the dynamical matrix, equation (3.16), is just an algebraic procedure that involves calculating its determinant and solving for the total corrected energy. It is convenient to use frequency units instead of energy.

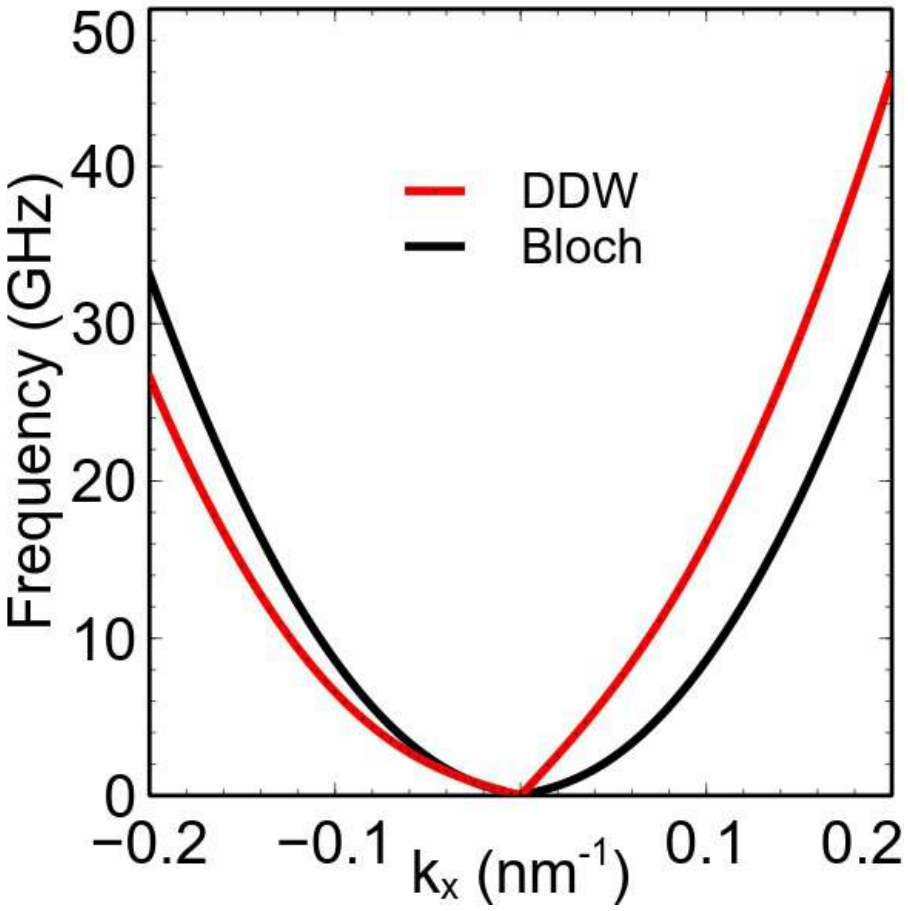

FIGURE 3.3: Spin wave dispersion for propagation along x. The black line corresponds to the dispersion found in a Bloch wall and is showed for comparison. The red line is the dispersion calculated using perturbation theory, equation (3.32), and exhibits a strong non-reciprocity.

The corrected frequency is,

$$\Omega_k^{N\pm} = \frac{2\gamma}{M_s}\left[\pm\frac{\pi D k_x}{4} + (K_o + K_\perp)\sqrt{\omega_{kx}\left(\omega_{kx} - \kappa + \frac{\pi D}{4(K_u + K_\perp)\lambda}\right)}\right], \tag{3.32}$$

and is presented in figure (3.3) along with the Bloch-type wall dispersion relation

$$\Omega_k^B = \frac{2\gamma K_o}{M_s}\sqrt{\omega_{kx}(\omega_{kx} + \kappa_B)}, \tag{3.33}$$

with $\kappa_B = K_\perp/K_o$ for comparison. An ellipticity in the precession arises from the term $\kappa_D - \mathrm{sech}(y/\lambda)$ and cancels out for the critical value, $D_c = 4\lambda K_\perp/\pi$, in which the static configuration completes its transition to a Néel type wall, (equation (2.21) in Chapter 2). The first term on the right hand side of equation (3.32) depends linearly on the wave vector k_x and is a result of the DMI terms $(D\lambda\,\mathrm{sech}(y/\lambda))\frac{\partial}{\partial x}$ in equation (3.27). This

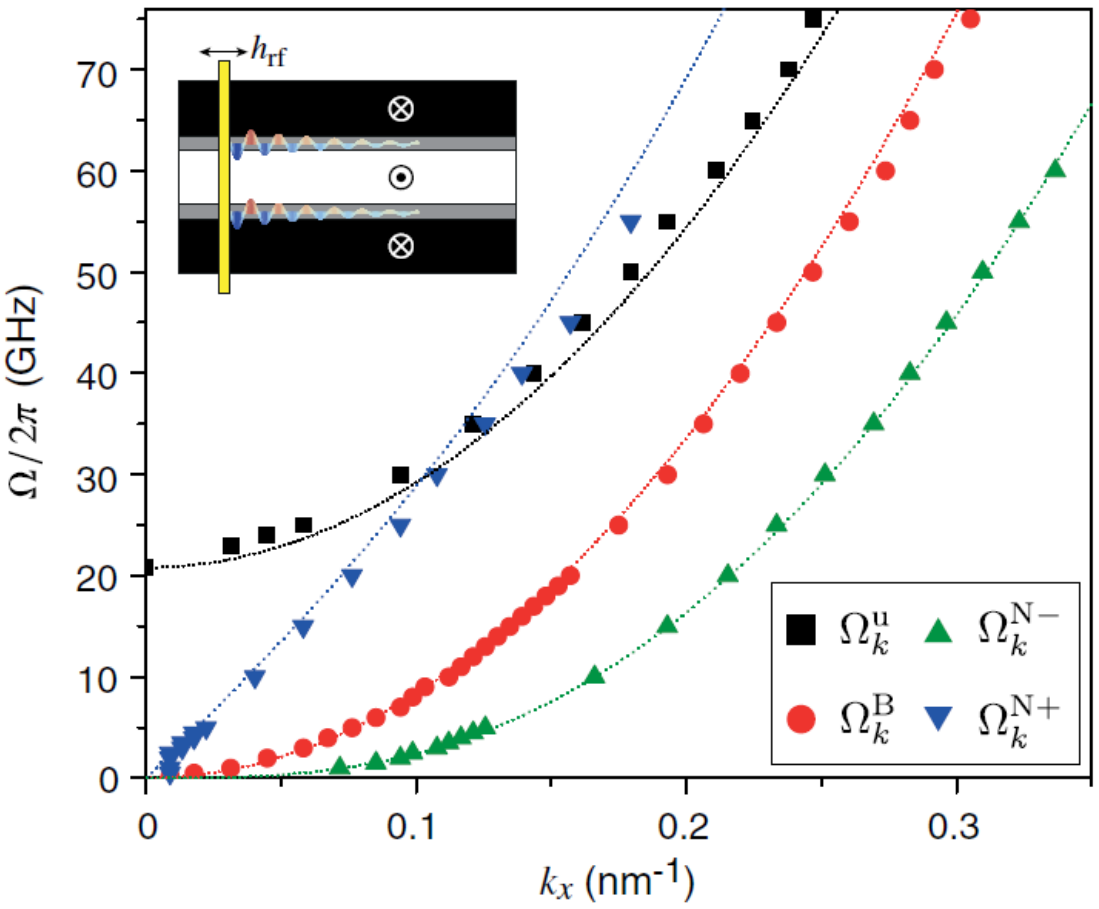

FIGURE 3.4: Simulated dispersion relation for channelled and bulk spin waves. Ω_k^u indicate bulk modes. The channelled modes for Bloch-type (Ω_k^B) and Néel-type ($\Omega_k^{N\pm}$) walls are computed, where $D = 3$ mJ/m^2 for the latter and the sign indicates propagation relative to the wall chirality. The points represent simulated values and lines are based on equations (3.32), (3.33), (3.34). The inset shows the three-domain geometry with two parallel domain wall channels.

is consistent with results found in other geometries [41, 42]. The dispersion relation becomes asymmetric with respect to $k_x = 0$, and exhibits a quasilinear variation for $k_x < 0$ and a quadratic form for $k_x > 0$ consistent with figure (3.3). Another critical value $D_{c2} = 4K_o\lambda/\pi$ is found in the limit when $\kappa \to 0$, $k_x \to 0$, consistent with previous works and that corresponds to the value for which the domain wall becomes unstable, $\sigma_D < 0$.

To verify the perturbation theory, the spin wave dispersion was studied using mumax3 [108]. Micromagnetic simulation software, such as mumax3, solves the phenomenological Landau-Lifshitz equation (3.3) taking into account the magnetostatic, exchange interaction and anisotropy interactions by dividing the magnetic structure into equal cubical cells. These simulations are useful to treat the long range demagnetising interaction

throughout the sample and not relying on a local approximation as is done in this work.

In figure (3.4) we show the simulations for a three domain structure comprising two parallel domain walls. The points are the numerical calculations and the curves the analytical calculations of the spin wave dispersion relations. We consider propagation along the x direction in three spin textures: red for a Bloch-type wall ($D = 0$), blue and green for Néel walls with opposite chirality and in black the dispersion relation of a uniformly magnetised film,

$$\Omega_k^u = \frac{2\gamma}{M_s}\left(Ak_x^2 + K_o\right). \tag{3.34}$$

In the inset of figure (3.4) we depict the geometry of the three domain structure that results in the two opposite chiralities of a Néel wall.

In all cases there is a good agreement between the analytical theory and the simulated dispersions. The small discrepancies are related to a limited wave vector resolution that results from the finite size of the simulation grid. For Néel type walls two frequency branches are observed, $\Omega_k^{N\pm}$, because the propagation happens for the two possible domain wall chiralities. The frequency difference between the two Néel branches,

$$\Delta\Omega_k^N = \Omega_k^{N+} - \Omega_k^{N-} = \frac{\gamma\pi D}{M_s}k_x, \tag{3.35}$$

is proportional to D and therefore a simultaneous measurement of the two branches in this geometry allows the DMI strength to be probed. We now further explore spin wave propagation in the centre of a domain wall.

Domain wall waveguide. The modes localised to the centre of the wall propagate freely in the plane parallel to the wall due to the confining potential, V_p. This statement is true for both Bloch and Néel-type profiles. In figures (3.5a and 3.5b) we show the results of micromagnetic simulations in which the localised modes in the centre of a domain wall are excited by an alternating field h_{rf}. It can be observed that spin waves propagate localised to the centre of the wall. In figure (3.5a) a Bloch-type wall is considered, and propagation is the same to the left and right directions. In a Néel type wall stabilised by the DMI, figure (3.5b), an asymmetry in the spin wave propagation can be observed as a result of the non-reciprocity in the dispersion due to the DMI.

Spin wave channelling in the centre of the wall allows for guides consisting of curved, narrow magnonic domain walls. Simulations of spin waves using domain walls in curved geometries are shown in figure (3.6) where a 200 nm wide curved track with a 90 ° bend

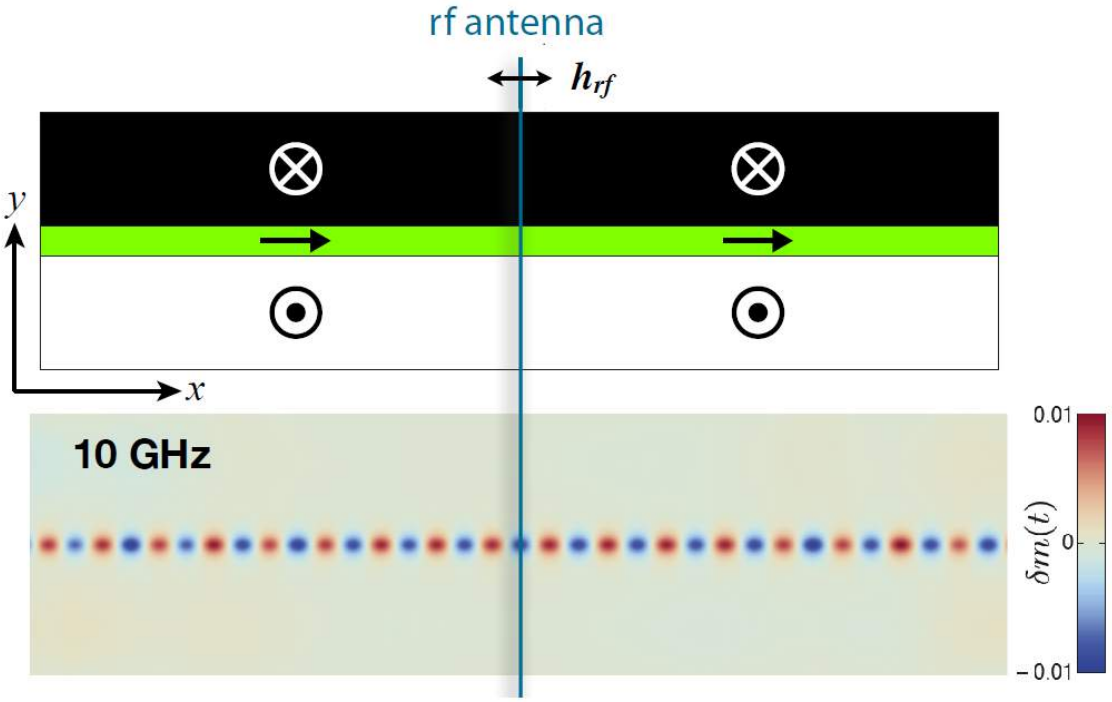

(A) Bloch wall

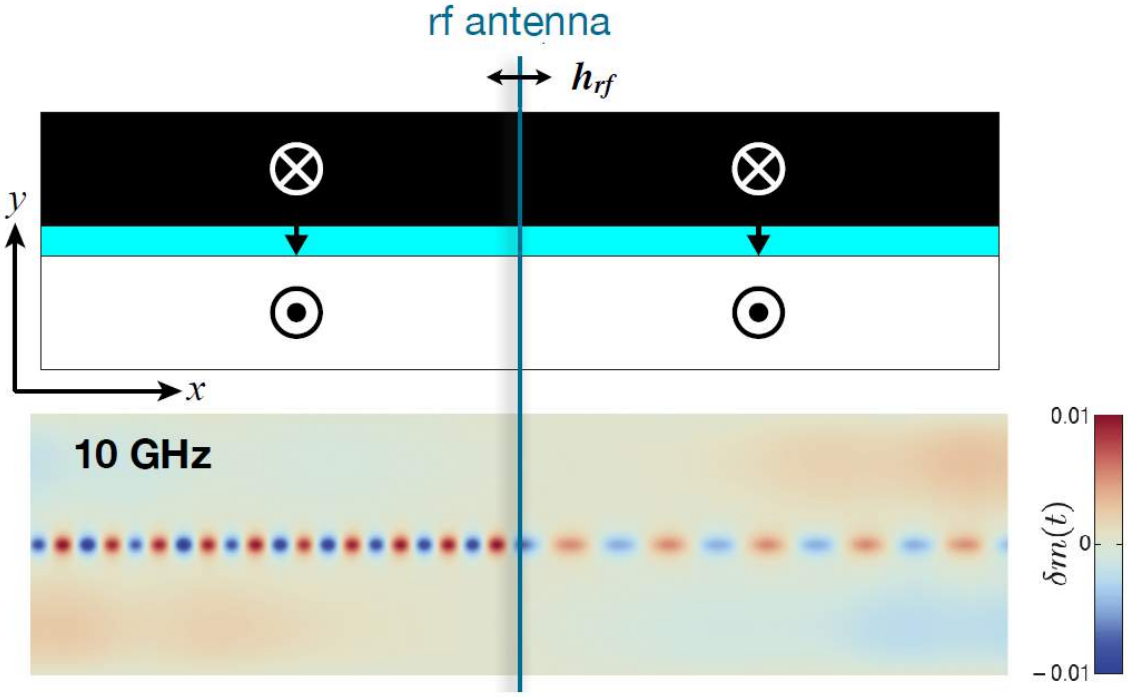

(B) Néel wall

FIGURE 3.5: Geometry for spin wave propagation along the centre of a domain wall, where a radio frequency antenna generating an alternating field h_{rf} excites spin waves that propagate along the x direction. In the bottom panel we show the simulation results of propagating modes for excitation field frequency of 10 GHZ for Bloch (A) and Néel (B) walls.

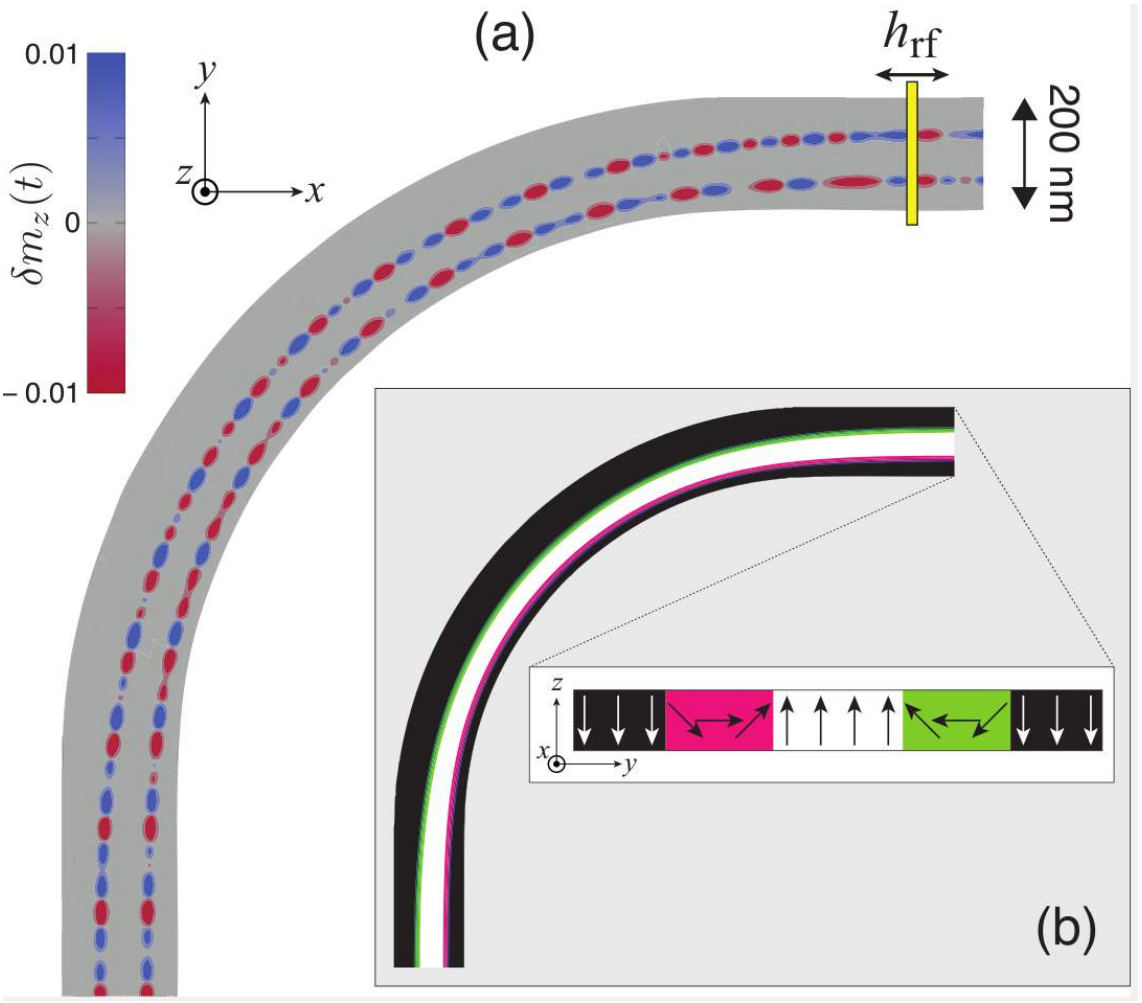

FIGURE 3.6: (a) Spin wave channelling around a curved track through two Néel-type domain walls ($D = 1$ mJ/m^2). Fluctuations in the m_z magnetization component are shown as a colour code for a microwave excitation frequency of 5 GHz, where the simulated microwave antenna is situated at the top of the track. The area of the simulated region is 1600 nm × 1600 nm. The width of the wire is 200 nm and the thickness is 1 nm. (b) Equilibrium configuration of the curved track comprising three domains. The inset shows a schematic of the magnetization profile in a cross section at the top of the track.

is considered with a radius of curvature of approximately 1600 nm for the outer edge. The magnetic state comprises a three-domain structure where the domain walls run parallel to the track edges. In order to stabilise this domain sate, a DMI of $D = 1$ mJ/m^2 was used in order to ensure that the domain walls are not expelled from the track because of dipolar interactions. Spin waves are excited with a microwave antenna at the end of the track and are effectively channelled along the track without any apparent scattering or loss of coherence due to the curved geometry. There is no perceptible interference between the two chiral channels where the non-reciprocity is preserved.

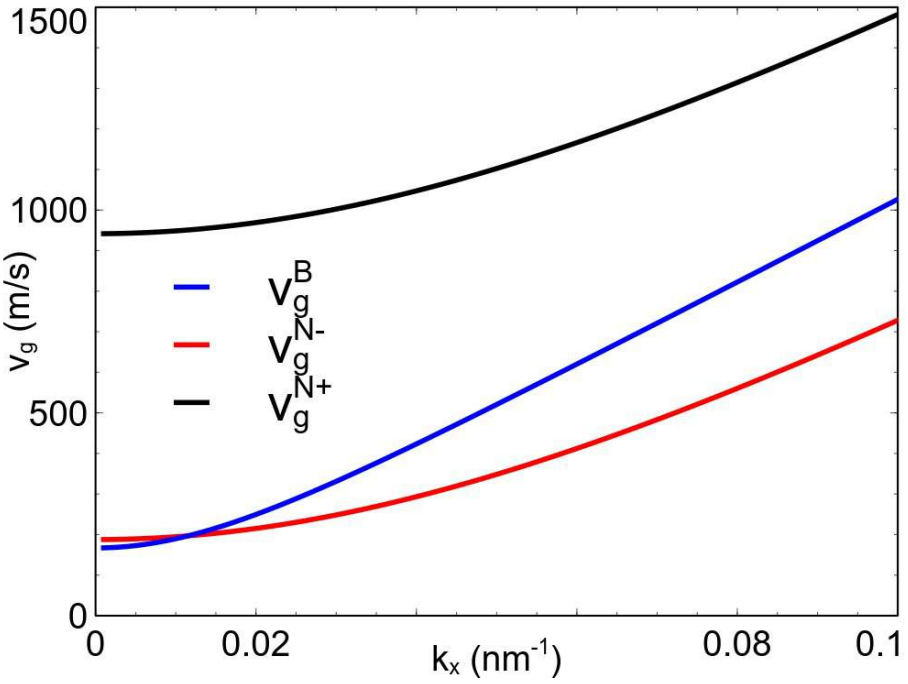

FIGURE 3.7: Group velocity for the channelled spin waves as a function of the wave vector k_x. The blue solid curve corresponds to the group velocity, v_g^B of spin waves propagating in a Bloch domain wall. The red and black curves are the group velocities, $v_g^{N\pm}$ in Néel domain walls of different chiralities defined by the $\pm$ sign.

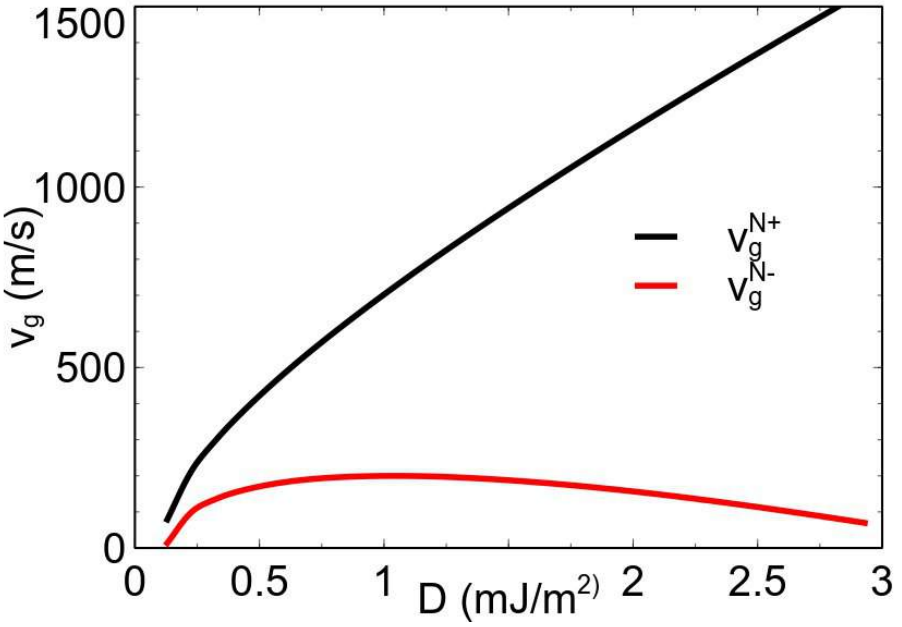

FIGURE 3.8: Group velocity for the two Néel wall modes $v_g^{N\pm}$ in the limit $k \to 0$ as a function of the Dzyaloshinskii-Moriya constant, D.

Another consequence that results from the dispersion relation, (equation (3.32)), of the localised modes of a Néel wall is found when the group velocity, $v_g^{N\pm} = \partial\Omega_k^{N\pm}/\partial k$, is calculated. In the long wavelength limit $k_x \to 0$, a Bloch-type wall has a group velocity, calculated from equation (3.33), $v_g^B(k_x = 0) = 2\gamma K_o \lambda \sqrt{\kappa_B}/M_s$, which is finite as a result of the weak ellipticity of the precession due to the dipole interaction at the centre of the wall. For the numerical values used in this work it is approximately 27 m/s [104, 109]. For Néel type walls the group velocity in the same long wavelength limit is described by

$$v_g^{N\pm}(k_x = 0) = \frac{2\gamma}{M_s}\left(\pm\frac{\pi D}{4} + \lambda(K_o + K_\perp)\sqrt{\frac{\pi D}{4\lambda(K_o + K_\perp)} - \kappa}\right). \tag{3.36}$$

For a moderate value of $D = 1.5$ mJ/m^2 it results in a group velocity of around 940 m/s for the positive branch. As the group velocity is usually related to the velocity at which information is conveyed along a wave [110], the above result can be useful for information technologies. The group velocity as a function of wave vector, figure (3.7), shows the two branches and their strong dependence on the direction of propagation. Figure (3.8) presents how they depend on D for $k_x = 0$, the branch Ω_k^{N-} tends to zero as D increases while Ω_k^{N+} behaves opposite increasing the group velocity. These features have many interesting possible applications for wave packet propagation as discussed in reference [104].

Edge channeling. In addition to stabilising Néel-type domain walls, the DMI also produces magnetisation tilting at the edges when the system is uniformly magnetised [111]. This can be explained by calculating the boundary conditions, equation (3.10), that arise from the variational procedure. With only $\epsilon = \epsilon_A + \epsilon_{K_0} + \epsilon_{K_\perp}$, one obtains the usual free boundary condition [112], $\frac{\partial \mathbf{m}}{\partial \mathbf{n}} = 0$ in the absence of any surface pinning. The inclusion of the DMI, however, requires satisfaction of twisted boundary conditions,

$$\begin{aligned} Dm_z + 2A\partial_y m_y &= 0; \\ -Dm_y + 2A\partial_y m_z &= 0; \\ Dm_z + 2A\partial_x m_x &= 0; \\ -Dm_x + 2A\partial_x m_z &= 0, \end{aligned} \tag{3.37}$$

and all other spatial derivatives in m vanishing, which couples the perpendicular magnetisation m_z with gradients in the transverse components $m_{x,y}$, and vice versa.

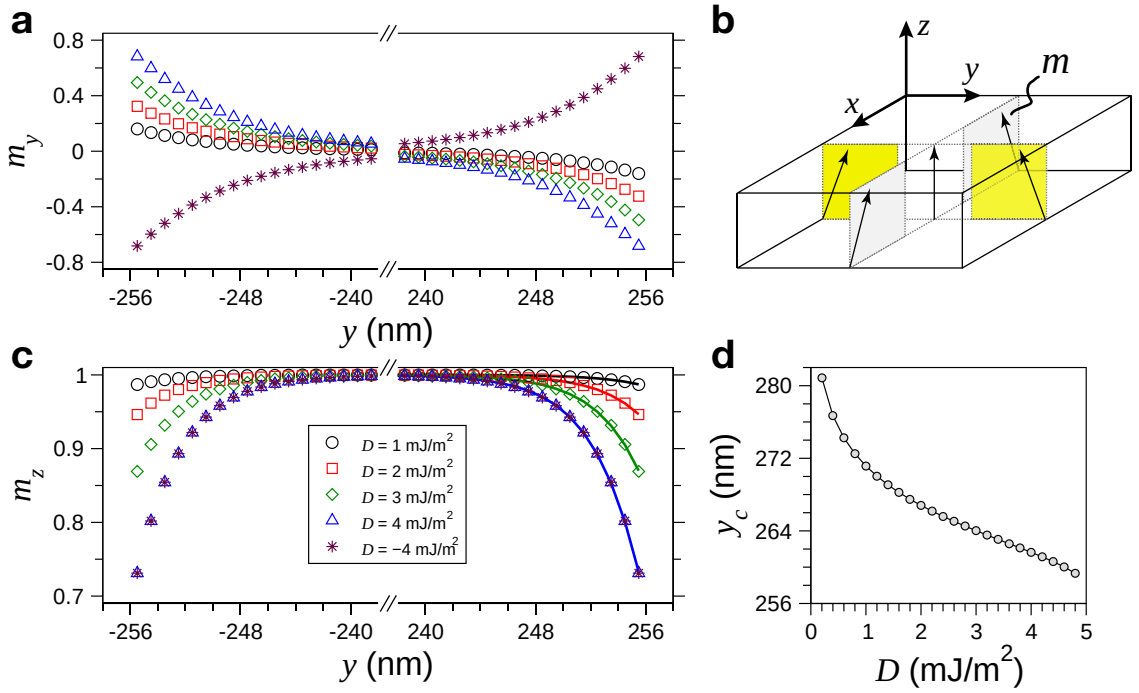

FIGURE 3.9: (a) The transverse m_y component of the magnetisation at the edges of a rectangular element along the y axis. (b) Schematic illustration of the magnetisation tilts for $D > 0$, with the yellow shaded regions representing the tilts shown in (a). In (c) we present the m_z component of the magnetisation at the boundary edges, where the solid lines correspond to the analytical form of a partial Néel wall profile, $m_z(y)$. (d) Variation of the partial wall centre Y_0 as a function of D. The partial wall enters progressivley the system as D increases.

These conditions, equation (3.37), indeed lead to tilts in the magnetisation at the edges whose profile are well described by partially expelled Néel domain walls [103]. In figure (3.9) we present micromagnetic simulations of a thin film with a length of 512 nm to describe this phenomenon. In figures (3.9(a),(b)) we show how the tilt of the magnetisation depends on the strength of the DMI parameter D and how the tilting reverses when $D < 0$. In figure (3.9(c)) we compare the numerical results with the analytical expression of a Néel wall presented by the solid curves. The position of the centre of a domain wall outside the film is shown in figure (3.9(d)) from where it is clear that as the strength increases the domain wall centre enters the film. The DMI interaction acts to pin a partial wall at the edges, because of the boundary conditions, equation (3.37), and the strength of the DMI interaction given by D determines the extent to which the wall enters the film.

In figure (3.10) we present the overview of non-reciprocal spin wave channelling, in (3.10(a)) we illustrate a Néel domain wall stabilised by the DMI, while in (3.10(c)) we show how the non-reciprocal propagation occurs. The right asymmetric red arrows show

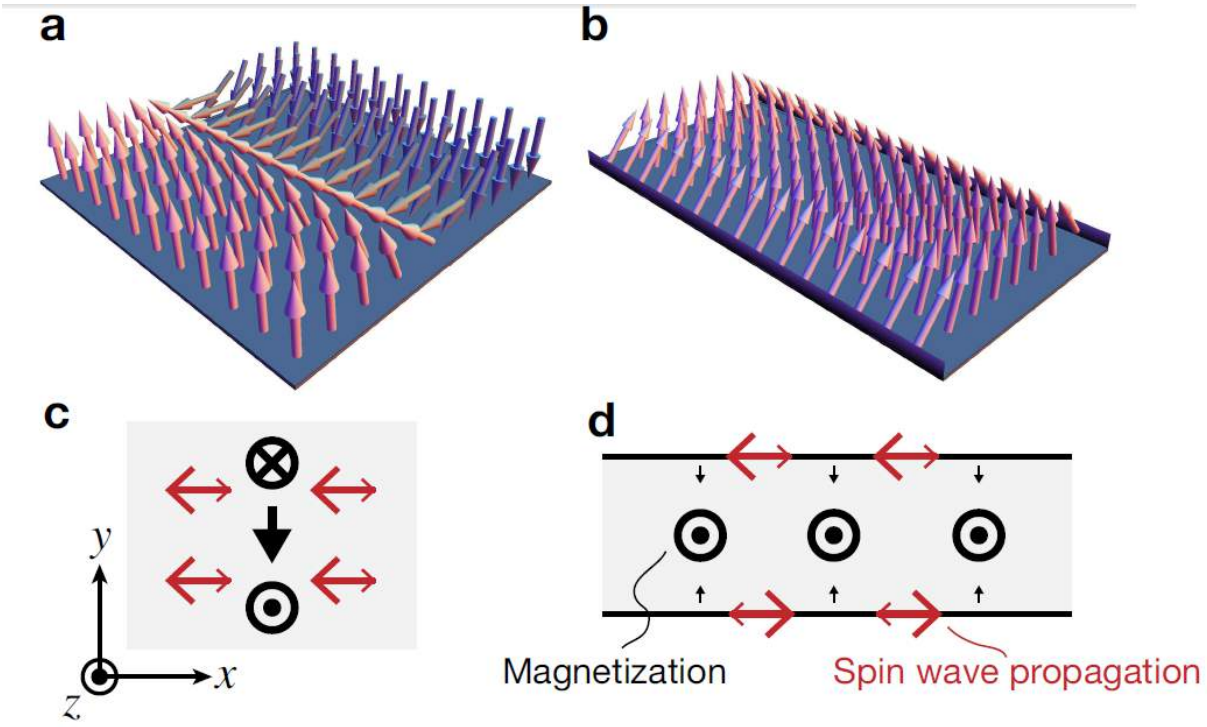

FIGURE 3.10: Overview of non-reciprocal spin wave channelling in spin textures driven by the DMI. (a,b) Illustration of chiral spin textures in ultra-thin films: Néel domain wall (a), and tilted edge magnetization in a thin rectangular stripe (b). (c,d) Illustration of non-reciprocal propagation of spin waves (red arrows) with respect to the magnetization textures (black arrows) for a Néel domain wall (c), and rectangular stripe (d). The different size of the propagation (red) arrowheads indicates the non-reciprocal propagation.

spin waves propagating along the wall. In (3.10(b)) we show how the magnetisation is tilted at the edges of a thin magnetic film. In (3.10(d)) we show spin wave propagation, where the non-reciprocity is inverted from one edge to the other because of the opposite chiralities at the edges.

In figure (3.11) we present the micromagnetic simulations for spin waves propagating at the edges of a thin film, in the top panel we identify the direction of propagation with the labels $(k_{top}, k_{cen}, k_{bot})$. An exciting field h_{rf} in the middle of the film drives the spin waves with a frequency of 16 GHz which propagate only at the edges as this frequency does not excite the uniform mode shoen in the bottom panel with a black curve. The non-reciprocity is observed by comparing opposite directions of propagation in both k_{top} and k_{bot}. In bottom panel we present the simulated dispersion relations for propagation along the edges and the centre of the film

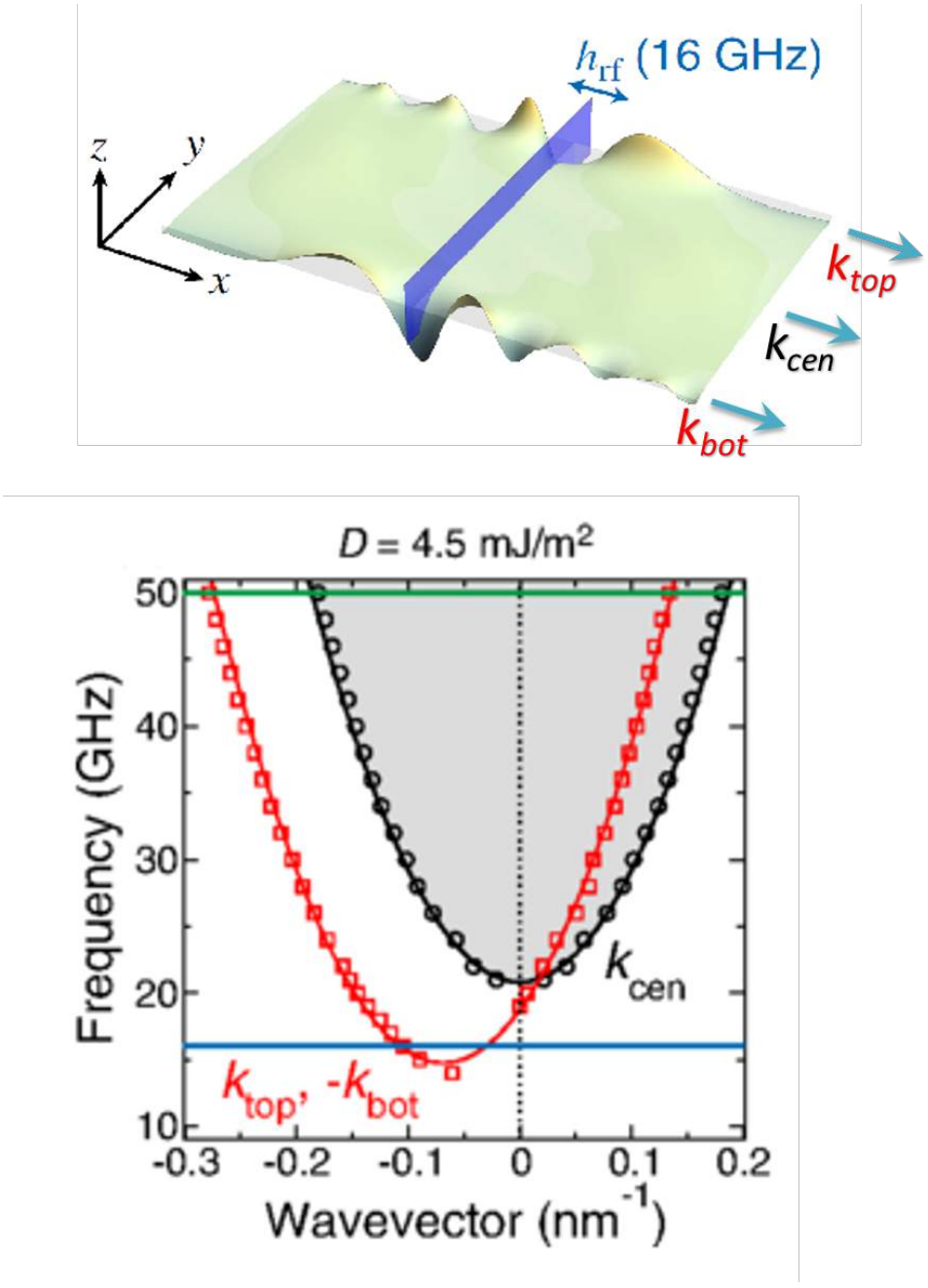

FIGURE 3.11: Nonreciprocal propagation in a thin film rectangular stripe. (a) Spatial profiles of the m_x component of magnetization resulting from an rf field excitation, $\mathbf{h}_r f(t) = h_0 \sin(2\pi f_{rf} t)\hat{\mathbf{x}}$, where $\mu_0 h_0 = 5$ mT, at a frequency f_{rf} of 16 GHz. In (a), the different wave vector components considered, k_{top} , k_{cen} , and k_{bot} , are illustrated. These wave vectors describe propagation along x at the top edge, centre, and bottom edge of the wire, respectively. The excitation frequency is in the gap of the bulk spin wave modes, represented by the solid black curve and gray shaded area in (b), and only edge modes are excited. (b) Dispersion relations for the top, centre, and bottom modes computed from micromagnetics simulations for $D = 4.5$ mJ/m^2 , with the excitation frequency used in (a) indicated by the blue horizontal line. The top and bottom modes follow a quadratic dispersion relation that is shifted from the origin due to the DM interaction. Dots represent results from micromagnetic simulations. The solid black curve (and gray shaded area) represents the theoretical dispersion relation for exchange modes using our material parameters.

3.2.2 Correction to the travelling modes

We now apply the perturbation theory using the travelling modes as the scattering basis. We calculate similar integrals as in equation (3.30), but using the travelling modes, ξ_k (equation (3.19)). We note that in the degenerate subspace given by equation (3.28) it is necessary to consider the degeneracy with respect to k_x and k_y. The explicit analytical form of the dispersion relation for these modes is plotted in figure (3.12) and discussed in the appendix (B). In figure (3.12(a) and (b)) we show the frequency dependence on the wave vector in the two possible directions of propagation k_x and k_y for opposite chiralities of a Néel wall determined by the sign of the D parameter. Two sheets appear as the DMI lifts the degeneracy with respect to propagation along the y axis. In (3.12(c) and (d)) we present the case where $k_y = 0$ and non-reciprocity appears similar to the localised modes. In (3.12(e)) we show the case $k_x = 0$, there is reciprocity in the dispersion and the two solid curves show the two possible chiralities of the wall. The dotted line indicates a Bloch wall ($D = 0$). This is an indication that spin waves are reflected by the Néel-type wall. This feature is discussed in detail in Chapter 4 using a different approach.

Discussion and Concluding Remarks for Chapter 3

It has been shown theoretically that Dzyaloshinskii domain walls modify the spin wave propagation in the two directions given by the plane of a thin film. For propagation parallel to the wall, (x), the DMI induces non-reciprocal channelling in the centre of the wall [103]. This phenomenon also occurs at the edges of wires where partial walls appear as a result of twisted boundary conditions. These results offer a means of measuring experimentally the DMI in multilayer systems relevant for spintronics. For the localised modes propagating freely in the centre of the wall these theoretical results are the foundations for a domain wall wave guide stabilised by the DMI in which the spin waves can be channelled even in curved geometries [104]. As the domain wall profile is given by the intrinsic magnetic properties of the material, fabrication issues become less relevant. Propagation of spin waves in curved geometries is important for magnonic circuit design and crucial for wave processing schemes based on spin wave interference. For propagation perpendicular to the wall plane, (y), the DMI lifts a degeneracy produced by the reflectionless feature of the wall potential by splitting the frequency domain, this topic will be discussed in chapter (4).

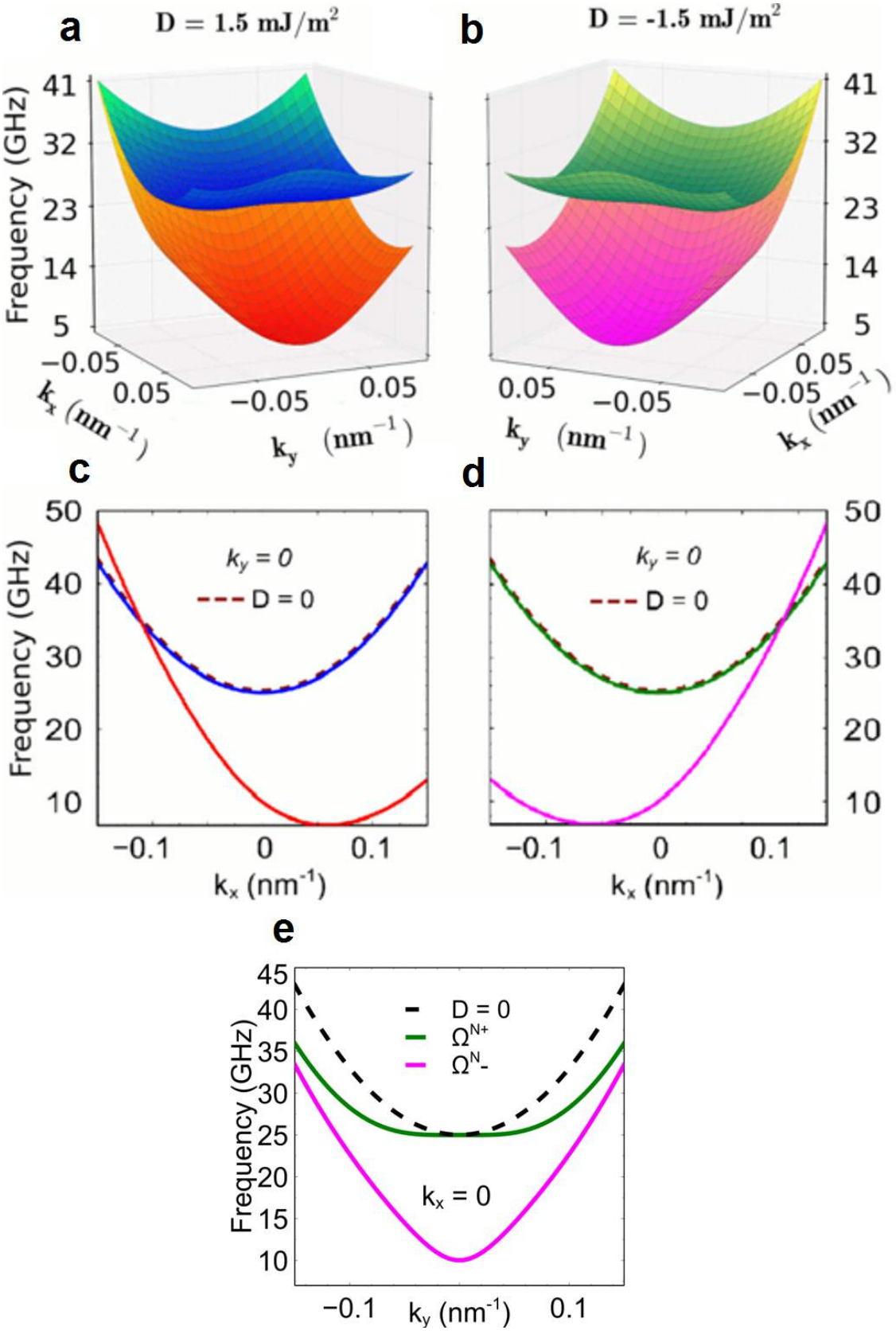

FIGURE 3.12: Spin wave dispersion relation calculated with perturbation theory using the travelling modes as the unperturbed eigenfunctions. (a) and (b) show the frequency as a function of the wave vectors k_x and k_y for opposite wall chiralities determined by the sign of $D = \pm 1.5$ mJ/m^2. The non-reciprocal dispersion is shown in (c)and (d) for the case $k_y = 0$. In (e) we show how the DMI lifts the degeneracy with respect the direction of propagation k_y.

Chapter 4

Spin wave reflection by a domain wall

As noted earlier, collective excitations around a domain wall static configuration receive the name of Winter modes [75, 77]. There are two families of these modes, a mode localised to the centre of the wall that propagates freely only in the direction parallel to the plane of the wall, and travelling modes that behave like plane waves far from the wall but have a distortion in the vicinity of it [69, 74], see also Chapter 3. The travelling modes are not reflected by the potential that describes the wall but only acquire a phase shift[83].

Possible magnonic applications such as domain wall logic gates are based on the reflectionless feature [113]. In Chapter 3 it was shown that the localised modes propagating parallel to the wall are affected when the induced, interface form of the DMI is included in the energy terms. A non-reciprocal channelling is the most important result. In this chapter it is demonstrated that the DMI affects the modes propagating perpendicular to the plane of the wall in a different way. Spin waves are partially reflected by the domain due to an extra chiral term in the effective potential associated with the domain wall leading to a hybridisation between the travelling modes and the local domain wall excitation. Spin wave reflection lifts a degeneracy and produces a splitting in the dispersion relation whose magnitude is proportional to the strength of the DMI. We propose a magnonic crystal in the form of a periodic array of Néel walls stabilised by the DMI. Transmitted and reflected contributions form standing waves at the edges of the Brillouin zone that produce gaps in the band structure.

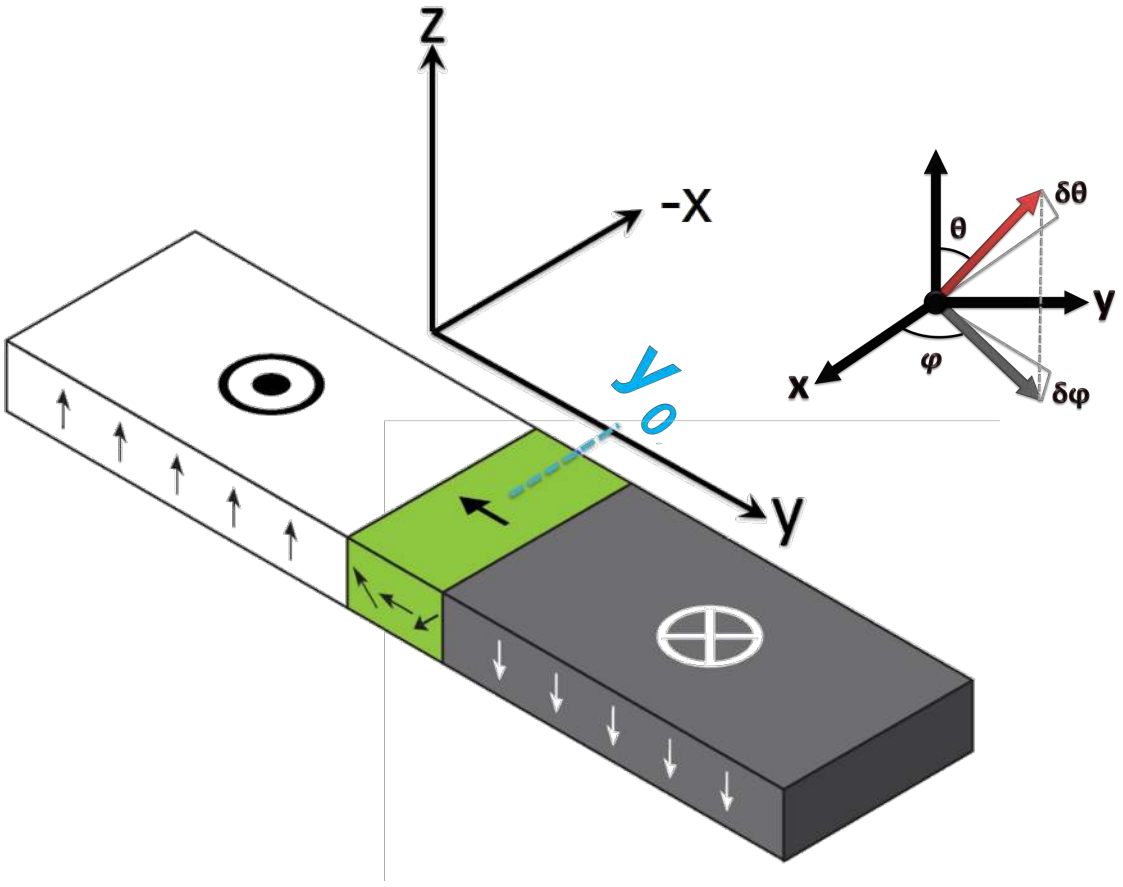

FIGURE 4.1: Geometry considered for the Néel-type Dzyaloshinskii domain wall. X_0 denotes the position of the wall center along the x axis. Translational invariance is assumed along the y direction and the magnetization is taken to be uniform across the thickness of the film in the z direction. Small fluctuations $(\delta\theta, \delta\phi)$ are presented when the magnetisation is parametrised in spherical coordinates.

4.1 Model and static wall profile

An ultrathin ferromagnetic wire is considered here in which a domain wall separates two uniformly-magnetized domains along the y axis, as shown in Figure (4.1). The energies we have considered account for the most important symmetries of the problem, and the magnetization orientation, represented by the unit vector $\mathbf{m}$, is parametrized using spherical coordinates as $\mathbf{m} = \mathbf{M}/|M_s| = (\sin\theta\cos\phi, \sin\theta\sin\phi, \cos\theta)$, where $\theta = \theta(\mathbf{r}, t)$, $\phi = \phi(\mathbf{r}, t)$ and M_s is the saturation magnetisation. The total magnetic energy of this

system is given by the functional $E[\theta(\mathbf{r}), \phi(\mathbf{r})]$,

$$E = \int dV \; \Big[A \left((\nabla\theta)^2 + \sin^2\theta \, (\nabla\phi)^2 \right) + D \left(\frac{\partial\theta}{\partial x}\cos\phi + \frac{\partial\theta}{\partial y}\sin\phi + \frac{1}{2}\sin 2\theta \left(\frac{\partial\phi}{\partial y}\cos\phi - \frac{\partial\phi}{\partial x}\sin\phi \right) \right) + K_\perp \sin^2\theta \sin^2\phi - K_o \cos^2\theta \Big] . \quad (4.1)$$

As discussed in section 2.2, the first term describes the isotropic part of the exchange interaction and where the exchange stiffness constant A is related within the continuum approximation to the exchange integral J. The second term describes the antisymmetric contribution to the exchange interaction given by the DMI. Unlike the isotropic part, this interaction is linear in the spatial derivatives of the magnetisation. The induced, interface form of the DMI relevant for our model is given in terms of the Lifshitz invariants $L^k_{ij} = m_i \frac{\partial m_j}{\partial x_k} - m_j \frac{\partial m_i}{\partial x_k}$ as $D\,(L^x_{zx} + L^y_{zy})$ [2, 25]. Finally, the third term describes the total anisotropy of the system. The constant $K_o = K_u - \mu_0 M_s^2/2$ is the effective anisotropy along the z axis, where K_u is related to the magnetocrystalline anisotropy and $-\mu_0 M_s^2/2$ accounts for the perpendicular demagnetizing field effect in the local approximation. The constant $K_\perp$, that favours a Bloch- over a Néel-type wall in the absence of DMI, is a magnetostatic anisotropy along the y axis related to the demagnetizing coefficient N_y by $K_\perp = \mu_0 N_y M_s^2/2$ in the local approximation.

As was done in section (2.2.3), the static profile of the domain wall is determined by minimising the energy functional in Equation (4.1) with respect to (θ_0, ϕ_0). We assume a straight wall so that there is translational invariance along the x direction. Furthermore, we assume a planar wall which requires $\phi(y) = \phi_0$. The equations satisfied by the static wall profile (θ_0, ϕ_0) are given by

$$\begin{aligned} \theta_0(y) &= -2\arctan\left[\exp\left(\frac{y - Y_0}{\lambda}\right)\right]; \\ \phi_0 &= \pi/2 \end{aligned} \quad (4.2)$$

where Y_0 denotes the wall centre, which is arbitrary, and $\lambda = \sqrt{\frac{A}{(K_o + K_\perp)}}$ is the domain wall width. This solution gives the configuration illustrated in Figure (4.1). We have shown in section (2.2.3) using energy considerations that a left-handed Néel wall is preferred energetically for $D > D_c = 4\lambda K_\perp/\pi > 0$.

4.2 Spin wave Hamiltonian

We are interested in linearised excitations or spin waves around the stable configuration. We follow a different procedure than the one presented in Chapter 3. This method is now based on the variables m_x, m_y, m_z expressed in spherical coordinates θ, ϕ. As the length of the magnetisation unit vector is conserved, $|\mathbf{m}|^2 = 1$, only two variables, θ, ϕ, are needed to describe the system [114]. We consider that the small deviations of the magnetisation $\mathbf{m}$ from the stable configuration $\mathbf{m_0}$ are given in spherical coordinates by the angles $\delta\theta$ and $\delta\phi$, depicted in the inset of figure (4.1), such that $\theta = \theta_0 + \delta\phi$ and $\phi = \phi_0 + \delta\phi$. The angles (θ_0, ϕ_0), equation (4.2), correspond to the profile of the stable configuration and are found through energy minimisation as was done in section (2.2.2). We expand the magnetic energy functional up to second order in the small fluctuations $(\delta\theta, \delta\phi)$ in order to obtain the spin wave Hamiltonian, δE. A more detailed derivation of the procedure is found in appendix (C). We find

$$\delta E = (K_o + K_\perp) \int dy \;\; \delta\theta \left[-\lambda^2 \partial_y^2 + V_P(y)\right] \delta\theta + \delta\phi \left[-\lambda^2 \partial_y^2 + V_P(y) + \frac{D}{\lambda(K_o + K_\perp)} \operatorname{sech}(y/\lambda) - \frac{K_\perp}{K_o + K_\perp}\right] \delta\phi, \quad (4.3)$$

where $V_P(y) = [1 - 2\operatorname{sech}^2(y/\lambda)]$. The physical picture of equation (4.3) can be thought of as a wave travelling through an effective potential, V_P, specified by the underlying domain wall, wherein the hyperbolic secant terms account for the domain wall structure. In particular, the DMI term, $D\operatorname{sech}(y/\lambda)$, results from the chiral symmetry breaking of the stable configuration given by a left handed Néel type wall. There is an elliptical precession in the fluctuations because of the extra terms in the $\delta\phi$ component due to the DMI and the $K_\perp$ which corresponds to the term $\kappa_D - \operatorname{sech}(y/\lambda)$ found in the perturbation part of the Hamiltonian, equation (3.27), in Chapter 3. Interestingly, while the $K_\perp$ produces a constant ellipticity, the DMI introduces a spatially dependent ellipticity through the $D\operatorname{sech}(y/\lambda)$ term.

The Schrödinger type operator, $-\lambda^2\partial_y^2 + V_P(y)$, has been widely studied and is used to describe spin waves in a Bloch type domain wall [69, 70, 77, 79]. Solutions to this operator include a single bound state (section (3.1.2)),

$$\xi_{loc}(y) = \frac{1}{\sqrt{2\lambda}} \operatorname{sech}(y/\lambda), \quad (4.4)$$

with zero corresponding energy, and continuum-travelling states,

$$\xi_k(y) = \frac{1}{\sqrt{\omega_k}} e^{iky}[\tanh(y/\lambda) - ik\lambda], \tag{4.5}$$

with eigenenergy given by $\omega_k = 1 + k^2\lambda^2$. The above states form a complete orthonormal set,

$$\begin{aligned} \int dV\ \xi_k^* \xi_{loc} &= 0, \\ \int dV\ \xi_k^* \xi_m &= \delta_{k,m}, \end{aligned} \tag{4.6}$$

with which we can now expand our solutions to include the effects of DMI as a perturbation.

We propose a linear superposition of the local and travelling modes,

$$\chi(y) = i\delta\phi(y) + \delta\theta(y) = ic_{loc}\xi_{loc}(y) + \sum_k d_k \xi_k(y), \tag{4.7}$$

with c_{loc} and d_k representing the amplitudes of the localised and travelling modes respectively, to calculate the spin wave energy. After the space integrals are computed, we find

$$\begin{aligned} \delta E = c_{loc}^2 \left(\frac{\pi D}{4\lambda} + K_\perp \right) + \sum_k \big[A'_k d_k^* d_k + B'_k (d_k^* d_{-k}^* + d_k d_{-k}) \\ + C_k c_{loc}(d_k + d_k^*)] + \sum_{km} U_{km}\, d_k^* d_m + V_{km}(d_k d_m + d_k^* d_m^*), \end{aligned} \tag{4.8}$$

where the coefficients are given by

$$\begin{aligned} A'_k &= \omega_k(K_u + K_\perp) - \frac{K_\perp}{2}, \\ B'_k &= \frac{K_\perp}{4}, \\ C_k &= \int dV\ \xi_{loc} \Delta(y)\, \xi_k, \\ U_{km} &= \int dV\ \xi_k^* \Delta(y)\, \xi_m, \\ V_{km} &= \int dV\ (\xi_k \Delta(y) \xi_m + \xi_k^* \Delta(x) \xi_m^*). \end{aligned} \tag{4.9}$$

The A'_k and B'_k terms denote elliptical spin precession as a result of the transverse anisotropy described by $K_\perp$, and correspond to the usual terms found in the Bloch wall

case [69, 104]. The C_k, U_{km} and V_{km} terms are proportional to the strength of D and depend on k because these terms result from the spatial dependent ellipticity.

The C_k term represents the coupling between the local and the travelling modes. It is small compared to the other terms so it will not be considered. U_{km} and V_{km} are scattering terms that describe the transition from a state with momentum $\hbar k$ to another state with $\hbar m$. If we focus on the maximum scattering strength then the specific form of the coefficients, $U_{km} \sim \mathrm{sech}(k-m)$ and $V_{km} \sim \mathrm{sech}(k+m)$, allows us to approximate U_{km} and V_{km} by delta functions δ_{km}, δ_{k-m} respectively. We can then approximate δE as

$$\delta E = c_{loc}^2 \left(\frac{\pi D}{4\lambda} + K_\perp \right) + \sum_k A_k d_k^* d_k + B_k (d_k^* d_{-k}^* + d_k d_{-k}), \tag{4.10}$$

where the first term on the right hand side is discussed below and the coefficients are

$$\begin{aligned} A_k &= \omega_k (K_o + K_\perp) - \frac{K_\perp}{2} + \frac{\pi D}{4\lambda} \frac{(1 + 2k^2\lambda^2)}{\omega_k}, \\ B_k &= \frac{K_\perp}{4} - \frac{\pi D}{8\lambda} \frac{(1 + 2k^2\lambda^2)}{\omega_k}. \end{aligned} \tag{4.11}$$

In the limit $D \to 0$, $K_\perp \to 0$, $B_k = 0$ and the frequency corresponds to that of a uniformly magnetised film, $\Omega_k^u = (1/\hbar)(Ak^2 + K_o)$. Equation (4.10) can be diagonalized by means of a Bogoliubov transformation, $c_k = u_k^+ d_k - u_k^- d_{-k}^*$, $u_k^\pm = \sqrt{(A_k \pm \hbar\Omega_k)/2\hbar\Omega_k}$, to obtain

$$\delta E = c_{loc}^2 \left(\frac{\pi D}{4\lambda} + K_\perp \right) + \sum_k \hbar\Omega_k c_k^* c_k. \tag{4.12}$$

We can write the total energy of the system as

$$E = \sigma + \delta E = \sigma + c_{loc}^2 \left(\frac{\pi D}{4\lambda} + K_\perp \right) + \sum_k \hbar\Omega_k c_k^* c_k, \tag{4.13}$$

where σ (equation (2.22) in Chapter 2) is the energy of the domain wall calculated by considering only the static profile. The term $\sum_k \hbar\Omega_k c_k^* c_k$ is the energy of the spin waves. We can identify the term $c_{loc}^2 \left(\frac{\pi D}{4\lambda} + K_\perp \right)$ with the kinetic energy of the domain wall. It is related to the wall mass that appears because the demagnetising field in the centre of the domain wall is changed due to the wall movement. We define $p^2/(2m_N) \sim c_{loc}^2(\frac{\pi D}{4\lambda} + K_\perp)$, where $m_N \sim 1/[2(\frac{\pi D}{4\lambda} + K_\perp)]$ is the Néel-type domain wall mass. The mass in a Bloch-type wall is $m_B \sim 1/(2K_\perp)$ [69, 70, 74, 100] so $m_N < m_B$ which agrees with a higher mobility in Dzyaloshinskii domain walls [64, 102].

The frequency Ω_k is given by

$$\Omega_k = \frac{(K_o + K_\perp)a^3}{\hbar}\sqrt{\omega_k\left(\omega_k - \frac{K_\perp}{K_o + K_\perp} + \frac{\pi D}{4\lambda(K_o + K_\perp)}\frac{(1 + 2k^2\lambda^2)}{(1 + k^2\lambda^2)}\right)}, \tag{4.14}$$

where $a \sim 0.3$ nm is the lattice constant. We find a critical value, $D_{c2} = 4\sqrt{AK_o}/\pi \sim 3.6$ mJ/m^2, in the limit $k \to 0$ that agrees with previous work [2, 65, 104], above which the domain wall becomes unstable. It is common to find a non-reciprocal dispersion in systems under the influence of the DMI, however, this is not the case for the direction of propagation considered here. It has been shown in previous studies [103, 104] and in section (3.2.1) that the non-reciprocity arises for propagation parallel to the plane of the wall, which in our geometry corresponds to propagation along the x direction. Still, an interesting consequence, related with the reflection of the spin waves, can be envisaged when we write the spin wave eigenmodes in terms of the amplitudes c_k, c^*_{-k},

$$\chi(y) = ic_{loc}\xi_{loc}(y) + \sum_k (c_k u_k^+ + c^*_{-k}u_k^-)\xi_k(y). \tag{4.15}$$

There is a hybridisation between the localised mode, $\xi_{loc}(y)$, and the travelling modes, $\xi_k(y)$ resulting from the DMI and $K_\perp$ which are the terms inducing the ellipticity in the precession. For clarity, we define $\theta_k = c_k + c_k^*$ and $\phi_k = (c_k - c_k^*)/i$, so that the small fluctuations are given by

$$\begin{aligned} \delta\theta(y) &= \sum_k \varepsilon^\theta\, \theta_k\, \xi_k(y), \\ \delta\phi(y) &= c_{loc}\xi_{loc}(y) + \sum_k \varepsilon^\phi\, \phi_k\, \xi_k(y), \end{aligned} \tag{4.16}$$

where the parameters $\varepsilon^\theta = (u_k^+ + u_k^-)/2$ and $\varepsilon^\phi = (u_k^+ - u_k^-)/2$ represent the ellipticity in the spin precession. In a totally symmetric system ($K_\perp = 0$, $D = 0$) the spins are circularly polarised, i.e $\varepsilon^\theta = \varepsilon^\phi = 1/2$.

4.3 Band structure in periodic wall arrays

We have discussed the effects of the DMI in the spin wave dispersion. We now examine how a DMI driven Néel type wall scatters the spin waves. The scattering potential for spin waves in a Bloch ($D = 0$) domain wall is represented by $-\lambda^2\partial_y^2 + V_P(y)$ which

is reflectionless but leads to a a phase shift when spin waves propagate through it [113, 115]. This reflectionless potential corresponds to a specific case of the so called modified Pöschl-Teller Hamiltonian [79],

$$\left[-\alpha^2\partial_y^2 - l(l-1)\,\mathrm{sech}^2(y/\alpha)\right]\,\psi = \epsilon\,\psi. \tag{4.17}$$

The parameter l describes the depth of the potential well, α has units of distance and ϵ is a dimensionless energy for the wave. For a Bloch-type wall, $l = 2$ and $\alpha = \lambda$. The transmission and reflection coefficients related to the wave propagation across this potential have been calculated for this Hamiltonian as a function of the depth

$$|R|^2 = \frac{1}{1+p^2}; \qquad |T|^2 = \frac{p^2}{1+p^2}, \tag{4.18}$$

with $p = \sinh(\pi k\alpha)/\sin(\pi l)$ [116]. From this result it can be seen by inspection that for $l\ \epsilon\ \mathbb{N}$, $|R|^2$ is zero. For the Dzyaloshinskii domain walls, the Hamiltonian is

$$\left[-\lambda^2\partial_y^2 - 2\,\mathrm{sech}^2(y/\lambda) - \frac{D\,\mathrm{sech}(y/\lambda)}{\lambda(K_u+K_\perp)}\right]\chi(y) = E\chi(y), \tag{4.19}$$

where the dimensionless energy is $E = \frac{\hbar\Omega_k}{(K_u+K_\perp)a^3} + \kappa - 1$. The first two terms on the right hand side are the Pöschl Teller potential, equation (4.17) with the depth parameter $l = 2$, the third term only depends on the DMI and is a result of the preferred handedness of the ground state. We define the dimensionless parameter $D' = D/(\lambda(K_o + K_\perp))$. It is possible to write Equation (4.19) as

$$\left[-\lambda^2\partial_x^2 - (2 + D'\cosh(y/\lambda))\,\mathrm{sech}^2(y/\lambda)\right]\chi(y) = E\chi(y), \tag{4.20}$$

from where we can relate the depth l in Equation (4.17) with the DMI part in the effective potential,

$$l(l-1) = 2 + D'\,\cosh y/\lambda \qquad l = \frac{1}{2}\left[1 \pm \sqrt{1 + 4\,(2 + D'\cosh(y/\lambda))}\right]. \tag{4.21}$$

The depth l now has a spatial dependence due to the DMI. To make further progress we examine the form of the total effective potential and compare it with the Bloch-type potential, they are shown as solid lines in Figure (4.2).

Although there is a small deformation in the total effective potential as compared to the Bloch-type one, the main effect of the DMI is to increase the depth l. As the depth is measured at $x = 0$ we then take $\cosh(x/\lambda) = 1$ in Equation (4.21). Furthermore, the

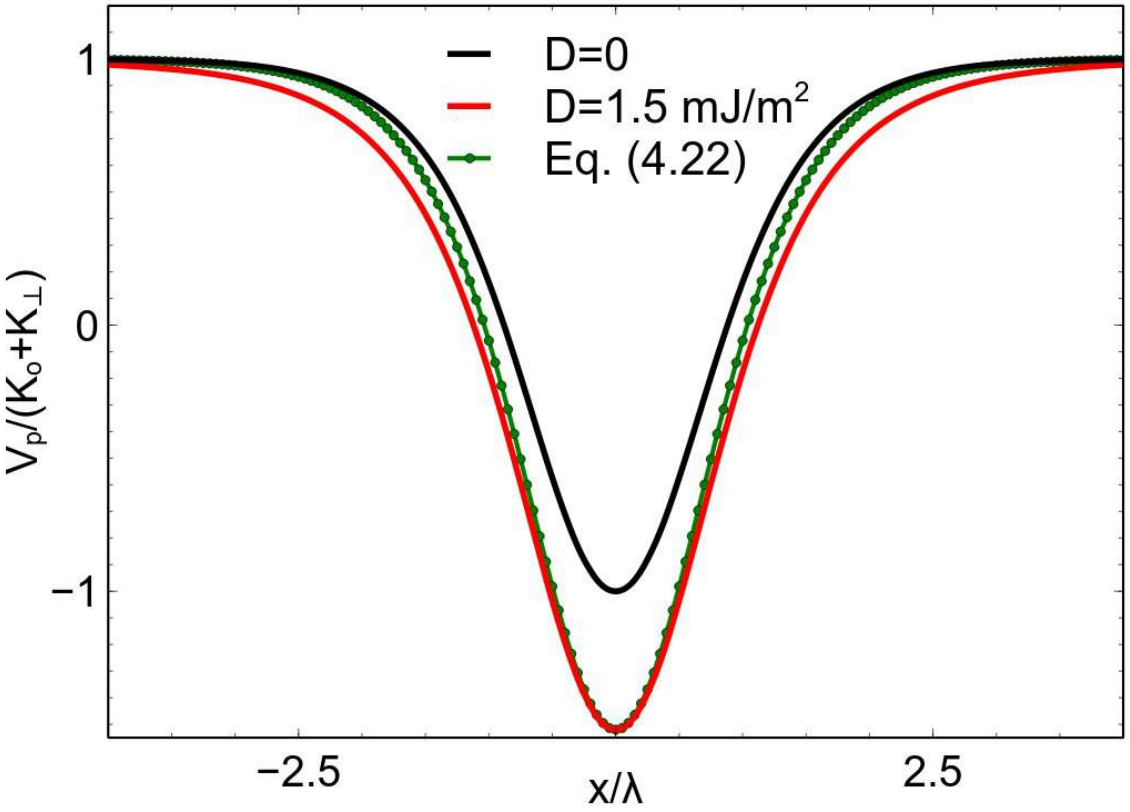

FIGURE 4.2: Effective potentials associated with the domain wall. The solid lines represent the exact form of the potentials, in black for a Bloch-type domain wall and in red for a Dzyaloshinskii domain wall with $D = 1.5$ mJ/m^2. The dotted line is the potential calculated using equation (4.22).

depth increases due to the DMI so that we take the positive root solution in Equation (4.21) as the physical solution. Under these assumptions the depth l is given by

$$l = \frac{1}{2}\left[1 + \sqrt{1 + 4\left(2 + \frac{D}{\lambda(K_u + K_\perp)}\right)}\right]. \tag{4.22}$$

We show the potential obtained using Equation (4.22) as the dotted curve in Figure (4.2), it corresponds to the exact form of a modified Pöschl Teller potential. In the domain wall region $-1 < y/\lambda < 1$ no deformation can be observed, the maximum deviation at $y/\lambda = \pm 1$ is less than a tenth of $V_P/(K_o + K_\perp)$. Note that considering the opposite chirality, $D < 0$, results in a decrease of the depth and then the negative root solution in Equation (4.21) would be the physical solution, and the same considerations apply.

Two transmission coefficients were calculated as a function of the wave vector k using Equation (4.18) and considering equation (4.22) as the depth parameter l. In Figure (4.3) we show as solid lines the analytical calculation of the transmission coefficients

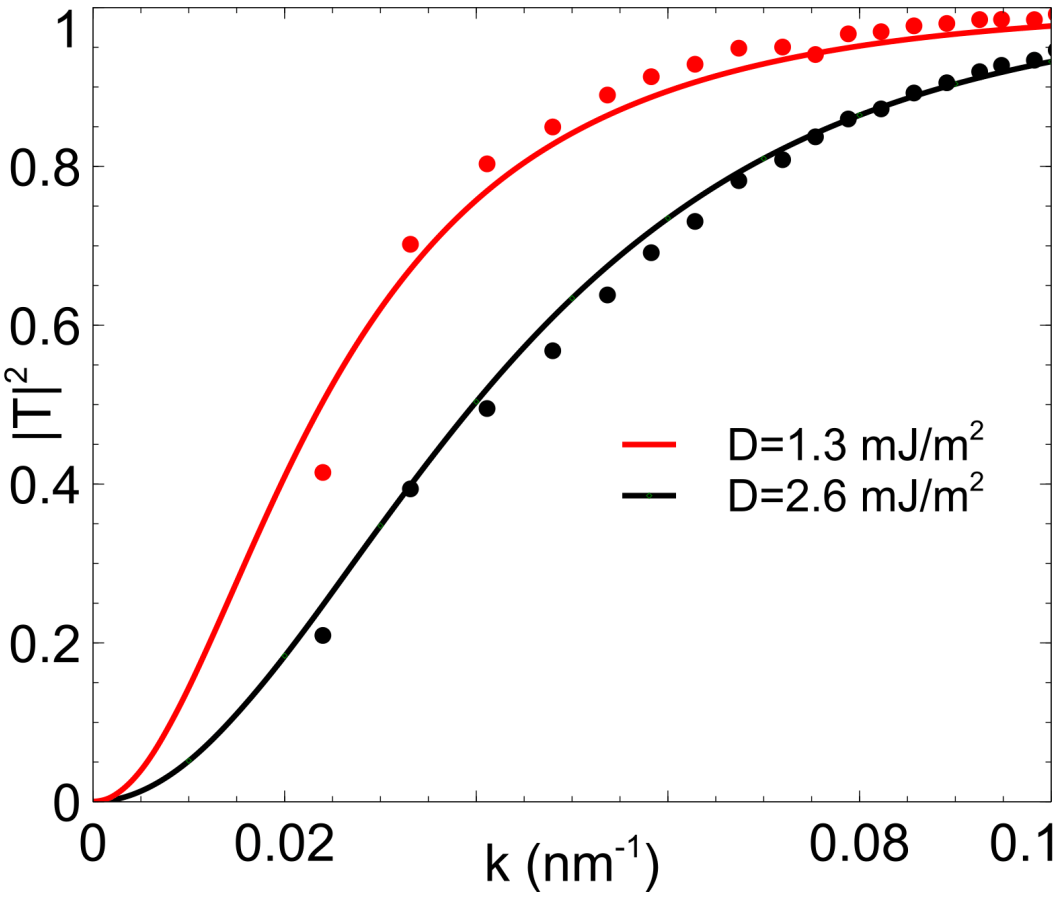

FIGURE 4.3: Transmission coefficient for $D = 1.3$ mJ/m^2 (red) and $D = 2.6$ mJ/m^2 (black). The solid lines result from using equation (4.22) and the points are numerical simulations as described in the text.

for two different values of D, we also present with points numerical calculations as described next.

We use numerical simulations to verify that the assumption made to obtain equation (4.22) is reasonable. The numerical calculations were performed within a micromagnetic model as discussed in section (3.2.1) in Chapter 3 and using the same parameter values [1, 2]. The geometry coincides with the one showed in figure (4.1) and the system size was $12800 \times 50 \times 1$ nm^3 with periodic boundary condition in y direction for numerical reasons. To compare exactly with the analytical model, the calculations were performed without damping term and demagnetizing field. A domain wall was introduced at the centre of the sample and then the system was excited with a monochromatic point source of 50 mT applied field, 1950 nm away from the domain wall. The amplitudes were calculated comparing the average envelope of the spin waves at both sides of the domain wall at the initial stages of the propagation. As D increases significant reflection

is found for larger values of k. This is a direct result of the scattering terms in Equation (4.8).

As a result of the DMI, the scattering effective potential associated with the domain wall produces reflection in the spin waves propagating through it. Spin wave reflection has been demonstrated due to the dipolar interaction in the absence of the DMI for propagation along the x and y direction [90]. In our model, spin waves propagating only along the y direction are reflected which makes it suitable for narrow nano-wires. Spin wave-driven domain wall motion has been explained in terms of linear momentum transfer [87]. When spin waves are reflected from the wall there is a linear momentum transfer. It has been shown that in the theoretical case when no damping is considered the linear momentum transfer leads to a rotation of the plane of the wall but not to domain wall motion [90]. We therefore expect that the inclusion of damping in our model would lead to a domain wall velocity, but the details are beyond the scope of this paper. It is important to emphasize that whatever physical mechanism is used to produce spin wave reflection damping is a key ingredient for linear momentum transfer-domain wall motion.

4.3.1 Magnonic crystal

To present the reflection in a clearer way and to highlight a consequence of the DMI for magnonics, we propose a periodic array of Bloch and Néel-type domain walls as shown in figure (4.4) and calculate the band structure. For any wave propagating in a crystal, Bragg reflection is the characteristic feature responsible for gaps at the edges of the first Brillouin zone, where the Bragg condition is satisfied. Similar to the ion cores in the nearly free electron model, in our case the periodicity of the crystal is determined by the periodic potential that describes the domain walls.

We rewrite the Schrödinger-like equation, equation (4.19),

$$\left[-\lambda^2\partial_y^2 + U(y)\right]\chi(y) = E\chi(y), \tag{4.23}$$

where the effective potential $U(y)$ is given by

$$U(y) = -2\,\mathrm{sech}^2(y/\lambda) - \frac{D\,\mathrm{sech}(y/\lambda)}{\lambda(K_u + K_\perp)}. \tag{4.24}$$

As we know that the effective potential is invariant under a crystal lattice translation, it may be expanded as Fourier series in the reciprocal lattice vectors,

$$U(y) = \sum_G U_G \exp(iGy), \tag{4.25}$$

where U_G are the Fourier coefficients of the potential.

Using Bloch's theorem, the wave function, $\chi(y)$, may be expressed as a Fourier series summed over all the values of the wave vector permitted, so that

$$\chi(y) = \sum_k C(k) \exp(iky). \tag{4.26}$$

The kinetic energy term can also be transformed as

$$-\lambda^2 \partial_y^2 \chi(y) = -\lambda^2 \sum_k k^2 C(k) \exp(iky). \tag{4.27}$$

Inserting equations (4.25), (4.26) and (4.27) in equation (4.19), we obtain

$$\sum_k \lambda^2 k^2 C(k) \exp(iky) + \sum_G \sum_k U_G C(k) \exp(i(k+G)y) = E \sum_k C(k) \exp(iky). \tag{4.28}$$

Each Fourier component must have the same coefficient on both sides of the equation. Thus we have the central equation [117]

$$\left(A\,k^2 - E\right) C(k) + \sum_G U_G C(k-G) = 0. \tag{4.29}$$

Equation (4.29) represents an infinite set of equations connecting the coefficients $C(k-G)$ for all reciprocal lattice vectors G. These equations are consistent if the determinant of the coefficients is zero. It is often only necessary to consider the determinant of a few coefficients. For our calculations an 11×11 matrix is used to numerically solve the central equation.

The period of the Dzyaloshinskii domain wall crystal can be determined with the Kooy-Enz formula that describes the stray field energy for an arrangement of parallel band domains separated by domain walls of zero width.[118] For a particular case of $D = 2.6$ mJ/m^2 and a film thickness of 2 nm, the period is found to be $L = 100$ nm. The order of magnitude of the calculated period agrees with previous experimental

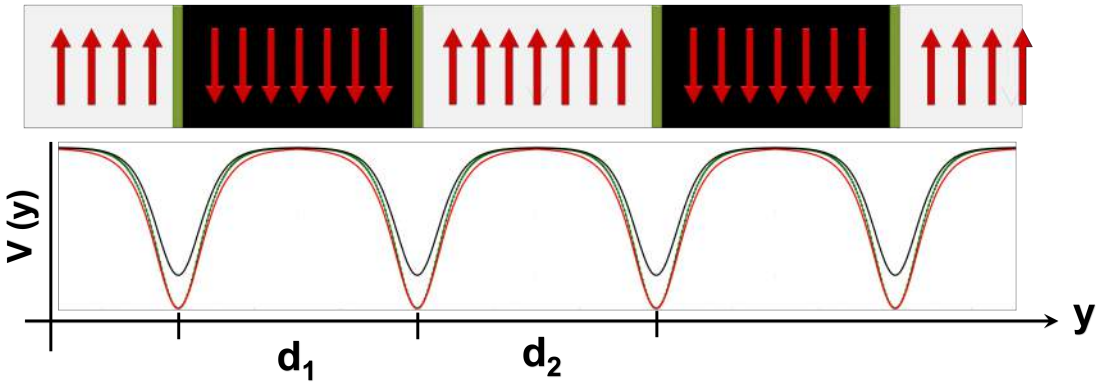

FIGURE 4.4: Periodic array of domain walls. A narrow nano-wire is considered with alternating domains that are denoted by the red arrows. In the lower part of the figure the effective potentials associated with Bloch and Néel type walls are presented. The period of the array is $d_1 + d_2$.

results obtained in a system of two monolayers of iron on top of tungsten where the magnetic period was found to be 50 ± 5 nm [65, 119]. We note also that this period depends on the magnitude of an external applied magnetic field, thus the periodicity can be adjusted with consequences on the band structure.

The calculated band structure of a domain wall crystal is shown in Figure (4.5). Our results are presented using the reduced zone scheme in which k is in the first zone, $-\pi/L \leq k \leq \pi/L$, and G is allowed to run over the appropriate reciprocal lattice points. The wave eigenfunctions at $k = \pm\pi/a$, where Bragg's condition is satisfied, are not travelling but standing waves formed by incident and reflected contributions. The origin of the gap can be understood by considering the probability densities. For a pure travelling wave, $\psi = \exp(iky)$, its probability density is $\rho = |\psi|^2 = 1$, which is independent of the space coordinate and therefore of k. In contrast, for standing waves, $\psi_s \sim \sin(\pi y/L)$, the probability density, $\rho = |\psi_s|^2 \propto \sin^2(\pi y/L)$, vanishes for $y = L$ which corresponds to the centre of the potential and to $\pm\pi/a$ in k space producing gaps. When the periodic array consists of Bloch-type walls (figure 4.5(a)) there is no reflected contribution and the spin wave travelling modes, $\chi_k(y)$ (equation 4.5), do not produce gaps. However, the DMI favours the formation of Néel-type walls (figure 4.5(b)) that reflect the spin waves described by the hybridised mode, $\chi(y)$ (equation 4.15), causing the gaps in the band structure. Note that the translational invariance prevents the formation of a band structure for propagation along the x axis.

Figure (4.6) shows the first gap frequencies as a function of $D < D_{c2}$ in $k = 0$ and $k = \pi/L$. For $k = 0$, the gap frequency increases monotonically for the values of D

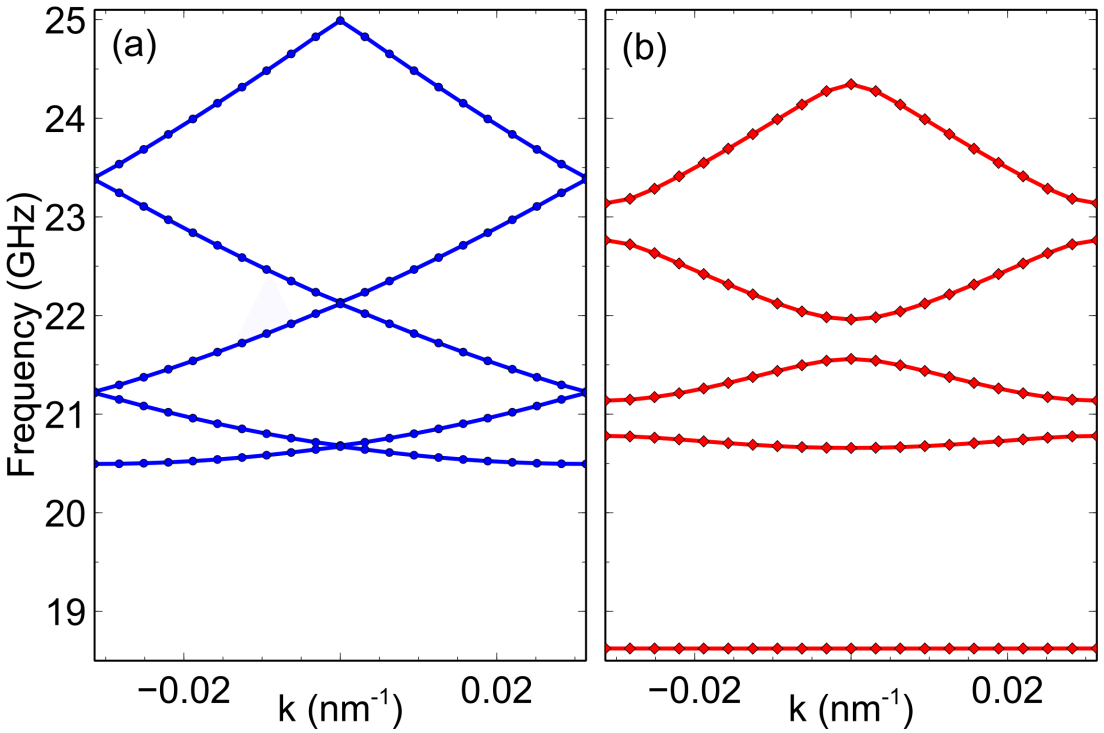

FIGURE 4.5: Calculated band structures of a domain wall crystal. No gaps at the edges of the Brillouin zone are found when the domain walls forming the periodic array are of the Bloch-type (a). In contrast, (b) shows the band structure of a periodic array of Dzyaloshinskii domain walls where gaps of different magnitudes determined by the strength of the DMI ($D = 1.56$ mJ/m^2) are found at the edges of the Brillouin zone.

considered, while for $k = \pi/L$ the gap reaches a maximum which for the parameters used in this work is $\Delta F \sim 0.5$ GHz.

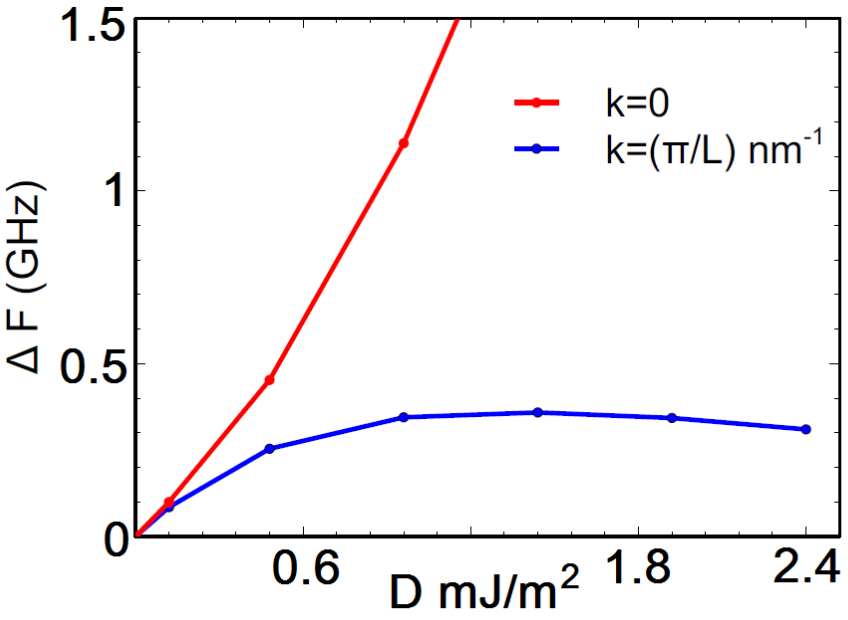

FIGURE 4.6: Frequency gaps ΔF at the Brillouin zone boundary as a function of D_c. $L = 100$ nm^{-1} is the period of the crystal.

Discussion and Concluding Remarks for Chapter 4

We have discussed the effects of the interface form of the DMI on spin waves propagating perpendicular to the plane of a DMI-driven Néel domain wall. Unlike the common non-reciprocal dispersion found in other systems with DMI [41, 42, 44], we find a frequency shift as compared to the dispersion found in Bloch-type walls. We calculate the spin wave eigenstate and find that the localised mode hybridises with the travelling modes as a result of an extra chiral term in the effective potential that describes the domain wall. While in Bloch-type walls spin waves are not reflected and only acquire a phase shift [83], we find that the DMI term in the effective potential scatters the spin waves and leads to reflection.

We propose a periodic array of domain walls to highlight the reflection phenomenon. The band structure of the array exhibits gaps that resemble the ones found in magnonic crystals [18, 120]. An advantage of our proposed model over magnonic crystals based on nanostructures with alternating magnetic parameters relies in the fact that an external, applied magnetic field can be adjusted to modify the width of the domains suggesting the possibility of a tunable device. Acoustic and optical bands, and control over the frequency gaps are immediate consequences of such a tunable crystal. Another advantage of our model comes from the fact that domain walls are natural elements that minimise the energy of a magnetic system and therefore would at least ease some

nanofabrication issues. Nevertheless, we recognise that the stabilisation of the domains would be rather difficult because of magnetostatic effects, treated here within a local approximation, that would prevent straight and planar walls to be formed. Narrow nanowires might relieve this problem. Moreover, spin wave damping is expected to be enhanced due to the spin-orbit origin of the DMI. While for the gaps in the band structure our proposal may still find applications in samples with relatively weak DMI with consequently small band gaps, another phenomenon may be enhanced: spin wave driven-domain wall motion due to linear momentum transfer is known to depend linearly on the damping [69, 121].

Chapter 5

Energy, and linear and angular momentum

In this chapter we use the symmetry properties of a magnetic Lagrangian that includes the interface form of the DMI to find the conserved physical quantities in a perpendicularly magnetised film. We use Noether's theorem [105, 106, 122] to find continuity equations for energy, linear momentum, and total angular momentum. The effect of the DMI on these systems is an interesting fundamental problem simply because of the nature of spin orbit coupling and so the conservation of the total angular momentum needs to be examined.

While the flux of energy is not affected by the DMI for perpendicular materials, we find that there is a contribution from the DMI to the energy flux in the direction consistent with a non-reciprocal spin wave dispersion found in previous studies [34, 41, 42]. We consider the linear momentum transfer from spin waves to a domain wall and find that the DMI exerts no extra pressure on the wall in perpendicular materials under consideration, but for in-plane geometries a non-vanishing DMI term increases the domain wall velocity in agreement with previous results [91]. Finally, we calculate the z component of the total angular momentum and find that it consists of an orbital and a spin part as in reference [90]. The z component of the total angular momentum is conserved as long as there is not a net flux of it through the system boundaries. The orbital part is not conserved because of the DMI. We demonstrate that angular momentum transfer from the orbital part to the spin part described by the magnetic moments needs to occur for the total angular momentum to be conserved. This angular momentum transfer leads to domain wall motion.

5.1 Energy-momentum Tensor

The phenomenological description of a ferromagnet with magnetisation vector $\mathbf{m}(\mathbf{r}, t)$ in the long wavelength approximation is given by the Landau-Lifshitz equation,

$$\frac{\partial \mathbf{m}}{\partial t} = -\gamma\mu_0 \left(\mathbf{m} \times \mathbf{H}_{\mathbf{eff}}\right). \tag{5.1}$$

Here, $\mathbf{H}_{\mathbf{eff}} = -(1/\mu_0 M_s)\delta H/\delta \mathbf{m}$ is the effective magnetic field obtained by calculating the variational derivative of the energy of the system, $H = \int dV\, \mathcal{H}$. In a thin film the form of the free magnetic energy density of the system is, as before (equation (4.1)),

$$\mathcal{H} = A(\nabla \mathbf{m})^2 + D[m_z(\nabla \cdot \mathbf{m}) - (\mathbf{m} \cdot \nabla)m_z] - K_o m_z^2. \tag{5.2}$$

Where the first term describes the isotropic part of the exchange interaction through the exchange stiffness constant A, the second term is the interface form of the DMI, and the third term is an effective uniaxial anisotropy along the z axis described by the constant $K_o = K_u - \mu_0 M_s^2/2$ which includes a magneto-crystalline part given by K_u and demagnetising effects in the local approximation. We can write the Lagrangian density of the system in terms of the projection $M_s m_z/\gamma$ of the angular momentum density vector $M_s\mathbf{m}/\gamma$ onto the z axis and the corresponding azimuthal angle $\phi = \arctan(m_y/m_x)$ as (see equation (3.4) in Chapter 4),

$$\mathcal{L} = \frac{M_s}{\gamma} m_z \dot{\phi} - \mathcal{H}, \tag{5.3}$$

where again we define a kinetic term $\frac{M_s}{\gamma} m_z \dot{\phi}$. The independent variables are ϕ, and m_z. Equation (5.1) results from calculating the Euler-Lagrange equations as in equation (3.9).

We now explore the symmetry properties of the Lagrangian to find the conserved quantities of the system. A transformation that changes the Lagrangian density only by a total derivative is symmetric. The absence of an explicit dependence on the coordinates t and x_i means that the Lagrangian is invariant under a transformation of those coordinates. In particular, invariance under time displacements leads to the conservation of energy, while spatial translational (rotational) symmetry implies conservation of linear (angular) momentum.

Noether's theorem formally describes the connection between invariance or symmetry properties and conserved quantities [122] (see e.g. [105, 106] for a more recent derivation).

It states that a continuous transformation of coordinates under which the action remains invariant yields the conservation of the corresponding physical quantity in terms of a continuity equation,

$$\frac{\partial \rho}{\partial t} + \nabla \cdot \mathbf{j} = 0, \tag{5.4}$$

where ρ is the conserved quantity and $\mathbf{j}$ is the current or flux of the conserved quantity. A common example is found in electromagnetism where ρ is the electric charge and $\mathbf{j}$ is the electric current [110]. The probability density in quantum mechanics [123] and the fluid density in fluid dynamics [124] are other examples.

The general form of Noether's theorem is rather complicated and is commonly given in tensor notation. It is based on the invariance of the action

$$S = \int dt\, L(q, \frac{\partial q}{\partial x}, x), \tag{5.5}$$

with $L = \int dV\, \mathcal{L}$, under transformations of the form $x \to x + \delta x$, and $q \to q + \delta q$, where x represents the spatio-temporal coordinates, (x, y, z, t) and q the generalised coordinates, (ϕ, m_z). To present it in a clearer way we consider a system that depends only on time, t, and the space coordinate, x. Generalisation to a system that depends on more space coordinates is immediate. Noether's theorem is,

$$\begin{aligned} &\frac{\partial}{\partial t}\left(\frac{\partial \mathcal{L}}{\partial(\partial q/\partial t)}\frac{\partial q}{\partial x}\delta x + \frac{\partial \mathcal{L}}{\partial(\partial q/\partial t)}\frac{\partial q}{\partial t}\delta t - \mathcal{L}\delta t - \frac{\partial \mathcal{L}}{\partial(\partial q/\partial t)}\delta q\right) + \\ &\frac{\partial}{\partial x}\left(\frac{\partial \mathcal{L}}{\partial(\partial q/\partial x)}\frac{\partial q}{\partial x}\delta x + \frac{\partial \mathcal{L}}{\partial(\partial q/\partial x)}\frac{\partial q}{\partial t}\delta t - \mathcal{L}\delta x - \frac{\partial \mathcal{L}}{\partial(\partial q/\partial x)}\delta q\right) = 0, \end{aligned} \tag{5.6}$$

where δx and δt denote the continuous transformation of the space and time coordinate respectively.

As was mentioned above, invariance of the Lagrangian under a time displacement yields the conservation of energy, so we consider $\delta x = \delta q = 0$ and $\delta t = \delta \epsilon$ an arbitrary infinitesimal translation of the time coordinate. In this case,

$$\frac{\partial}{\partial t}\left(\frac{\partial \mathcal{L}}{\partial(\partial q/\partial t)}\frac{\partial q}{\partial t} - \mathcal{L}\right) + \frac{\partial}{\partial x}\left(\frac{\partial \mathcal{L}}{\partial(\partial q/\partial x)}\frac{\partial q}{\partial t}\right) = 0, \tag{5.7}$$

which is in the form of a continuity equation. The first term under the time derivative is the energy density of the system, while the term under the space derivative is the energy flux. They are discussed in detail below.

Invariance of the Lagrangian under a continuous space transformation results in the conservation of the linear momentum of the system. In this case $\delta t = \delta q = 0$ and $\delta x = \delta\epsilon$,

$$\frac{\partial}{\partial t}\left(\frac{\partial \mathcal{L}}{\partial(\partial q/\partial t)}\frac{\partial q}{\partial x}\right) + \frac{\partial}{\partial x}\left(\frac{\partial \mathcal{L}}{\partial(\partial q/\partial x)}\frac{\partial q}{\partial x} - \mathcal{L}\right) = 0, \tag{5.8}$$

and we can repeat the argument to see that linear momentum density is the first term on the left and the term under the space derivative is the momentum current. These physical quantities are treated in detail later in this Chapter.

Throughout these calculations there has been no mathematical distinction between space and time, they are both treated as coordinates. It is possible to compact the notation with the help of the so called energy-momentum tensor also considering a dependence on x and y,

$$T_{\mu\nu} = \frac{\partial q}{\partial x_\mu}\frac{\partial \mathcal{L}}{\partial(\partial q/\partial x_\nu)} - \delta_{\mu\nu}\mathcal{L}, \tag{5.9}$$

where $\delta_{\mu\nu}$ is the Kronecker delta and μ, ν are the spatio-temporal coordinates, t, x and y. This tensor is the conserved quantity of the system under a spatio-temporal translational invariance, with the following continuity equations for the energy and components of the linear momentum,

$$\begin{aligned}
\frac{\partial \mathcal{H}}{\partial t} =& \frac{\partial T_{tt}}{\partial t} = -\nabla \cdot (T_{tx}, T_{ty})\,; \\
\frac{\partial p_x}{\partial t} =& \frac{\partial T_{xt}}{\partial t} = -\nabla \cdot (T_{xx}, T_{xy})\,; \\
\frac{\partial p_y}{\partial t} =& \frac{\partial T_{yt}}{\partial t} = -\nabla \cdot (T_{yx}, T_{yy})\,.
\end{aligned} \tag{5.10}$$

The conserved physical quantities are on the left hand side acted by the time derivative operator, on the right hand side under the space derivative operator are the currents. We now address the effects of the DMI in these conserved quantities.

5.1.1 Energy

The T_{tt} component of the tensor is the energy density of the system, $\mathcal{H}$, while the T_{ti} components are the energy flux in the i direction. They satisfy the continuity equation,

$$\frac{\partial \mathcal{H}}{\partial t} = \frac{\partial T_{tt}}{\partial t} = -\frac{\partial T_{ti}}{\partial x_i}. \tag{5.11}$$

The T_{ti} components,

$$\begin{aligned} T_{tx} &= -2A\left(\dot{\mathbf{m}}\cdot\frac{\partial\mathbf{m}}{\partial x}\right) + D\left(m_x\dot{m}_z - \dot{m}_x m_z\right); \\ T_{ty} &= -2A\left(\dot{\mathbf{m}}\cdot\frac{\partial\mathbf{m}}{\partial y}\right) + D\left(m_y\dot{m}_z - \dot{m}_y m_z\right), \end{aligned} \tag{5.12}$$

calculated from equation (5.9), have the first term related to the isotropic exchange and the second to the DMI. Just as in the case where the Poynting vector, quadratic in the amplitude of the electric and magnetic fields, transports the electromagnetic energy, in this case the spin waves are responsible for the energy flux. The spin waves are small fluctuations, circularly polarised in the XY plane described by

$$\begin{aligned} m_+ &= m_x + i\,m_y = \rho_k \exp[i(\mathbf{k}\cdot\mathbf{r} - \Omega_k t)]; \\ m_- &= m_x - i\,m_y = \rho_k^* \exp[-i(\mathbf{k}\cdot\mathbf{r} - \Omega_k t)], \end{aligned} \tag{5.13}$$

where ρ_k, $\mathbf{k}$, and Ω_k are the spin wave amplitude, wave vector, and frequency respectively.

In this case, it can be seen by inspection that the DMI does not affect the energy flux in the film as $\dot{m}_z = 0$ and the terms $\dot{m}_i m_z$ are not quadratic in the amplitudes, i.e., $\dot{m}_i m_z \simeq (\dot{m}_+ + \dot{m}_-)/2$, since $m_z \simeq 1$. It is instructive to derive the contribution from the isotropic part of the exchange interaction to the energy flux as the procedure is used in following calculations. The energy flux along the x direction is given by the T_{tx} component of the energy-momentum tensor,

$$T_{tx} = -2A\left(\frac{\partial m_x}{\partial t}\frac{\partial m_x}{\partial x} + \frac{\partial m_y}{\partial t}\frac{\partial m_y}{\partial y}\right) = -A\left(\frac{\partial m_+}{\partial t}\frac{\partial m_-}{\partial x} + \frac{\partial m_-}{\partial t}\frac{\partial m_+}{\partial x}\right), \tag{5.14}$$

using equation (5.13) and calculating the derivatives we obtain

$$T_{tx} = 2A\,|\rho_k|^2\,\Omega_k\,k_x = \frac{\hbar\Omega_k}{a^3}\,v_x^g\,|\rho_k|^2, \tag{5.15}$$

where $v_x^g = \partial\Omega_k/\partial k_x$ is the spin wave group velocity obtained from the dispersion relation of a uniformly magnetised film, $\Omega_k = a^3/(\hbar)(Ak^2 + K_o)$ with $a \sim 0.3$ nm the lattice parameter.

The above calculations were performed for spin waves with wave vector, k_x. To obtain the total contribution to the energy flux we need to sum over all the possible wave vectors. After summation, an interesting corpuscular interpretation can be given. The squared amplitude is related to the number of magnons per unit volume, $n_k = |\rho_k|^2/a^3$,

with momentum $\hbar k_x$ so that the total energy flux is

$$T_{ti} = \sum_{k_i} \hbar\Omega_k \, v_i^g \, n_k \tag{5.16}$$

which states that the energy flux associated with the spin waves is in fact the magnon energy flux.

However, it is known that the DMI tilts the magnetisation at the edges of the sample because the DMI acts like a pinning term in the boundary conditions [103]. Suppose that the magnetisation is tilted an angle θ_0 with respect to the normal of the film in the plane $\phi_0 = \pi/2$ in agreement with the boundary conditions, equation (3.10) in Chapter 3. In this case the magnetisation components are described in spherical coordinates as

$$\begin{aligned} m_x &= -\delta\phi \, \sin\theta_0 \\ m_y &= \sin\theta_0 + \, \delta\theta \, \cos\theta_0 \\ m_z &= \cos\theta_0 - \delta\theta \, \sin\theta_0, \end{aligned} \tag{5.17}$$

where the small fluctuations, $(\delta\theta(x,y,t), \delta\phi(x,y,t))$, or spin waves, are the energy transporters. We introduce $\psi = i\delta\theta + \delta\phi$ and its complex conjugate $\psi^* = -i\delta\theta + \delta\phi$ to calculate the DMI part of the energy flux following the procedure used to obtain equation (5.14). While in the y direction the DMI produces no energy flux, in the x direction the flux is

$$T_{tx} = D\left(m_x \dot{m}_z - \dot{m}_x m_z\right) = D\frac{\sin^2\theta_0}{2i}\left(\psi^*\frac{\partial\psi}{\partial t} - \frac{\partial\psi^*}{\partial t}\psi\right), \tag{5.18}$$

where we have only kept terms that are quadratic in the fluctuations because these are the terms relevant for the energy flux. It has the form of a current as expected. By inspection we note that the case $\theta_0 = 0$ which corresponds to a uniformly magnetised film along the z direction agrees with our claim that the DMI does not affect the energy flux. For $\theta_0 = \pi/2$ the DMI contribution is maximum. This case corresponds to an in-plane geometry or to the centre of a domain wall where the magnetisation lies in the plane.

Considering ψ as a plane wave similar to $m_\pm$ described above we can calculate the time derivative to obtain

$$T_{tx}^D = -D\sum_{k_x} \Omega_k \, |\rho_k|^2. \tag{5.19}$$

It has been shown that for in-plane magnetisation the dispersion relation exhibits a strong non reciprocity which depends on the DMI [41, 42]. The fact that the DMI induces an extra energy flux in the x direction but not in the y direction is related with the non-reciprocal dispersion. To show this we write the total energy flux in the x direction, including the isotropic exchange

$$T_{tx} = \sum_{k_x} \Omega_k (2Ak - D)|\rho_k|^2. \tag{5.20}$$

Relating the term $(2Ak - D)$ with the group velocity as was done in equation (5.15), $\partial\Omega_k/\partial k = a^3/(\hbar)(2Ak - D)$, it is possible to see the non-reciprocal dispersion, after integration over k_x. A term linear in the wave vector appears, $D\,k_x$, making the dispersion asymmetric with respect to $k_x = 0$. This is consistent with previous results [44, 45, 47], namely that the in-plane field tilts the magnetisation at an angle θ_0 from the z axis and hence allows to measure the non-reciprocity and give an experimental value of the DMI parameter D.

In summary, we observe that the non-reciprocity dispersion found for certain geometries and under the influence of the DMI leads to a net energy flux along the direction of the non-reciprocity.

5.1.2 Linear Momentum

We now turn to the linear momentum part of the energy-momentum tensor. The components T_{it} represent the i components of the linear momentum density and are,

$$p_i = T_{it} = \frac{M_s}{\gamma} m_z \frac{\partial \phi}{\partial x_i}. \tag{5.21}$$

Note that the units on the right hand side are [A/m·sJ/(Am^2)· 1/m]=[Kg·m/s·(1/m^3)] and correspond to a linear momentum density. Again we make a connection with a corpuscular interpretation of linear momentum. To do so we express the z component of the magnetisation in terms of the amplitudes of the spin waves as $m_z = 1 - |\rho_k|^2/2$ [125]. The linear momentum density is then

$$p_i = \frac{M_s}{\gamma}\frac{\partial \phi}{\partial x_i} - \frac{M_s}{\gamma}\frac{|\rho_k|^2}{2}\frac{\partial \phi}{\partial x}, \tag{5.22}$$

where the first term on the right hand side does not depend on the spin waves and can be considered as the momentum associated with the static magnetic structure. For a domain wall, the angle ϕ determines the plane of the wall which is a constant for the static case. However, when the wall moves, the wall magnetic moments are tilted from the rotation plane [88, 89]. The second term depends on the number of magnons through the relation $n_k = M_s|\rho_k|^2/(2\hbar\gamma)$ [125]. Then the linear momentum density can be written as

$$p_i = \frac{M_s}{\gamma}\frac{\partial\phi}{\partial x_i} - n_k\hbar k_i \tag{5.23}$$

where we have calculated $\partial\phi/\partial x$ using equation (5.13) and following the same procedure that led to (5.14).

The continuity equation for the linear momentum,

$$\frac{\partial p_i}{\partial t} = -\left(\frac{\partial T_{ix}}{\partial x} + \frac{\partial T_{iy}}{\partial y}\right), \tag{5.24}$$

states that the variation of the linear momentum with time is equal to the space divergence of a linear momentum current, (T_{ix}, T_{iy}). The spatial part of the tensor T_{ij} is the force per unit area in the direction i acting on an element of surface oriented in the j direction. The diagonal components,

$$\begin{aligned} T_{xx} &= -\left[2A\left(\frac{\partial\mathbf{m}}{\partial x}\right)^2 + D\left(m_z\frac{\partial m_x}{\partial x} - m_x\frac{\partial m_z}{\partial x}\right) + \mathcal{L}\right]; \\ T_{yy} &= -\left[2A\left(\frac{\partial\mathbf{m}}{\partial y}\right)^2 + D\left(m_z\frac{\partial m_y}{\partial y} - m_y\frac{\partial m_z}{\partial y}\right) + \mathcal{L}\right], \end{aligned} \tag{5.25}$$

with $\mathcal{L}$ given by equation (5.3), correspond to pressures, while the off-diagonal components,

$$\begin{aligned} T_{xy} &= -\left[2A\left(\frac{\partial\mathbf{m}}{\partial x}\cdot\frac{\partial\mathbf{m}}{\partial y}\right) + D\left(m_z\frac{\partial m_y}{\partial x} - m_y\frac{\partial m_z}{\partial x}\right)\right]; \\ T_{yx} &= -\left[2A\left(\frac{\partial\mathbf{m}}{\partial x}\cdot\frac{\partial\mathbf{m}}{\partial y}\right) + D\left(m_z\frac{\partial m_x}{\partial y} - m_x\frac{\partial m_z}{\partial y}\right)\right], \end{aligned} \tag{5.26}$$

are shears.

Conservation of linear momentum can give us information about the dynamics of a domain wall. Consider two domains in the XY plane separated by a 180° domain wall, see figure (3.1). For $y < 0$ the magnetisation, M_s, points along the z. We calculate the momentum current in the two domains where the z component of the magnetisation is

nearly a constant $M_s m_z \simeq M_s$. The considered geometry results in a one-dimensional problem where only the difference in the pressure, T_{yy}, from one domain to the other is relevant,

$$T_{yy}(I) - T_{yy}(II) = 2\frac{M_s}{\gamma} m_z \dot{\phi} + D\left(m_z \frac{\partial m_x}{\partial x} - m_x \frac{\partial m_z}{\partial x}\right) \tag{5.27}$$

where region I and II are $y < 0$ and $y > 0$ respectively. The carriers of linear momentum are the spin waves of the system, and as for any current it must be quadratic in the wave amplitude. As $m_z \simeq 1$, the second term on the right hand side associated with the DMI does not contribute to the linear momentum transfer. Note, however, that for an in-plane magnetised material the DMI term does not vanish and enhances the linear momentum transfer as has been reported in reference [91].

Conservation of linear momentum assures the $\partial \mathbf{P}/\partial t = 0$. The system has contributions from the domain wall, $\mathbf{P}^{dw}$, and from the magnons $\mathbf{P}^{m}$, such that

$$0 = \frac{\partial \mathbf{P}}{\partial t} = \frac{\partial(\mathbf{P}^{dw} + \mathbf{P}^{m})}{\partial t}. \tag{5.28}$$

Considering only the y direction we integrate equation (5.22) over y to get the total linear momentum, and take the time derivative to obtain

$$0 = \frac{\partial(P_y^{dw} + P_y^{m})}{\partial t} = \frac{2M_s \dot{\phi}}{\gamma} - \frac{M_s}{\gamma}\frac{|\rho_k|^2}{2} v^g \, k_y \tag{5.29}$$

where $\dot{\phi} = (\partial\phi/\partial y)(\partial y/\partial t) = (\partial\phi/\partial y) v^g$ has been used in the last term on the right hand side. The above equation explicitly shows that the linear momentum exerted from the spin waves to the domain wall leads to a rotation of the plane of the wall, $\dot{\phi}$.

Domain wall motion results when Gilbert damping,$\alpha \mathbf{m} \times \dot{\mathbf{m}}$, is included in the system. In this case it is known [121] that domain wall motion is given by

$$\dot{Y} = \alpha\lambda\dot{\phi} = \alpha\lambda\frac{|\rho_k|^2}{4} v^g \, k_y = \alpha\lambda\frac{\hbar\gamma}{2M_s} n_k v^g \, k_y, \tag{5.30}$$

where Y is the centre of the domain wall. This result is in agreement with previous studies [71, 86, 91] and relates the wall velocity with the number of magnons with momentum $\hbar \, k_y$ propagating with a velocity v^g. The motion of the wall is in the same direction as the propagating magnons, this is a common signature of linear momentum transfer-domain wall motion [87, 126].

Our starting point was spin wave reflection by the domain wall. It is known that, in special cases, spin waves are not reflected by domain walls [70, 79, 83]. The inclusion of an explicit dipole interaction in the energy leads to spin wave reflection [90]. We showed in Chapter 4 that the interface form of the DMI also results in spin wave reflection by a domain wall. Whatever mechanism is used to produce spin wave reflection, it is the damping torque that allows domain wall mobility, otherwise there is only a rotation of the plane of the wall [90].

5.1.3 Orbital angular momentum

Another physical quantity can be readily obtained from the energy-momentum tensor. The orbital angular momentum density, l_z, of the system can be calculated in the usual way, in particular the z component is given by

$$l^z = x\, p_y - y\, p_x = x\, T_{yt} - y\, T_{xt}. \tag{5.31}$$

The time rate of change of the z component of total orbital angular momentum, $L_z = \int dV\, l_z$, is

$$\frac{dL^z}{dt} = \int dV \left(x \frac{\partial p_y}{\partial t} - y \frac{\partial p_x}{\partial t} \right) = \int dV \left(x \frac{\partial T_{yt}}{\partial t} - y \frac{\partial T_{xt}}{\partial t} \right), \tag{5.32}$$

written in terms of the corresponding components of the energy-momentum tensor.

We apply the continuity equation, (5.10), to obtain

$$\frac{dL^z}{dt} = -\int dV \left[x \left(\frac{\partial T_{yx}}{\partial x} + \frac{\partial T_{yy}}{\partial y} \right) - y \left(\frac{\partial T_{xx}}{\partial x} + \frac{\partial T_{xy}}{\partial y} \right) \right], \tag{5.33}$$

integration by parts converts this expression to

$$\frac{dL^z}{dt} = -\int dV \frac{\partial}{\partial x_i} \left(x\, T_{yi} - y\, T_{xi} \right) + \int dV \, \left(T_{xy} - T_{yx} \right). \tag{5.34}$$

The first term on the right hand side is in the form of a total divergence integrated over the volume, so it can be transformed to an integral over the surface enclosing the volume. As long as there is no flux of angular momentum flowing through the surface, the first integral vanishes. This may not be the case for systems under the influence of the DMI as the spin orbit coupling interaction is provided by the heavy atoms of the substrate. The second integral on the right hand side depends on the symmetry of the

energy-momentum tensor. For a symmetric tensor, $T_{xy} = T_{yx}$, and L^z is conserved as the second integral is identically zero. However, the DMI leads to an antisymmetric tensor,

$$T_{xy} - T_{yx} = D\left[\left(m_z\frac{\partial m_x}{\partial y} - m_x\frac{\partial m_z}{\partial y}\right) - \left(m_z\frac{\partial m_y}{\partial x} - m_y\frac{\partial m_z}{\partial x}\right)\right], \tag{5.35}$$

and L^z is not conserved. This result finds an analogy in thick films where magnetostatic effects play an important role and cannot be treated with a local approximation as is done in this work. In that case, the dipolar interaction also leads to an antisymmetric energy-momentum tensor and the orbital angular momentum is not conserved [127, 128]. However, a conserved quantity associated with the total angular momentum must be found since the system possesses axial symmetry under spatial rotation around the z axis as long as the DMI is in its interface form. We consider this situation in the next section.

5.2 Total angular momentum

Noether's theorem assures us that for every symmetry in a physical system there is a corresponding conserved quantity. While spatio-temporal translational symmetry results in the continuity equation for the energy-momentum tensor, a rotational symmetry leads to the conservation of angular momentum. For a thin film with a uniaxial anisotropy, the kinetic term, $m_z\dot{\phi}$, in the Lagrangian (equation (5.3)) is invariant only under rotations around the z axis. We introduce the infinitesimal parameters that lead to a rotation around the z axis as $\delta x = -y\delta\epsilon$, $\delta y = x\delta\epsilon$, $\delta m_x = -m_y\delta\epsilon$, $\delta m_y = m_x\delta\epsilon$, and $\delta m_z = 0$, where $\delta\epsilon$ is the infinitesimal rotation parameter and use Noether's theorem, (equation (5.6)), to calculate the conserved quantity associated with this symmetry. We obtain the total angular momentum density by calculating the quantity that is under the action of the time derivative. Using the infinitesimal parameters defined above with equation (5.6),

$$\frac{\partial}{\partial t}\left[\frac{m_z}{(m_x^2+m_y^2)}\left(y\,m_y\frac{\partial m_x}{\partial x} - x\,m_y\frac{\partial m_x}{\partial y} + x\,m_x\frac{\partial m_y}{\partial y} - y\,m_x\frac{\partial m_y}{\partial x} - (m_x^2+m_y^2)\right)\right]. \tag{5.36}$$

The quantity under the time derivative operator is the z component of the total angular momentum density, which we define as j_t^z. It can be written in a more compact notation

as

$$j_t^z = \frac{M_s}{\gamma}\left[-m_z + m_z(\mathbf{r}\times\nabla\phi)_z\right]. \tag{5.37}$$

The first term in the right hand side of equation (5.37) corresponds to the spin angular momentum density, $M_s m_z/\gamma$, and the second to an orbital angular momentum density since it can be written as $(\mathbf{r}\times\mathbf{p})_z$ with $\mathbf{p} = M_s m_z \nabla\phi/\gamma$ the linear momentum density found in equation (5.21).

We calculate the angular momentum current in a similar way as for equation (5.36), only this time we are interested in the quantities associated with the space derivatives,

$$\begin{aligned}\frac{\partial}{\partial x}\left[-y\,T_{xx} + x\,T_{yx} - 2A\left(m_y\frac{\partial m_x}{\partial x} - m_x\frac{\partial m_y}{\partial x}\right) - D(m_z\,m_y)\right] + \\ \frac{\partial}{\partial y}\left[-y\,T_{xy} + x\,T_{yy} - 2A\left(m_y\frac{\partial m_x}{\partial y} - m_x\frac{\partial m_y}{\partial y}\right) + D(m_z\,m_x)\right].\end{aligned} \tag{5.38}$$

The quantities under the space derivatives correspond to the current due to the z component of the angular momentum density and comprise a vector with components (j_x^z, j_y^z).

The continuity equation for the z component of the total angular momentum is

$$\frac{\partial j_t^z}{\partial t} = -\nabla\cdot(j_x^z, j_y^z). \tag{5.39}$$

We now analyse in detail the form of the right hand side of the above equation. The divergence of the angular momentum current, $\nabla\cdot(j_x^z, j_y^z)$, needs to consist of an orbital contribution and a spin contribution as the angular momentum density, as defined by equation (5.37). The spin part is given by the torque equation, (5.1), with z component,

$$\begin{aligned}\frac{M_s}{\gamma}\frac{\partial m_z}{\partial t} =& 2A\left(m_y\frac{\partial^2 m_x}{\partial x^2} + m_y\frac{\partial^2 m_x}{\partial x^2} - m_y\frac{\partial^2 m_x}{\partial x^2} - m_y\frac{\partial^2 m_x}{\partial x^2}\right) \\ &+ 2D\left(m_y\frac{\partial m_z}{\partial x} - m_x\frac{\partial m_z}{\partial y}\right),\end{aligned} \tag{5.40}$$

while the orbital contribution is given by equation (5.34). We write this below in its explicit form

$$\frac{dl^z}{dt} = \frac{\partial}{\partial x_i}\left(x\,T_{yi} - y\,T_{xi}\right) + D\left[\left(m_z\frac{\partial m_x}{\partial y} - m_x\frac{\partial m_z}{\partial y}\right) - \left(m_z\frac{\partial m_y}{\partial x} - m_y\frac{\partial m_z}{\partial x}\right)\right]. \tag{5.41}$$

Combining the spin contribution (equation (5.40)) and the orbital contribution (equation (5.41)) we can write the continuity condition, (5.39), as,

$$\frac{\partial J^z}{\partial t} = -\int dV \, \frac{\partial}{\partial x_i} \left(x \, T_{yi} - y \, T_{xi} \right) + \int dV \, \left[\frac{M_s}{\gamma} \frac{\partial m_z}{\partial t} - \left(T_{xy} - T_{yx} \right) \right], \tag{5.42}$$

where $J^z = \int dV \, j_t^z$. The first integral on the right hand side is in the form of a total divergence integrated over the whole volume and vanishes if there is no angular momentum flow through the surface as discussed above. The second integral on the right hand side of equation (5.42) must be zero as the z component of the angular momentum is conserved inside the volume.

The following condition is then found by writing the explicit form of $T_{xy} - T_{yx}$, (equation (5.35)):

$$\int dV \, \frac{\partial m_z}{\partial t} = \frac{\gamma}{M_s} \int dV \, D \left[\left(m_z \frac{\partial m_x}{\partial y} - m_x \frac{\partial m_z}{\partial y} \right) - \left(m_z \frac{\partial m_y}{\partial x} - m_y \frac{\partial m_z}{\partial x} \right) \right] \tag{5.43}$$

This is the central result of the chapter. It relates the dynamic behaviour of the z component of the magnetisation with a torque-like term that resembles the non-adiabatic damping term [69]. It depends only on the DMI,

$$\frac{\partial m_z}{\partial t} = \frac{D\gamma}{M_s} \left[\Big(\mathbf{m} \times (\hat{i} \cdot \nabla) \mathbf{m} \Big)_{\hat{i}} + \Big(\mathbf{m} \times (\hat{j} \cdot \nabla) \mathbf{m} \Big)_{\hat{j}} \right]. \tag{5.44}$$

To find the other components of the torque it is necessary to repeat the procedure for the x and y components of the total angular momentum. However, the Lagrangian, equation (5.3), is not invariant with respect to rotations about the x or y axis due to the DMI and the effective uniaxial anisotropy that fixes the z axis as the rotational axis. Then, Noether's theorem cannot be applied directly for the symmetry that we have considered. To calculate the continuity equation for the other components of the total (orbital and spin), it is necessary to find a different rotational symmetry.

5.3 Application

It is clear that the condition given in equation (5.43) is fulfilled in the case of perpendicularly magnetised film. The left hand side is zero, $m_z \simeq 1$, while the right hand side

does not involve quadratic terms in the spin wave amplitude because m_z is in every term.

However, it is interesting to apply the conservation condition to a non-uniform spin texture. A suitable texture is a Néel domain wall as this is the stable configuration when the interface form of DMI is considered. The domain wall profile is given by $\phi_0 = \pi/2$ and $\theta_0 = -2\arctan(\exp(\xi))$ and we consider small fluctuations $(\delta\phi, \delta\theta)$ around the equilibrium so that the magnetisation components are, up to first order in the fluctuations,

$$\begin{aligned} m_x &= \delta\phi - \sin\theta_0\,\delta\phi, \\ m_y &= \cos\theta_0\,\delta\theta + \sin\theta_0, \\ m_z &= \cos\theta_0 - \sin\theta_0\,\delta\theta. \end{aligned} \tag{5.45}$$

Equation (5.45) is different from equation (5.17) in that the angle θ_0 now has a spatial dependence, the domain wall profile. Moreover, if we assign to ξ a temporal dependence through the domain wall centre position, $Y(t)$, then $\xi = \frac{y-Y(t)}{\lambda}$, where λ is the domain wall width. The fluctuations depend on ξ and t. Then, the left hand side becomes

$$\int dV\,\frac{\partial m_z}{\partial t} = \int d\xi\,\lambda\,\frac{\partial}{\partial t}\left[-\tanh(\xi) + \operatorname{sech}(\xi)\,\delta\theta(\xi,t)\right]. \tag{5.46}$$

The fluctuations $(\delta\theta, \delta\phi)$ are related to the domain wall spin wave eigenmodes, ψ_k, through $\psi_k = i\delta\theta + \delta\phi$. It is known that there are two kinds of domain wall spin wave eigenmodes. A localised branch that is related to the deformation of the wall and travelling states similar to plane waves but deformed in the vicinity of the wall. As we are interested in the angular momentum transport and because we assume a rigid wall we are only interested in the travelling family, (see section 3.1.2),

$$\psi_k(\xi) = \rho_k \exp\left[i(k_y\lambda\xi - \Omega_k t)\right](\tanh(\xi) - i\,k_y\,\lambda) \tag{5.47}$$

After the time derivative and space integral are computed the result is

$$\partial_t M_z = 2\dot{Y}(t) \tag{5.48}$$

Note that after the integration the spin wave frequency, Ω_k, does not contribute to the dynamical behaviour of $M_z = \int dV\,m_z$.

After integration, and retaining only quadratic terms in the amplitude, the right hand side of equation (5.43) becomes,

$$\frac{\gamma}{M_s}\int dV\, D\left[\left(m_z\frac{\partial m_x}{\partial y}-m_x\frac{\partial m_z}{\partial y}\right)-\left(m_z\frac{\partial m_y}{\partial x}-m_y\frac{\partial m_z}{\partial x}\right)\right]=-2D\,\frac{\gamma\,\rho_k^2}{M_s}\,k_y\lambda. \tag{5.49}$$

We can identify the term $2\gamma D/M_s$ as a velocity previously called the Dzyaloshinskii-Moriya velocity for spin waves [129] which for typical values of $D = 1.5$ mJ/m^2 and $M_s = 1100$ kA/m is of around 76 m/s. Equating (5.48) and (5.49) we obtain,

$$\dot{Y}(t) = -D\frac{\gamma|\rho_k|^2}{M_s}\,k_y\lambda. \tag{5.50}$$

This equation relates the velocity of the domain wall through the coordinate of the centre of the wall with the number of magnons through the squared amplitude of the spin wave with a velocity determined by the DMI parameter, D. The domain wall velocity is opposite to the spin wave propagation in agreement with previous results in which angular momentum transfer is the mechanism to move the wall [86, 91, 126].

The total wall velocity consists of two contributions, one due to linear momentum transfer, equation (5.30), and the one that arises as a result of angular momentum conservation, equation (5.50). While the first requires spin wave damping, the second one does not.

Discussion and Concluding Remarks for Chapter 5

We calculated the energy-momentum of a perpendicularly magnetised film with the interface form of the DMI. While for the considered geometry the DMI does not affect the energy flux nor the linear momentum current, in an in-plane geometry the DMI modifies the energy flux consistent with a non-reciprocal spin wave dispersion usually found in DMI systems [41, 42, 44]. Using the continuity equation for linear momentum we calculated the pressure exerted from the magnons to a domain wall. It is found that the DMI has no explicit effect on the spin wave pressure, unlike the case where an in plane geometry is considered and conservation of linear momentum requires an additional DMI pressure term [91].

The DMI, however, has an implicit effect on domain wall motion by linear momentum transfer in perpendicular materials. The DMI is responsible for the spin wave reflection which is the underlying physical mechanism of linear momentum transfer. Although the dipolar interaction also results in strong spin wave reflection, it needs spin wave propagation oblique to the plane of a sharp wall [90]. DMI-driven reflection has been found for spin waves propagating only perpendicularly to the wall, thus making it suitable for narrow nano-wires. Moreover, damping plays a crucial part in the wall motion process [121]. Without damping, spin wave reflection results in the rotation of the plane of the wall, and it is only the inclusion of a damping torque that allows the domain wall to move. In DMI systems the damping is enhanced by the DMI and hence the domain wall velocity is expected to be larger.

The energy-momentum stress tensor also allows us to calculate the orbital angular momentum of the system by considering the off-diagonal components of the tensor. It is found that under the local approximation of the demagnetising energy made in our work, the antisymmetric nature of the tensor depends entirely on the DMI. Previous results have shown that for thick films in which the dipolar interaction plays an important role, tensor antisymmetry results from this interaction [90]. In both cases the consequence is that the orbital angular momentum is not conserved. However, the symmetry of the system described in terms of the Lagrangian demands the conservation of an angular momentum-related physical quantity.

We obtained the total angular momentum continuity equation. The z component of the total angular momentum density consists of an orbital and a spin part. We found that because of the not conserved orbital part, an angular momentum transfer must occur in the system to satisfy the conservation requirement. In particular, we derived

the form of the angular momentum transfer and applied it to the case of a Néel wall. Domain wall motion can be achieved by spin waves transferring angular momentum to the wall. Consistent with previous works, the direction of the wall velocity is opposite to the propagation of the spin waves [87].

Chapter 6

Conclusions and outlook

We have used an analytical approach within the continuum approximation to observe the effect of the Dzyaloshinskii-Moriya interaction on spin waves in magnetic domain walls in ultra thin ferromagnetic films. The results have allowed us to propose novel possible applications in the field of magnonics to manipulate the spin waves. A non-reciprocal dispersion together with spin wave channelling along the centre of the wall leads to a magnonic wave guide. Spin wave reflection in a periodic array of domain walls results in a tunable device with a band structure that resembles a magnonic crystal. Spin wave driven-domain wall motion is possible due to angular momentum transfer related with the DMI.

We calculated the spin wave dispersion using a perturbative formalism where the DMI interaction is taken as the perturbation. We distinguish two main results depending on the spin wave direction of propagation with respect to the domain wall. We find that for propagation parallel to the wall plane, x direction, the spin waves exhibit a non-reciprocal dispersion, i.e., the frequency Ω is different for spin propagating in opposite directions, $\Omega(k_x) \neq \Omega(-k_x)$. The domain wall acts as a confining potential and spin waves are channelled along the centre of the wall. A magnonic wave guide is based on this phenomenon which we further explore by considering curved tracks stabilised by the DMI.

We find that spin waves propagate through curved geometries without any scattering or loss of coherence. The capacity to propagate spin waves along curved paths is essential for any form of circuit design and is crucial for wave processing schemes that rely on spin wave interference. Furthermore, we show that the group velocity of the channelled spin waves can exceed 1 km/s in the long wavelength limit, useful for information

technologies. The number, spacing, and shape of domain walls can be modified with applied, external fields or with spin-polarised currents resulting in reconfigurable wave guide schemes.

Usual complications related to nanofabrictaion are eased as the spin structure of domain walls are determined primarily by intrinsic magnetic properties. However, we recognise that achieving the stable configuration is a difficult task because of magnetostatic effects that prevent the formation of totally planar domain walls. Increasing the magnitude of the DMI is an option for an enhanced stabilisation, but control over the DMI strength is still at its initial stage. Moreover, there exists a critical D value above which a domain wall is no longer stable.

For propagation perpendicular to the plane of the wall, y direction, spin waves are reflected by the domain wall. Reflection is induced by the DMI distorting the otherwise reflectionless potential used to describe the domain wall. We propose a periodic array of domain walls stabilised by the DMI and calculate the band structure. Frequency gaps, similar to the ones found in a magnonic crystal, appear on the edges of the Brillouin zone. The gaps can act as a filter or wave guide, only allowing spin waves of certain frequency to propagate through the array. An applied, external field can vary the period of the domain wall array leading to control of the frequency gaps. Additionally, the external field can modulate the width of the alternating domains, which we expect can result in the formation of an acoustic and optical branch.

Unlike magnonic crystals, our proposed model does not depend on the nano-fabrication of meta-materials with alternating magnetic properties. However, for our analytical calculations we assumed a planar, straight domain wall, while in reality it is known that the magnetostatic interaction in the centre of the domain wall tend to twist the wall. Considering a narrow nano-wire can minimise the magnetostatic effect. Although a different stable configuration requires more analytical detail we expect the reflection phenomenon to be preserved.

Because of the spin-orbit interaction origin of the DMI we expect a strong damping, which was neglected throughout the calculations. A compromise must be made between the magnitude of the gaps and the propagation length of the spin waves. Still, large damping can result in another phenomenon useful in the magnonics field related to data storage. Spin wave reflection is usually associated with domain wall motion resulting from a linear momentum transfer mechanism. A damping torque, together with spin wave reflection, is necessary to achieve a wall velocity. Physical mechanisms such as

the dipole interaction lead to spin wave reflection which result in domain wall motion. In our case the DMI induces the reflection and increases the damping. Micromagnetic simulations and/or experiments are needed to demonstrate this phenomenon.

Finally, we investigate the conservation of the total angular momentum in a thin magnetic film under the influence of the DMI. We find that the total angular momentum has an orbital contribution and a spin contribution. While the DMI prevents the conservation of each contribution separately, the total angular momentum is conserved under the condition of angular momentum transfer form the orbital part related with the DMI to the spin part given, in the continuum approximation, by the magnetic moments.

The angular momentum transfer is in the form of a torque. We anticipate that for systems influenced by the interface form of the DMI this torque needs to be included in the general equation of motion for the magnetic moments. The analytical form of the torque resembles the non-adiabatic damping contribution (see equation (5.44)) and further investigation in this sense needs to be conducted. Micromagnetic simulations and comparison with experiments can provide further physical insight in this matter by identifying the different contributions to the angular momentum.

We calculate the angular momentum transfer mechanism by considering spin waves propagating in a domain wall. We show that spin wave driven-domain wall motion is achievable. We find that the domain wall velocity direction is opposite to the spin wave propagation. This is the usual signature of angular momentum transfer-domain wall motion. Magnetostatic effects, as the DMI, result in antisymmetric energy-momentum tensor. It is important to determine the effect of the dipole interaction and compare with the effect produced by the DMI. We intend to run micromagnetic simulations to include magnetostatic effects that have been treated in this work within the local approximation.

We have discussed important aspects of the influence of the DMI on spin waves. We have used the results to present possible applications. Still, issues related with the non-linear regime and thermal dependence of the spin waves remain open questions. In particular, we showed that, in perpendicularly magnetised materials, the energy flux and the linear momentum (equations (5.12),(5.25), and (5.26)) involve processes that are cubic or quartic in the spin wave amplitude. Investigation of these higher order terms is necessary. While the formalism used in Chapter 4 deals with thermal magnons, the spin wave driven-domain wall motion phenomenon can be investigated in more

detail. For example, a temperature gradient can be used to initiate the magnon flow necessary to move the wall.

Appendix A

Derivation of the domain wall profile

In this appendix we derive the domain wall profile in the absence of the DMI. We consider equation (2.15),

$$\sin 2\,\theta_0 - 2\lambda_{B,N}^2 \frac{d^2\theta_0}{dy^2} = 0. \tag{A.1}$$

To solve this differential equation we multiply by $-\partial\theta/\partial y$, to obtain

$$2\lambda_{B,N}^2 \frac{\partial\theta}{\partial y}\frac{d^2\theta_0}{dy^2} - \frac{\partial\theta}{\partial y}\sin 2\,\theta_0 = 0. \tag{A.2}$$

We note that the above equation can be written as a total derivative

$$0 = \lambda_{B,N}^2 \frac{\partial}{\partial y}\left(\frac{\partial\theta}{\partial y}\right)^2 + \frac{1}{2}\frac{\partial}{\partial y}(\cos 2\,\theta_0) = \frac{\partial}{\partial y}\left(\lambda_{B,N}^2\left(\frac{\partial\theta}{\partial y}\right)^2 + \frac{1}{2}(\cos 2\,\theta_0)\right), \tag{A.3}$$

so that the term under the y derivative must be a constant,

$$\lambda_{B,N}^2\left(\frac{\partial\theta}{\partial y}\right)^2 + \frac{1}{2}(\cos 2\,\theta_0) = C. \tag{A.4}$$

The constant C is determined by the boundary conditions. The magnetisation far from the wall is aligned along the z direction, i.e. $\theta = 0$. Also, the magnetisation does not

vary far from the wall, so the boundary conditions,

$$\begin{aligned} \theta(y=-\infty) &= 0; \\ \left.\frac{\partial\theta}{\partial y}\right|_{y=-\infty} &= 0, \end{aligned} \tag{A.5}$$

result in $C = 1/2$.

Using the trigonometric relation $\frac{1}{2}(\cos 2\theta - 1) = -\sin^2\theta$, we obtain

$$\lambda_{B,N}^2 \left(\frac{\partial\theta}{\partial y}\right)^2 - \sin^2\theta = 0, \tag{A.6}$$

from where the important relation

$$\frac{\partial\theta}{\partial y} = \pm\frac{1}{\lambda_{B,N}}\sin\theta \tag{A.7}$$

is found. This equation determines the sense of rotation of the domain wall, in the absence of the DMI the energy of the domain wall is degenerate with respect to taking the plus or minus sign, which means that the enegy is degenerate with respect to the chirality of the wall.

The solution to the differential equation (A.7) is found by integrating

$$\int \frac{d\theta}{\sin\theta} = \int \frac{dy}{\lambda} \tag{A.8}$$

from where the domain wall profile, equation (2.16) is obtained,

$$\theta_0(y) = \pm 2\arctan\left[\exp\left(\frac{y - Y_0}{\lambda_{B,N}}\right)\right]. \tag{A.9}$$

Appendix B

Perturbation theory

In this appendix we present the correction to the frequency when the DMI and the dipolar term in the centre of the wall are treated as a perturbation to the magnetic Hamiltonian. We use as the scattering basis the travelling modes, ξ_{loc}, equation (3.19), and repeat the procedure used to calculate the correction using the localised modes, (see equations (3.30) and (3.31)). The corrected frequency is

$$\begin{aligned}\Omega^{D}_{tr,a} &= \frac{2\gamma}{M_s}\left[\pm\frac{\pi D k_x}{2} f(k_y)(1+\operatorname{sech}(\pi k_y \lambda)) + (K_o + K_\perp)\sqrt{\omega_{\mathbf{k}}\left(\omega_{\mathbf{k}} - \kappa + \frac{\pi D}{2(K_o+K_\perp)\lambda} f(k_y)\right)}\right] \\ \Omega^{D}_{tr,b} &= \frac{2\gamma}{M_s}\left[\pm\frac{\pi D k_x}{2} f(k_y)(1-\operatorname{sech}(\pi k_y \lambda)) + (K_o + K_\perp)\sqrt{\omega_{\mathbf{k}}\left(\omega_{\mathbf{k}} - \kappa\right)}\right],\end{aligned} \tag{B.1}$$

where

$$f(k_y) = \frac{1+2k_y^2\lambda^2}{1+k_y^2\lambda^2}. \tag{B.2}$$

Unlike the correction to the localised modes, in this case we have four possible frequencies. This is related to the fact that the DMI lifts the degeneracies for both directions of propagation. In figure (3.12(a)) we present the dispersion relation as a function of k_y and k_x. We observe that in addition to the non-reciprocity found in the k_x direction, there appears two frequency sheets. These sheets correspond to the to the lifting of the degeneracy in the k_y direction. They are symmetric with respect to $k_y = 0$. For the travelling modes there is a clear distinction of the direction in which the domain wall

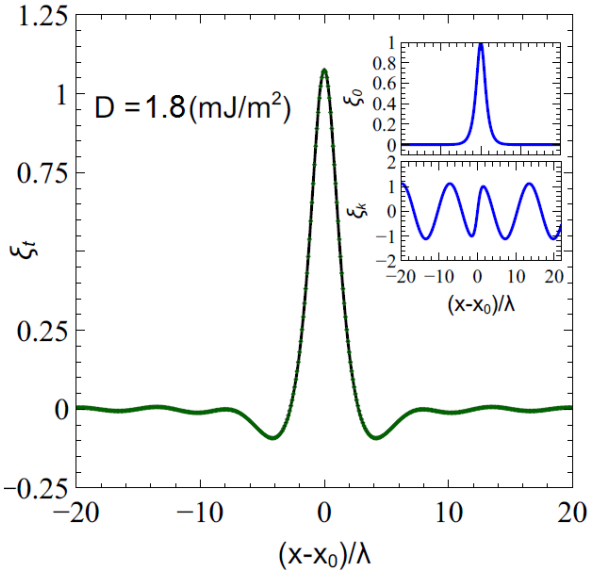

FIGURE B.1: The eigenfunctions of the Pöschl Teller potential that describe the domain wall are shown in the inset of the figure and correspond to the case $D = 0$. For a finite value of the DMI, $D = 1.8$ mJ/m^2 a hybridisation of the modes can be observed. The hybridisation is stronger in the vicinity of the wall

varies. This is a hint that the domain wall reflectionless feature is lost. This effect is discussed in Chapter (4).

To analyse the last statement in more detail, propagation only along the (y) direction is considered and perturbation theory is applied to calculate the corrected eigenfunctions. As the degeneracy in the (x) is not considered, it is necessary to take the two families of solutions as the unperturbed basis. The only term that remains for this direction of propagation is $(D/\lambda)\,\mathrm{sech}(y/\lambda)$. The corrected eigenfunction is given by,

$$\xi_{corr} = \xi_{loc} + \sum_k \frac{\langle \xi_k | D\,\mathrm{sech}(y/\lambda) | \xi_{loc} \rangle}{\omega_k} \xi_k. \tag{B.3}$$

In figure (B.1), we present the calculation of equation (B.3) for $D = 1.8$ mJ/m^2. When $D = 0$ there are two eigenfunctions for the Pöschl Teller potential that describes the domain wall, presented in the inset of figure (B.1). However, for a finite DMI the two families hybridise.

Appendix C

Taylor expansion of the energy functional

In this appendix we derive the spin wave Hamiltonian , equation (4.3), from the energy functional, (4.1). We consider small fluctuations $(\delta\theta, \delta\phi)$ and expand the energy in a functional Taylor series around them using the equilibrium state given by (θ_0, ϕ_0). We assume a one dimensional system depending on x a generalisation to more spatial dimensions is immediate. The Taylor functional expansion is [130]

$$\begin{aligned} E[\theta_0+\delta\theta, \phi_0+\delta\phi] = E[\theta_0,\phi_0]+ \\ + \int dy' \left.\frac{\delta E}{\delta\theta(y')}\right|_{\theta_0,\phi_0} \delta\theta(y') + \int dy' \left.\frac{\delta E}{\delta\phi(y')}\right|_{\theta_0,\phi_0} \delta\phi(y')+ \\ \int dy'dy'' \left.\frac{\delta^2 E}{\delta\theta(y')\delta\phi(y'')}\right|_{\theta_0,\phi_0} \delta\theta(y')\delta\phi(y'')+ \\ +\frac{1}{2}\int dy'dy'' \left.\frac{\delta^2 E}{\delta\theta(y')\delta\theta(y'')}\right|_{\theta_0,\phi_0} \delta\theta(x')\delta\theta(y'')+\frac{1}{2}\int dy'dy'' \left.\frac{\delta^2 E}{\delta\phi(y')\delta\phi(y'')}\right|_{\theta_0,\phi_0} \delta\phi(y')\delta\phi(y'')+ \\ +\cdots \end{aligned} \tag{C.1}$$

The first term on the right hand side is the energy due to the equilibrium configuration, it corresponds to equation (2.17). The second and third terms vanish as these are the equilibrium conditions that allowed us to find the domain wall profile. They correspond to the Euler Lagrange equations (2.14). The last three terms on the right hand side give the second order contribution to the energy, the spin wave contribution.

We consider the magnetic energy of the system and expand it up to first order in fluctuations, $(\delta\theta, \delta\phi)$. It is convenient to treat each energy term separately. For clarity we only analyse the one dimensional case as the generalisation to more spatial dimensions is immediate.

The isotropic exchange interaction is given in spherical coordinates as

$$\epsilon_A = A\left[\left(\frac{\partial\theta}{\partial y}\right)^2 + \sin^2\theta\left(\frac{\partial\phi}{\partial y}\right)^2\right], \tag{C.2}$$

The angles (θ, ϕ) have a stable part $(\theta_0, \phi_0$ and fluctuations $(\delta\theta, \delta\phi)$. After performing the trigonometrical expansion of the terms, neglecting the terms that are quadratic in the fluctuations and the terms that only contribute to the static energy

$$\delta\epsilon_A = 2A\left[\frac{\partial\theta_0}{\partial y}\frac{\partial\delta\theta}{\partial y} + \sin^2\theta_0\frac{\partial\phi_0}{\partial y}\frac{\partial\delta\phi}{\partial y} + \delta\theta\cos\theta_0\left(\frac{\partial\phi}{\partial y}\right)^2\right] \tag{C.3}$$

.

We separate the $\delta\theta(y)$ and $\delta\phi(y)$ terms and take the functional derivative with respect to $\delta\theta(y')$ and $\delta\phi(y')$ to calculate the second order terms in the Taylor expansion, equation (C.1)

$$\frac{\delta\epsilon_A}{\delta\theta(y')} = 2A\left[\frac{\partial\theta_0}{\partial y}\frac{\partial\delta\theta/\partial y}{\delta\theta(y')} + \frac{\delta\theta(y)}{\delta\theta(y')}\frac{\sin 2\theta_0}{2}\left(\frac{\partial\phi}{\partial y}\right)^2\right]. \tag{C.4}$$

We use the following identities [130],

$$\begin{aligned}\frac{\delta u(y)}{\delta u(y')} &= \delta(y-y');\\ \frac{\partial\delta u(y)/\partial y}{\delta u(y')} &= \frac{\partial}{\partial y}\delta(y-y'),\end{aligned} \tag{C.5}$$

to obtain

$$\frac{\delta\epsilon_A}{\delta\theta(y')} = 2A\left[\frac{\partial\theta_0}{\partial y}\frac{\partial}{\partial y}\delta(y-y') + \delta(y-y')\frac{\sin 2\theta_0}{2}\left(\frac{\partial\phi}{\partial y}\right)^2\right]. \tag{C.6}$$

We repeat the procedure to get the second order derivative

$$\frac{\delta^2\epsilon_A}{\delta\theta(y')\delta\theta(y'')} = 2A\left[\frac{\partial}{\partial y}\delta(y-y'')\frac{\partial}{\partial y}\delta(y-y') - \delta(y-y')\delta(y-y'')\cos 2\theta_0\left(\frac{\partial\phi}{\partial y}\right)^2\right]. \tag{C.7}$$

For the $\delta\phi$ part the second order derivative is

$$\frac{\delta^2\epsilon_A}{\delta\phi(y')\delta\phi(y'')} = 2A\sin^2\theta_0\frac{\partial}{\partial y}\delta(y-y'')\frac{\partial}{\partial y}\delta(y-y') \tag{C.8}$$

We insert the second order derivatives calculated, equations (C.7) and (C.8) in the Taylor expansion, equation (C.1).

$$\frac{1}{2}\int dy'dy''\left.\frac{\delta^2 E_A}{\delta\theta(y')\delta\theta(y'')}\right|_{\theta_0,\phi_0}\delta\theta(x')\delta\theta(y'') + \frac{1}{2}\int dy'dy''\left.\frac{\delta^2 E_A}{\delta\phi(y')\delta\phi(y'')}\right|_{\theta_0,\phi_0}\delta\phi(y')\delta\phi(y'') = \frac{1}{2}\int dy\, 2A\left[\left(\frac{\partial\delta\theta}{\partial y}\right)^2 - \delta\theta^2\cos 2\theta_0\left(\frac{\partial\phi}{\partial y}\right)^2 + \sin^2\theta_0\left(\frac{\partial\phi}{\partial y}\right)^2\right]. \tag{C.9}$$

We now insert the stable domain wall profile, equation (4.2).

The same procedure is repeated for the effective anisotropies. We note that the mixed partials for these energy terms are identically zero. We then calculate the DMI term to obtain,

$$\begin{aligned}\delta E = (K_o + K_\perp)\int dy\ \ &\delta\theta\left[-\lambda^2\partial_y^2 + 1 - 2\,\mathrm{sech}^2(y/\lambda)\right]\delta\theta \\ &+ \delta\phi\left[-\lambda^2\partial_y^2 + 1 - 2\,\mathrm{sech}^2(y/\lambda) + \frac{D}{\lambda(K_o+K_\perp)}\,\mathrm{sech}(y/\lambda) - \frac{K_\perp}{K_o+K_\perp}\right]\delta\phi,\end{aligned} \tag{C.10}$$

which is the same as equation (4.3) in Chapter 4 when the definition $V_P(y) = 1 - 2\,\mathrm{sech}^2(y/\lambda)$ is considered. It is important to note that with this unidimensional calculation, only in the direction perpendicular to the plane of the wall the non-reciprocity cannot be obtained. The mixed derivatives are not zero for the DMI term. The consideration of the x direction results in a term that contains a derivative with respect to x from where the non-reciprocity appears.

Bibliography

[1] J.-P. Tetienne, T. Hingant, L. J. Martínez, S. Rohart, A. Thiaville, L. Herrera Diez, K. Garcia, J.-P. Adam, J.-V. Kim, J.-F. Roch, I. M. Miron, G. Gaudin, L. Vila, B. Ocker, D. Ravelosona, and V. Jacques. The nature of domain walls in ultrathin ferromagnets revealed by scanning nanomagnetometry. *Nat Commun*, 6, April 2015. URL http://www.nature.com/ncomms/2015/150401/ncomms7733/full/ncomms7733.html.

[2] André Thiaville, Stanislas Rohart, Émilie Jué, Vincent Cros, and Albert Fert. Dynamics of Dzyaloshinskii domain walls in ultrathin magnetic films. *EPL*, 100 (5):57002, December 2012. ISSN 0295-5075. doi: 10.1209/0295-5075/100/57002. URL http://iopscience.iop.org/0295-5075/100/5/57002.

[3] G. Binasch, P. Grünberg, F. Saurenbach, and W. Zinn. Enhanced magnetoresistance in layered magnetic structures with antiferromagnetic interlayer exchange. *Phys. Rev. B*, 39(7):4828–4830, March 1989. doi: 10.1103/PhysRevB.39.4828. URL http://link.aps.org/doi/10.1103/PhysRevB.39.4828.

[4] M. N. Baibich, J. M. Broto, A. Fert, F. Nguyen Van Dau, F. Petroff, P. Etienne, G. Creuzet, A. Friederich, and J. Chazelas. Giant Magnetoresistance of (001)Fe/(001)Cr Magnetic Superlattices. *Phys. Rev. Lett.*, 61(21):2472–2475, November 1988. doi: 10.1103/PhysRevLett.61.2472. URL http://link.aps.org/doi/10.1103/PhysRevLett.61.2472.

[5] F. Bloch. Zur Theorie des Ferromagnetismus. *Z. Physik*, 61(3-4):206–219, March 1930. ISSN 0044-3328. doi: 10.1007/BF01339661. URL http://link.springer.com/article/10.1007/BF01339661.

[6] T. Holstein and H. Primakoff. Field Dependence of the Intrinsic Domain Magnetization of a Ferromagnet. *Phys. Rev.*, 58(12):1098–1113, December 1940. doi: 10.1103/PhysRev.58.1098. URL http://link.aps.org/doi/10.1103/PhysRev.58.1098.

[7] Conyers Herring and Charles Kittel. On the Theory of Spin Waves in Ferromagnetic Media. *Phys. Rev.*, 81(5):869–880, March 1951. doi: 10.1103/PhysRev.81.869. URL http://link.aps.org/doi/10.1103/PhysRev.81.869.

[8] Freeman J. Dyson. General Theory of Spin-Wave Interactions. *Phys. Rev.*, 102 (5):1217–1230, June 1956. doi: 10.1103/PhysRev.102.1217. URL http://link.aps.org/doi/10.1103/PhysRev.102.1217.

[9] Yaroslav Tserkovnyak, Arne Brataas, and Gerrit E. W. Bauer. Enhanced Gilbert damping in thin ferromagnetic films. *Phys. Rev. Lett.*, 88:117601, Feb 2002. doi: 10.1103/PhysRevLett.88.117601. URL http://link.aps.org/doi/10.1103/PhysRevLett.88.117601.

[10] D. C. Ralph and M. D. Stiles. Spin transfer torques. *Journal of Magnetism and Magnetic Materials*, 320(7):1190–1216, April 2008. ISSN 0304-8853. doi: 10.1016/j.jmmm.2007.12.019. URL http://www.sciencedirect.com/science/article/pii/S0304885307010116.

[11] M. I. D'Yakonov and V. I. Perel'. Possibility of Orienting Electron Spins with Current. *Soviet Journal of Experimental and Theoretical Physics Letters*, 13:467, June 1971.

[12] J. E. Hirsch. Spin Hall effect. *Phys. Rev. Lett.*, 83:1834–1837, Aug 1999. doi: 10.1103/PhysRevLett.83.1834. URL http://link.aps.org/doi/10.1103/PhysRevLett.83.1834.

[13] V V Kruglyak, S O Demokritov, and D Grundler. Magnonics. *Journal of Physics D: Applied Physics*, 43(26):264001, July 2010. ISSN 0022-3727, 1361-6463. doi: 10.1088/0022-3727/43/26/264001. URL http://stacks.iop.org/0022-3727/43/i=26/a=264001?key=crossref.7d59bbfceddaf0f03df576a620cfcdf3.

[14] A A Serga, A V Chumak, and B Hillebrands. YIG magnonics. *Journal of Physics D: Applied Physics*, 43(26):264002, July 2010. ISSN 0022-3727, 1361-6463. doi: 10.1088/0022-3727/43/26/264002. URL http://stacks.iop.org/0022-3727/43/i=26/a=264002?key=crossref.6a073bfc1c8ba106fa1ba87bbfe37df3.

[15] B. Lenk, H. Ulrichs, F. Garbs, and M. Münzenberg. The building blocks of magnonics. *Physics Reports*, 507(4–5):107–136, October 2011. ISSN 0370-1573. doi: 10.1016/j.physrep.2011.06.003. URL http://www.sciencedirect.com/science/article/pii/S0370157311001694.

[16] V. V. Kruglyak and R. J. Hicken. Magnonics: Experiment to prove the concept. *Journal of Magnetism and Magnetic Materials*, 306(2):191–194, November 2006. ISSN 0304-8853. doi: 10.1016/j.jmmm.2006.02.242. URL http://www.sciencedirect.com/science/article/pii/S0304885306005889.

[17] Robert L Stamps, Stephan Breitkreutz, Johan Åkerman, Andrii V Chumak, YoshiChika Otani, Gerrit E W Bauer, Jan-Ulrich Thiele, Martin Bowen, Sara A Majetich, Mathias Kläui, Ioan Lucian Prejbeanu, Bernard Dieny, Nora M Dempsey, and Burkard Hillebrands. The 2014 magnetism roadmap. *Journal of Physics D: Applied Physics*, 47(33):333001, 2014. URL http://stacks.iop.org/0022-3727/47/i=33/a=333001.

[18] Z. K. Wang, V. L. Zhang, H. S. Lim, S. C. Ng, M. H. Kuok, S. Jain, and A. O. Adeyeye. Observation of frequency band gaps in a one-dimensional nanostructured magnonic crystal. *Applied Physics Letters*, 94(8):083112, February 2009. ISSN 0003-6951, 1077-3118. doi: 10.1063/1.3089839. URL http://scitation.aip.org/content/aip/journal/apl/94/8/10.1063/1.3089839.

[19] Lord Rayleigh Sec. R.S. XXVI. On the remarkable phenomenon of crystalline reflexion described by Prof. Stokes. *Philosophical Magazine Series 5*, 26(160): 256–265, 1888. doi: 10.1080/14786448808628259. URL http://dx.doi.org/10.1080/14786448808628259.

[20] Eli Yablonovitch. Inhibited spontaneous emission in solid-state physics and electronics. *Phys. Rev. Lett.*, 58:2059–2062, May 1987. doi: 10.1103/PhysRevLett.58.2059. URL http://link.aps.org/doi/10.1103/PhysRevLett.58.2059.

[21] Sajeev John. Strong localization of photons in certain disordered dielectric superlattices. *Phys. Rev. Lett.*, 58:2486–2489, Jun 1987. doi: 10.1103/PhysRevLett.58.2486. URL http://link.aps.org/doi/10.1103/PhysRevLett.58.2486.

[22] I. Dzyaloshinsky. A thermodynamic theory of "weak" ferromagnetism of antiferromagnetics. *Journal of Physics and Chemistry of Solids*, 4(4):241–255, 1958. ISSN 0022-3697. doi: 10.1016/0022-3697(58)90076-3. URL http://www.sciencedirect.com/science/article/pii/0022369758900763.

[23] Tôru Moriya. Anisotropic Superexchange Interaction and Weak Ferromagnetism. *Phys. Rev.*, 120(1):91–98, October 1960. doi: 10.1103/PhysRev.120.91. URL http://link.aps.org/doi/10.1103/PhysRev.120.91.

[24] Tôru Moriya. New Mechanism of Anisotropic Superexchange Interaction. *Phys. Rev. Lett.*, 4(5):228–230, March 1960. doi: 10.1103/PhysRevLett.4.228. URL http://link.aps.org/doi/10.1103/PhysRevLett.4.228.

[25] A. N. Bogdanov and U. K. Rößler. Chiral Symmetry Breaking in Magnetic Thin Films and Multilayers. *Phys. Rev. Lett.*, 87(3):037203, June 2001. doi: 10.1103/PhysRevLett.87.037203. URL http://link.aps.org/doi/10.1103/PhysRevLett.87.037203.

[26] A. Bogdanov and A. Hubert. Thermodynamically stable magnetic vortex states in magnetic crystals. *Journal of Magnetism and Magnetic Materials*, 138(3):255–269, December 1994. ISSN 0304-8853. doi: 10.1016/0304-8853(94)90046-9. URL http://www.sciencedirect.com/science/article/pii/0304885394900469.

[27] F. Jonietz, S. Mühlbauer, C. Pfleiderer, A. Neubauer, W. Münzer, A. Bauer, T. Adams, R. Georgii, P. Böni, R. A. Duine, K. Everschor, M. Garst, and A. Rosch. Spin Transfer Torques in MnSi at Ultralow Current Densities. *Science*, 330(6011): 1648–1651, December 2010. ISSN 0036-8075, 1095-9203. doi: 10.1126/science.1195709. URL http://www.sciencemag.org/content/330/6011/1648.

[28] Junichi Iwasaki, Masahito Mochizuki, and Naoto Nagaosa. Universal current-velocity relation of skyrmion motion in chiral magnets. *Nat Commun*, 4:1463, February 2013. doi: 10.1038/ncomms2442. URL http://www.nature.com/ncomms/journal/v4/n2/full/ncomms2442.html.

[29] J. Sampaio, V. Cros, S. Rohart, A. Thiaville, and A. Fert. Nucleation, stability and current-induced motion of isolated magnetic skyrmions in nanostructures. *Nat Nano*, 8(11):839–844, November 2013. ISSN 1748-3387. doi: 10.1038/nnano.2013.210. URL http://www.nature.com/nnano/journal/v8/n11/full/nnano.2013.210.html.

[30] Yurii A Izyumov. Modulated, or long-periodic, magnetic structures of crystals. *Soviet Physics Uspekhi*, 27(11):845, 1984. URL http://stacks.iop.org/0038-5670/27/i=11/a=R04.

[31] M. Bode, M. Heide, K. von Bergmann, P. Ferriani, S. Heinze, G. Bihlmayer, A. Kubetzka, O. Pietzsch, S. Blugel, and R. Wiesendanger. Chiral magnetic order at surfaces driven by inversion asymmetry. *Nature*, 447(7141):190–193, May 2007. ISSN 0028-0836. doi: 10.1038/nature05802. URL http://dx.doi.org/10.1038/nature05802.

[32] Stefan Heinze, Kirsten von Bergmann, Matthias Menzel, Jens Brede, André Kubetzka, Roland Wiesendanger, Gustav Bihlmayer, and Stefan Blügel. Spontaneous atomic-scale magnetic skyrmion lattice in two dimensions. *Nat Phys*, 7 (9):713–718, September 2011. ISSN 1745-2473. doi: 10.1038/nphys2045. URL http://www.nature.com/nphys/journal/v7/n9/full/nphys2045.html.

[33] A. Fert and Peter M. Levy. Role of Anisotropic Exchange Interactions in Determining the Properties of Spin-Glasses. *Phys. Rev. Lett.*, 44(23):1538–1541, June 1980. doi: 10.1103/PhysRevLett.44.1538. URL http://link.aps.org/doi/10.1103/PhysRevLett.44.1538.

[34] L. Udvardi and L. Szunyogh. Chiral Asymmetry of the Spin-Wave Spectra in Ultrathin Magnetic Films. *Phys. Rev. Lett.*, 102(20):207204, May 2009. doi: 10.1103/PhysRevLett.102.207204. URL http://link.aps.org/doi/10.1103/PhysRevLett.102.207204.

[35] Kh. Zakeri, Y. Zhang, J. Prokop, T.-H. Chuang, N. Sakr, W. X. Tang, and J. Kirschner. Asymmetric Spin-Wave Dispersion on Fe(110): Direct Evidence of the Dzyaloshinskii-Moriya Interaction. *Phys. Rev. Lett.*, 104(13):137203, March 2010. doi: 10.1103/PhysRevLett.104.137203. URL http://link.aps.org/doi/10.1103/PhysRevLett.104.137203.

[36] A. Hrabec, N. A. Porter, A. Wells, M. J. Benitez, G. Burnell, S. McVitie, D. McGrouther, T. A. Moore, and C. H. Marrows. Measuring and tailoring the Dzyaloshinskii-Moriya interaction in perpendicularly magnetized thin films. *Phys. Rev. B*, 90(2):020402, July 2014. doi: 10.1103/PhysRevB.90.020402. URL http://link.aps.org/doi/10.1103/PhysRevB.90.020402.

[37] Soong-Geun Je, Duck-Ho Kim, Sang-Cheol Yoo, Byoung-Chul Min, Kyung-Jin Lee, and Sug-Bong Choe. Asymmetric magnetic domain-wall motion by the Dzyaloshinskii-Moriya interaction. *Phys. Rev. B*, 88:214401, Dec 2013. doi: 10.1103/PhysRevB.88.214401. URL http://link.aps.org/doi/10.1103/PhysRevB.88.214401.

[38] M Vaňatka, J-C Rojas-Sánchez, J Vogel, M Bonfim, M Belmeguenai, Y Roussigné, A Stashkevich, A Thiaville, and S Pizzini. Velocity asymmetry of Dzyaloshinskii domain walls in the creep and flow regimes. *Journal of Physics: Condensed Matter*, 27(32):326002, 2015. URL http://stacks.iop.org/0953-8984/27/i=32/a=326002.

[39] A. T. Costa, R. B. Muniz, S. Lounis, A. B. Klautau, and D. L. Mills. Spin-orbit coupling and spin waves in ultrathin ferromagnets: The spin-wave Rashba effect. *Phys. Rev. B*, 82(1):014428, July 2010. doi: 10.1103/PhysRevB.82.014428. URL http://link.aps.org/doi/10.1103/PhysRevB.82.014428.

[40] M. Kostylev. Interface boundary conditions for dynamic magnetization and spin wave dynamics in a ferromagnetic layer with the interface Dzyaloshinskii-Moriya interaction. *Journal of Applied Physics*, 115(23):233902, June 2014. ISSN 0021-8979, 1089-7550. doi: 10.1063/1.4883181. URL http://scitation.aip.org/content/aip/journal/jap/115/23/10.1063/1.4883181.

[41] Jung-Hwan Moon, Soo-Man Seo, Kyung-Jin Lee, Kyoung-Whan Kim, Jisu Ryu, Hyun-Woo Lee, R. D. McMichael, and M. D. Stiles. Spin-wave propagation in the presence of interfacial Dzyaloshinskii-Moriya interaction. *Phys. Rev. B*, 88 (18):184404, November 2013. doi: 10.1103/PhysRevB.88.184404. URL http://link.aps.org/doi/10.1103/PhysRevB.88.184404.

[42] D Cortés-Ortuño and P Landeros. Influence of the Dzyaloshinskii–Moriya interaction on the spin-wave spectra of thin films. *Journal of Physics: Condensed Matter*, 25(15):156001, April 2013. ISSN 0953-8984, 1361-648X. doi: 10.1088/0953-8984/25/15/156001. URL http://stacks.iop.org/0953-8984/25/i=15/a=156001?key=crossref.d1a5a9b3c9d9f67a0235c534db7903d5.

[43] Kai Di, Vanessa Li Zhang, Hock Siah Lim, Ser Choon Ng, Meng Hau Kuok, Xuepeng Qiu, and Hyunsoo Yang. Asymmetric spin-wave dispersion due to Dzyaloshinskii-Moriya interaction in an ultrathin Pt/CoFeB film. *Applied Physics Letters*, 106(5):052403, February 2015. ISSN 0003-6951, 1077-3118. doi: 10.1063/1.4907173. URL http://scitation.aip.org/content/aip/journal/apl/106/5/10.1063/1.4907173.

[44] Kai Di, Vanessa Li Zhang, Hock Siah Lim, Ser Choon Ng, Meng Hau Kuok, Jiawei Yu, Jungbum Yoon, Xuepeng Qiu, and Hyunsoo Yang. Direct observation of the Dzyaloshinskii-Moriya Interaction in a Pt/Co/Ni film. *Phys. Rev. Lett.*, 114: 047201, Jan 2015. doi: 10.1103/PhysRevLett.114.047201. URL http://link.aps.org/doi/10.1103/PhysRevLett.114.047201.

[45] A. A. Stashkevich, M. Belmeguenai, Y. Roussigné, S. M. Cherif, M. Kostylev, M. Gabor, D. Lacour, C. Tiusan, and M. Hehn. Experimental study of spin-wave

dispersion in Py/Pt film structures in the presence of an interface Dzyaloshinskii-Moriya interaction. *Phys. Rev. B*, 91:214409, Jun 2015. doi: 10.1103/PhysRevB.91.214409. URL http://link.aps.org/doi/10.1103/PhysRevB.91.214409.

[46] Vanessa Li Zhang, Kai Di, Hock Siah Lim, Ser Choon Ng, Meng Hau Kuok, Jiawei Yu, Jungbum Yoon, Xuepeng Qiu, and Hyunsoo Yang. In-plane angular dependence of the spin-wave nonreciprocity of an ultrathin film with Dzyaloshinskii-Moriya interaction. *Applied Physics Letters*, 107(2):022402, 2015. doi: http://dx.doi.org/10.1063/1.4926862. URL http://scitation.aip.org/content/aip/journal/apl/107/2/10.1063/1.4926862.

[47] Mohamed Belmeguenai, Jean-Paul Adam, Yves Roussigné, Sylvain Eimer, Thibaut Devolder, Joo-Von Kim, Salim Mourad Cherif, Andrey Stashkevich, and André Thiaville. Interfacial Dzyaloshinskii-Moriya interaction in perpendicularly magnetized Pt/Co/AlO ultrathin films measured by Brillouin light spectroscopy. *Phys. Rev. B*, 91(18):180405, May 2015. doi: 10.1103/PhysRevB.91.180405. URL http://link.aps.org/doi/10.1103/PhysRevB.91.180405.

[48] Hans T. Nembach, Justin M. Shaw, Mathias Weiler, Emilie Jue, and Thomas J. Silva. Linear relation between Heisenberg exchange and interfacial Dzyaloshinskii-Moriya interaction in metal films. *Nat Phys*, advance online publication, August 2015. ISSN 1745-2481. URL http://dx.doi.org/10.1038/nphys3418.

[49] Jaehun Cho, Nam-Hui Kim, Sukmock Lee, June-Seo Kim, Reinoud Lavrijsen, Aurelie Solignac, Yuxiang Yin, Dong-Soo Han, Niels J. J. van Hoof, Henk J. M. Swagten, Bert Koopmans, and Chun-Yeol You. Thickness dependence of the interfacial Dzyaloshinskii-Moriya interaction in inversion symmetry broken systems. *Nat Commun*, 6, July 2015. doi: 10.1038/ncomms8635. URL http://www.nature.com/ncomms/2015/150708/ncomms8635/full/ncomms8635.html.

[50] Arne Brataas. Spintronics: Chiral domain walls move faster. *Nat Nano*, 8(7):485–486, July 2013. ISSN 1748-3387. URL http://dx.doi.org/10.1038/nnano.2013.126.

[51] Stuart S. P. Parkin, Masamitsu Hayashi, and Luc Thomas. Magnetic Domain-Wall Racetrack Memory. *Science*, 320(5873):190–194, November 2008. ISSN 0036-8075, 1095-9203. doi: 10.1126/science.1145799. URL http://www.sciencemag.org/content/320/5873/190.

[52] D. A. Allwood, G. Xiong, C. C. Faulkner, D. Atkinson, D. Petit, and R. P. Cowburn. Magnetic Domain-Wall Logic. *Science*, 309(5741):1688–1692, September 2005. ISSN 0036-8075, 1095-9203. doi: 10.1126/science.1108813. URL http://www.sciencemag.org/content/309/5741/1688.

[53] Roland Weiss, Roland Mattheis, and Günter Reiss. Advanced giant magnetoresistance technology for measurement applications. *Measurement Science and Technology*, 24(8):082001, August 2013. ISSN 0957-0233, 1361-6501. doi: 10.1088/0957-0233/24/8/082001. URL http://stacks.iop.org/0957-0233/24/i=8/a=082001?key=crossref.85e144120a72037a087d8babe89f5f1a.

[54] Djemoui Bouzidi and Harry Suhl. Motion of a Bloch domain wall. *Phys. Rev. Lett.*, 65(20):2587–2590, November 1990. doi: 10.1103/PhysRevLett.65.2587. URL http://link.aps.org/doi/10.1103/PhysRevLett.65.2587.

[55] Dennis Ilgaz, Mathias Klaui, Lutz Heyne, Olivier Boulle, Fabian Zinser, Stephen Krzyk, Mikhail Fonin, Ulrich Rüdiger, Dirk Backes, and Laura J. Heyderman. Selective domain wall depinning by localized Oersted fields and Joule heating. *Applied Physics Letters*, 93(13):132503, 2008. doi: http://dx.doi.org/10.1063/1.2990629. URL http://scitation.aip.org/content/aip/journal/apl/93/13/10.1063/1.2990629.

[56] June-Seo Kim, Mohamad-Assaad Mawass, André Bisig, Benjamin Krüger, Robert M. Reeve, Tomek Schulz, Felix Büttner, Jungbum Yoon, Chun-Yeol You, Markus Weigand, Hermann Stoll, Gisela Schütz, Henk J. M. Swagten, Bert Koopmans, Stefan Eisebitt, and Mathias Kläui. Synchronous precessional motion of multiple domain walls in a ferromagnetic nanowire by perpendicular field pulses. *Nat Commun*, 5, March 2014. doi: 10.1038/ncomms4429. URL http://www.nature.com/ncomms/2014/140324/ncomms4429/full/ncomms4429.html.

[57] L. Berger. Low field magnetoresistance and domain drag in ferromagnets. *Journal of Applied Physics*, 49(3):2156–2161, 1978. doi: http://dx.doi.org/10.1063/1.324716. URL http://scitation.aip.org/content/aip/journal/jap/49/3/10.1063/1.324716.

[58] L. Berger. Exchange interaction between ferromagnetic domain wall and electric current in very thin metallic films. *Journal of Applied Physics*, 55(6):1954–1956, 1984. doi: http://dx.doi.org/10.1063/1.333530. URL http://scitation.aip.org/content/aip/journal/jap/55/6/10.1063/1.333530.

[59] J.C. Slonczewski. Current-driven excitation of magnetic multilayers. *Journal of Magnetism and Magnetic Materials*, 159(1-2):L1–L7, jun 1996. doi: 10.1016/0304-8853(96)00062-5. URL http://dx.doi.org/10.1016/0304-8853(96)00062-5.

[60] A. Yamaguchi, T. Ono, S. Nasu, K. Miyake, K. Mibu, and T. Shinjo. Real-Space Observation of Current-Driven Domain Wall Motion in Submicron Magnetic Wires. *Phys. Rev. Lett.*, 92(7):077205, February 2004. doi: 10.1103/PhysRevLett.92.077205. URL http://link.aps.org/doi/10.1103/PhysRevLett.92.077205.

[61] G. S. D. Beach, M. Tsoi, and J. L. Erskine. Current-induced domain wall motion. *Journal of Magnetism and Magnetic Materials*, 320(7):1272–1281, April 2008. ISSN 0304-8853. doi: 10.1016/j.jmmm.2007.12.021. URL http://www.sciencedirect.com/science/article/pii/S0304885307010141.

[62] D. Ravelosona, D. Lacour, J. A. Katine, B. D. Terris, and C. Chappert. Nanometer scale observation of high efficiency thermally assisted current-driven domain wall depinning. *Phys. Rev. Lett.*, 95:117203, Sep 2005. doi: 10.1103/PhysRevLett.95.117203. URL http://link.aps.org/doi/10.1103/PhysRevLett.95.117203.

[63] Satoru Emori, Eduardo Martinez, Kyung-Jin Lee, Hyun-Woo Lee, Uwe Bauer, Sung-Min Ahn, Parnika Agrawal, David C. Bono, and Geoffrey S. D. Beach. Spin Hall torque magnetometry of Dzyaloshinskii domain walls. *Phys. Rev. B*, 90(18):184427, November 2014. doi: 10.1103/PhysRevB.90.184427. URL http://link.aps.org/doi/10.1103/PhysRevB.90.184427.

[64] Kwang-Su Ryu, Luc Thomas, See-Hun Yang, and Stuart Parkin. Chiral spin torque at magnetic domain walls. *Nat Nano*, 8(7):527–533, July 2013. ISSN 1748-3387. doi: 10.1038/nnano.2013.102. URL http://www.nature.com/nnano/journal/v8/n7/full/nnano.2013.102.html.

[65] M. Heide, G. Bihlmayer, and S. Blügel. Dzyaloshinskii-Moriya interaction accounting for the orientation of magnetic domains in ultrathin films: Fe/W(110). *Phys. Rev. B*, 78(14):140403, October 2008. doi: 10.1103/PhysRevB.78.140403. URL http://link.aps.org/doi/10.1103/PhysRevB.78.140403.

[66] G. Chen, J. Zhu, A. Quesada, J. Li, A. T. N'Diaye, Y. Huo, T. P. Ma, Y. Chen, H. Y. Kwon, C. Won, Z. Q. Qiu, A. K. Schmid, and Y. Z. Wu. Novel chiral magnetic domain wall structure in Fe/Ni/Cu(001) films. *Phys. Rev. Lett.*, 110:177204, 2013.

[67] E. H. Hall. On a new action of the magnet on electric currents. *American Journal of Mathematics*, 2(3):287, sep 1879. doi: 10.2307/2369245. URL http://dx.doi.org/10.2307/2369245.

[68] Jun-ichiro Ohe and Bernhard Kramer. Dynamics of a Domain Wall and Spin-Wave Excitations Driven by a Mesoscopic Current. *Phys. Rev. Lett.*, 96(2):027204, January 2006. doi: 10.1103/PhysRevLett.96.027204. URL http://link.aps.org/doi/10.1103/PhysRevLett.96.027204.

[69] Yann Le Maho, Joo-Von Kim, and Gen Tatara. Spin-wave contributions to current-induced domain wall dynamics. *Phys. Rev. B*, 79(17):174404, May 2009. doi: 10.1103/PhysRevB.79.174404. URL http://link.aps.org/doi/10.1103/PhysRevB.79.174404.

[70] Jun-ichiro Kishine and A. S. Ovchinnikov. Adiabatic and nonadiabatic spin-transfer torques in the current-driven magnetic domain wall motion. *Phys. Rev. B*, 81(13):134405, April 2010. doi: 10.1103/PhysRevB.81.134405. URL http://link.aps.org/doi/10.1103/PhysRevB.81.134405.

[71] Gen Tatara, Hiroshi Kohno, and Junya Shibata. Microscopic approach to current-driven domain wall dynamics. *Physics Reports*, 468(6):213–301, November 2008. ISSN 0370-1573. doi: 10.1016/j.physrep.2008.07.003. URL http://www.sciencedirect.com/science/article/pii/S0370157308002597.

[72] Gen Tatara and Hiroshi Kohno. Theory of Current-Driven Domain Wall Motion: Spin Transfer versus Momentum Transfer. *Phys. Rev. Lett.*, 92(8):086601, February 2004. doi: 10.1103/PhysRevLett.92.086601. URL http://link.aps.org/doi/10.1103/PhysRevLett.92.086601.

[73] Z. Li and S. Zhang. Domain-Wall Dynamics and Spin-Wave Excitations with Spin-Transfer Torques. *Phys. Rev. Lett.*, 92(20):207203, May 2004. doi: 10.1103/PhysRevLett.92.207203. URL http://link.aps.org/doi/10.1103/PhysRevLett.92.207203.

[74] Jun-ichiro Kishine and A. S. Ovchinnikov. Canonical formulation of magnetic domain-wall motion. *Physics Letters A*, 375(17):1824–1830, April 2011. ISSN 0375-9601. doi: 10.1016/j.physleta.2011.02.019. URL http://www.sciencedirect.com/science/article/pii/S0375960111001988.

[75] J. M. Winter. Bloch Wall Excitation. Application to Nuclear Resonance in a Bloch Wall. *Phys. Rev.*, 124(2):452–459, October 1961. doi: 10.1103/PhysRev.124.452. URL http://link.aps.org/doi/10.1103/PhysRev.124.452.

[76] J. Goldstone. Field theories with superconductor solutions. *Il Nuovo Cimento (1955-1965)*, 19(1):154–164, 1961. doi: 10.1007/BF02812722. URL http://dx.doi.org/10.1007/BF02812722.

[77] A. A. Thiele. Excitation spectrum of magnetic domain walls. *Phys. Rev. B*, 7: 391–397, Jan 1973. doi: 10.1103/PhysRevB.7.391. URL http://link.aps.org/doi/10.1103/PhysRevB.7.391.

[78] Alexander Szameit, Felix Dreisow, Matthias Heinrich, Stefan Nolte, and Andrey A. Sukhorukov. Realization of reflectionless potentials in photonic lattices. *Phys. Rev. Lett.*, 106:193903, May 2011. doi: 10.1103/PhysRevLett.106.193903. URL http://link.aps.org/doi/10.1103/PhysRevLett.106.193903.

[79] John Lekner. Reflectionless eigenstates of the squared hyperbolic secant potential. *American Journal of Physics*, 75(12):1151–1157, December 2007. ISSN 0002-9505, 1943-2909. doi: 10.1119/1.2787015. URL http://scitation.aip.org/content/aapt/journal/ajp/75/12/10.1119/1.2787015.

[80] John Lekner. Nonreflecting stratifications. *Canadian Journal of Physics*, 68(9):738–742, 1990. doi: 10.1139/p90-106. URL http://dx.doi.org/10.1139/p90-106.

[81] R. K. Dodd, J. C. Eilbeck, J. D. Gibbon, and H. C. Morris. *Solitons and Nonlinear Wave Equations. London UK.*, volume 1. Academic Press 1982., 1982. ISBN 10: 0122191226.

[82] Fred Cooper, Avinash Khare, and Uday Sukhatme. Supersymmetry and quantum mechanics. *Physics Reports*, 251(5–6):267 – 385, 1995. ISSN 0370-1573. doi: http://dx.doi.org/10.1016/0370-1573(94)00080-M. URL http://www.sciencedirect.com/science/article/pii/037015739400080M.

[83] C. Bayer, Helmut Schultheiss, Burkard Hillebrands, and Robert L. Stamps. Phase shift of spin waves travelling through a 180 degree Bloch-domain wall. *Magnetics, IEEE Transactions on*, 41(10):3094–3096, Oct 2005. ISSN 0018-9464. doi: 10.1109/TMAG.2005.855233.

[84] Riccardo Hertel, Wulf Wulfhekel, and Jürgen Kirschner. Domain-Wall Induced Phase Shifts in Spin Waves. *Phys. Rev. Lett.*, 93(25):257202, December 2004. doi:

10.1103/PhysRevLett.93.257202. URL http://link.aps.org/doi/10.1103/PhysRevLett.93.257202.

[85] Dong-Soo Han, Sang-Koog Kim, Jun-Young Lee, Sebastian J. Hermsdoerfer, Helmut Schultheiss, Britta Leven, and Burkard Hillebrands. Magnetic domain-wall motion by propagating spin waves. *Applied Physics Letters*, 94(11):112502, 2009. doi: http://dx.doi.org/10.1063/1.3098409. URL http://scitation.aip.org/content/aip/journal/apl/94/11/10.1063/1.3098409.

[86] Xi-guang Wang, Guang-hua Guo, Yao-zhuang Nie, Guang-fu Zhang, and Zhi-xiong Li. Domain wall motion induced by the magnonic spin current. *Phys. Rev. B*, 86:054445, Aug 2012. doi: 10.1103/PhysRevB.86.054445. URL http://link.aps.org/doi/10.1103/PhysRevB.86.054445.

[87] P. Yan, X. S. Wang, and X. R. Wang. All-Magnonic Spin-Transfer Torque and Domain Wall Propagation. *Phys. Rev. Lett.*, 107(17):177207, October 2011. doi: 10.1103/PhysRevLett.107.177207. URL http://link.aps.org/doi/10.1103/PhysRevLett.107.177207.

[88] W. Döring. About the inertia of walls. *Zeist. f. Naturforschung*, (3a):373, 1948.

[89] C. Kittel. Note on the inertia and damping constant of ferromagnetic domain boundaries. *Phys. Rev.*, 80:918–918, Dec 1950. doi: 10.1103/PhysRev.80.918. URL http://link.aps.org/doi/10.1103/PhysRev.80.918.

[90] Peng Yan, Akashdeep Kamra, Yunshan Cao, and Gerrit E. W. Bauer. Angular and linear momentum of excited ferromagnets. *Phys. Rev. B*, 88(14):144413, October 2013. doi: 10.1103/PhysRevB.88.144413. URL http://link.aps.org/doi/10.1103/PhysRevB.88.144413.

[91] Weiwei Wang, Maximilian Albert, Marijan Beg, Marc-Antonio Bisotti, Dmitri Chernyshenko, David Cortés-Ortuño, Ian Hawke, and Hans Fangohr. Magnon-Driven Domain-Wall Motion with the Dzyaloshinskii-Moriya Interaction. *Phys. Rev. Lett.*, 114(8):087203, February 2015. doi: 10.1103/PhysRevLett.114.087203. URL http://link.aps.org/doi/10.1103/PhysRevLett.114.087203.

[92] G.C. Hadjipanayis. *Magnetic Storage Systems Beyond 2000*. Nato Science Series II:. Springer Netherlands, 2012. ISBN 9789401006248.

[93] W. B. Zeper, F. J. A. M. Greidanus, P. F. Carcia, and C. R. Fincher. Perpendicular magnetic anisotropy and magneto optical Kerr effect of vapor deposited

Co/Pt layered structures. *Journal of Applied Physics*, 65(12):4971–4975, 1989. doi: http://dx.doi.org/10.1063/1.343189. URL http://scitation.aip.org/content/aip/journal/jap/65/12/10.1063/1.343189.

[94] Felix Bloch. Zur theorie des austauschproblems und der remanenzerscheinung der ferromagnetika. In *Zur Theorie des Austauschproblems und der Remanenzerscheinung der Ferromagnetika*, pages 295–335. Springer Berlin Heidelberg, 1932. ISBN 978-3-662-40658-8. doi: 10.1007/978-3-662-41138-4_1. URL http://dx.doi.org/10.1007/978-3-662-41138-4_1.

[95] L. Landau and E. Lifhsitz. Domain walls. *Physik A, Soviet Union*, 8:153, 1935.

[96] L. Néel. Domain walls. *Chiers Phys.*, 25:1–20, 1944.

[97] L.D. Landau and E.M. Lifshitz. *Statistical Physics*. Number v. 5. Elsevier Science, 2013. ISBN 9780080570464.

[98] W. Heisenberg. Zur theorie des ferromagnetismus. *Zeitschrift fur Physik*, 49 (9-10):619–636, sep 1928. doi: 10.1007/bf01328601. URL http://dx.doi.org/10.1007/BF01328601.

[99] P. A. M. Dirac. Quantum mechanics of many-electron systems. *Proceedings of the Royal Society A: Mathematical, Physical and Engineering Sciences*, 123(792): 714–733, apr 1929. doi: 10.1098/rspa.1929.0094. URL http://dx.doi.org/10.1098/rspa.1929.0094.

[100] A. Hubert and R. Schäfer. *Magnetic Domains: The Analysis of Magnetic Microstructures*. Springer Berlin Heidelberg, 2008. ISBN 9783540850540.

[101] A. Mougin, M. Cormier, J. P. Adam, P. J. Metaxas, and J. Ferré. Domain wall mobility, stability and Walker breakdown in magnetic nanowires. *EPL (Europhysics Letters)*, 78(5):57007, 2007. URL http://stacks.iop.org/0295-5075/78/i=5/a=57007.

[102] Satoru Emori, Uwe Bauer, Sung-Min Ahn, Eduardo Martinez, and Geoffrey S. D. Beach. Current-driven dynamics of chiral ferromagnetic domain walls. *Nat Mater*, 12(7):611–616, July 2013. ISSN 1476-1122. URL http://dx.doi.org/10.1038/nmat3675.

[103] Felipe Garcia-Sanchez, Pablo Borys, Arne Vansteenkiste, Joo-Von Kim, and Robert L. Stamps. Nonreciprocal spin-wave channeling along textures driven by

the Dzyaloshinskii-Moriya interaction. *Phys. Rev. B*, 89(22):224408, June 2014. doi: 10.1103/PhysRevB.89.224408. URL http://link.aps.org/doi/10.1103/PhysRevB.89.224408.

[104] Felipe Garcia-Sanchez, Pablo Borys, Rémy Soucaille, Jean-Paul Adam, Robert L. Stamps, and Joo-Von Kim. Narrow Magnonic Waveguides Based on Domain Walls. *Phys. Rev. Lett.*, 114(24):247206, June 2015. doi: 10.1103/PhysRevLett.114.247206. URL http://link.aps.org/doi/10.1103/PhysRevLett.114.247206.

[105] Herbert Goldstein, Charles P. Poole, and John L. Safko. *Classical Mechanics (3rd Edition)*. Addison-Wesley, Jun 2001.

[106] P.J. Olver. *Applications of Lie Groups to Differential Equations*. Applications of Lie Groups to Differential Equations. Springer New York, 2000. ISBN 9780387950006.

[107] M. V. Berry. Quantal phase factors accompanying adiabatic changes. *Proceedings of the Royal Society A: Mathematical, Physical and Engineering Sciences*, 392 (1802):45–57, mar 1984. doi: 10.1098/rspa.1984.0023. URL http://dx.doi.org/10.1098/rspa.1984.0023.

[108] Arne Vansteenkiste, Jonathan Leliaert, Mykola Dvornik, Mathias Helsen, Felipe Garcia-Sanchez, and Bartel Van Waeyenberge. The design and verification of mumax3. *AIP Advances*, 4(10):107133, 2014. doi: http://dx.doi.org/10.1063/1.4899186. URL http://scitation.aip.org/content/aip/journal/adva/4/10/10.1063/1.4899186.

[109] Ioan Mihai Miron, Thomas Moore, Helga Szambolics, Liliana Daniela Buda-Prejbeanu, Stéphane Auffret, Bernard Rodmacq, Stefania Pizzini, Jan Vogel, Marlio Bonfim, Alain Schuhl, and Gilles Gaudin. Fast current-induced domain-wall motion controlled by the Rashba effect. *Nature Materials*, 10(6):419–423, may 2011. doi: 10.1038/nmat3020. URL http://dx.doi.org/10.1038/nmat3020.

[110] J.D. Jackson. *Classical electrodynamics*. Wiley, 1975. ISBN 9780471431329.

[111] S. Rohart and A. Thiaville. Skyrmion confinement in ultrathin film nanostructures in the presence of Dzyaloshinskii-Moriya interaction. *Phys. Rev. B*, 88:184422, Nov 2013. doi: 10.1103/PhysRevB.88.184422. URL http://link.aps.org/doi/10.1103/PhysRevB.88.184422.

[112] A. Aharoni. *Introduction to the Theory of Ferromagnetism*. International Series of Monographs on Physics. Clarendon Press, 2000. ISBN 9780198508090.

[113] Riccardo Hertel, Wulf Wulfhekel, and Jürgen Kirschner. Domain-Wall Induced Phase Shifts in Spin Waves. *Phys. Rev. Lett.*, 93(25):257202, December 2004. doi: 10.1103/PhysRevLett.93.257202. URL http://link.aps.org/doi/10.1103/PhysRevLett.93.257202.

[114] H. Suhl. Ferromagnetic resonance in nickel ferrite between one and two kilomegacycles. *Phys. Rev.*, 97:555–557, Jan 1955. doi: 10.1103/PhysRev.97.555.2. URL http://link.aps.org/doi/10.1103/PhysRev.97.555.2.

[115] C. Bayer, H. Schultheiss, B. Hillebrands, and R.L. Stamps. Phase shift of spin waves traveling through a 180 degree Bloch domain wall. In *Magnetics Conference, 2005. INTERMAG Asia 2005. Digests of the IEEE International*, pages 827–828, April 2005. doi: 10.1109/INTMAG.2005.1463842.

[116] Siegfried. Flugge. *Practical quantum mechanics*, volume 1. Springer Berlin, 1971.

[117] C. Kittel. *Introduction to Solid State Physics*. Wiley, 2004. ISBN 9780471415268.

[118] C Kooy and U Enz. Experimental and theoretical study of the domain configuration in thin layers of BaFe. *Philips Res. Rep*, 15(7):181, 1960.

[119] A. Kubetzka, M. Bode, O. Pietzsch, and R. Wiesendanger. Spin-polarized scanning tunneling microscopy with antiferromagnetic probe tips. *Phys. Rev. Lett.*, 88: 057201, Jan 2002. doi: 10.1103/PhysRevLett.88.057201. URL http://link.aps.org/doi/10.1103/PhysRevLett.88.057201.

[120] V. V. Kruglyak and A. N. Kuchko. Spectrum of spin waves propagating in a periodic magnetic structure. *Physica B: Condensed Matter*, 339(2–3):130–133, December 2003. ISSN 0921-4526. doi: 10.1016/j.physb.2003.08.124. URL http://www.sciencedirect.com/science/article/pii/S0921452603006215.

[121] A.P. Malozemoff and J.C. Slonczewski. *Magnetic domain walls in bubble materials*. Applied solid state science: Supplement. Academic Press, 1979. ISBN 9780120029518.

[122] E. Noether. Invariante variationsprobleme. *Nachrichten von der Gesellschaft der Wissenschaften zu Göttingen, Mathematisch-Physikalische Klasse*, 1918:235–257, 1918. URL http://eudml.org/doc/59024.

[123] J.J. Sakurai and J. Napolitano. *Modern Quantum Mechanics*. Addison-Wesley, 2011. ISBN 9780805382914.

[124] L.D. Landau and E.M. Lifshitz. *Fluid Mechanics*. Number v. 6. Elsevier Science, 2013. ISBN 9781483140506.

[125] A.G. Gurevich and G.A. Melkov. *Magnetization Oscillations and Waves*. Taylor & Francis, 1996. ISBN 9780849394607.

[126] D. Hinzke and U. Nowak. Domain Wall Motion by the Magnonic Spin Seebeck Effect. *Phys. Rev. Lett.*, 107(2):027205, July 2011. doi: 10.1103/PhysRevLett.107.027205. URL http://link.aps.org/doi/10.1103/PhysRevLett.107.027205.

[127] N. Papanicolaou and T.N. Tomaras. Dynamics of magnetic vortices. *Nuclear Physics B*, 360(2–3):425 – 462, 1991. ISSN 0550-3213. doi: http://dx.doi.org/10.1016/0550-3213(91)90410-Y. URL http://www.sciencedirect.com/science/article/pii/055032139190410Y.

[128] Peng Yan. Angular and linear momentum of excited ferromagnets. *Phys. Rev. B*, 88(14), 2013. doi: 10.1103/PhysRevB.88.144413.

[129] Aurélien Manchon, Papa Birame Ndiaye, Jung-Hwan Moon, Hyun-Woo Lee, and Kyung-Jin Lee. Magnon-mediated Dzyaloshinskii-Moriya torque in homogeneous ferromagnets. *Phys. Rev. B*, 90(22):224403, December 2014. doi: 10.1103/PhysRevB.90.224403. URL http://link.aps.org/doi/10.1103/PhysRevB.90.224403.

[130] P.M. Chaikin and T.C. Lubensky. *Principles of Condensed Matter Physics*. Cambridge University Press, 2000. ISBN 9780521794503.